THE DIELECTRIC CONSTANT OF SANDSTONES, 5 HZ TO 13 MHZ

A DISSERTATION

SUBMITTED TO THE DEPARTMENT OF GEOPHYSICS

AND THE COMMITTEE ON GRADUATE STUDIES

OF STANFORD UNIVERSITY

IN PARTIAL FULFILLMENT OF THE REQUIREMENTS

FOR THE DEGREE OF

DOCTOR OF PHILOSOPHY

By

Rosemary Jane Knight

November 1984

ABSTRACT

The dielectric constant of 13 sandstones has been measured across the frequency range of 5Hz to 13 MHz as a function of water saturation and pore fluid salinity. Complex impedance plots of the data are used as an aid in identifying the various components in the frequency response and in determining an equivalent electrical circuit for the rock samples. There are two regions in the frequency response - a low frequency and high frequency region; the frequency separating these two regions in any particular rock sample depends upon the d.c. resistance of the sample. Within each region the dielectric constant shows a power law dependence upon frequency.

A Debye circuit provides a good equivalent circuit with which to approximately model the response of the samples. The Debye circuit contains two capacitors - one in series and one in parallel with the d.c. resistance of the sample. It is evident from the sample response that the values of the two capacitors are approximately 10^{-8} and 10^{-11} Farads respectively, the former dominating the low frequency, the latter the high frequency response. The low frequency capacitance is interpreted as representing double layer polarization, the high frequency capacitance as representing dipolar polarization. A significant part of the observed frequency dependence in the dielectric constant reflects the presence of these two capacitances with values differing approximately eight orders of magnitude.

There exists in the data a frequency dependence that cannot be modelled by a Debye circuit. This non-Debye behavior can be modelled by the inclusion of a frequency dependent admittance term in the equivalent electrical circuit. This admittance has a specific form such that the real and imaginary parts show

the same power law dependence upon frequency and the dissipation factor is constant with respect to frequency. The dependence of the power law exponent in this term on the level of water saturation and the surface area to volume ratio of the pore space of the sample, suggests that the frequency dependence is closely related to the internal geometry and microstructure of the sample. It appears possible to model this term using infinite equivalent circuits in the form of three-dimensional random networks.

The observed change of the dielectric constant with water saturation is interpreted as reflecting the presence of bound and free water in the pore space of a rock sample. When the frequency dependence is superimposed on the saturation dependence, the result is a rapid increase in the dielectric constant at low saturation up to some critical saturation above which the dielectric constant increases linearly and more gradually with saturation. The critical saturation is interpreted as reflecting the percentage of bound water in the rock and is thus proportional to the surface area to volume ratio of the pore space.

TABLE OF CONTENTS

CHAPTER 1

INTRODUCTION

The electrical properties of rocks are used in a wide variety of geophysical applications as a means of determining *in-situ* conditions. Examples of this are the use of resistivity logging in hydrocarbon exploration, and induced polarization and electromagnetic surveys in mineral exploration. The interpretation of data obtained from use of these methods is often based upon empirical relationships between electrical properties and rock properties. As the need for higher resolution is increasing, so is the need for a better understanding of the physical mechanisms controlling the electrical response of rocks.

The use of the dielectric constant as a well-logging tool has become a topic of great interest within the last decade. Table 1.1, taken from Poley et al. (1968) illustrates the potential usefulness of the dielectric constant as a means of measuring the level of water saturation in a reservoir. The dielectric constant of water is 80, significantly different from that of the rock matrix (approximately 6) or that of oil (2.2) or gas (1). Schlumberger has developed a dielectric logging tool known as an EPL (Electromagnetic Propogation Log) which operates in the GHz range (Calvert et al., 1977) and Texaco has developed several dielectric constant logging tools, one of which operates in the MHz range (Meander and Cox, 1975). There is interest in extending the logging frequency to even lower frequencies to further increase the investigation depth of the tool.

Despite the fact that dielectric logging tools are presently in use, there is little real understanding of the measured dielectric constant and the effect of such variables as clays and salinity of pore fluid. In laboratory measurements enormous values of the dielectric constant at low frequencies and a pronounced

Substance	dielectric constant ϵ'
Quartz (bulk)	4.5 – 4.7
Calcite (bulk)	7 – 8
Shale	13 – 15
Gas	1
Oil	2.2
Water	80

Table 1.1 The dielectric constant of materials commonly found in a reservoir.

dispersion have been observed, neither of which have been satisfactorily explained. It is the aim of this study to provide, through laboratory measurements and their interpretation, information about the electrical response of sedimentary rocks that can be used to develop a better understanding of the dielectric constant. The frequency is varied from 5Hz to 13 MHz; the other variables are the petrography of the sample, the level of water saturation and the salinity of the pore fluids.

Excellent discussions of the basic theory and definitions in electrical measurements are given by Von Hippel (1954), Sharbaugh and Roberts (1959), and Olhoeft (1981). Here only selected points relevant to this study are briefly summarized.

The following relations are valid in materials which exhibit electromagnetically linear behavior:

$$D = \varepsilon E$$
$$J = \sigma E$$
$$B = \mu H$$

where

E = electric field intensity (volt/meter)

H = magnetic field intensity (ampere - turn/meter)

D = electrical displacement (coulomb/m^2)

B = magnetic induction (weber/m^2)

J = electric current density (ampere/m^2)

ε = dielectric permittivity (farad/m)

σ = electrical conductivity (mho/m or siemens/m)

μ = magnetic permeability (henry/m)

There are two components in the electrical response of a material to an applied electric field, one in phase with the applied voltage (the conduction or loss component) and one out of phase with the applied voltage (the displacement or

storage component). The equation for total current density, J_T, is

$$J_T = \nabla \cdot H = \sigma E + \frac{\varepsilon \partial E}{\partial t}$$

where σE is the conduction current component and $\frac{\varepsilon \partial E}{\partial t}$ is the displacement current component.

For an applied alternating field, E = $E_o e^{i\omega t}$

$$J_T = (\sigma + i\omega\varepsilon) E_o e^{i\omega t}$$

where ω is frequency (radians/sec); t is time.

A total electrical conductivity (σ_T) can be defined as containing both free carrier conduction (σ) and dielectric displacement (ε):

$$\sigma_T = (\sigma_T' + i\sigma_T'') = \sigma + i\omega\varepsilon$$

where ' indicates the real part and " the imaginary part of a complex variable. Both σ and ε may be complex (Fuller and Ward, 1970), therefore:

$$\sigma_T' = \sigma' + \omega\varepsilon''$$
$$\sigma_T'' = \sigma'' + \omega\varepsilon'$$

The total resistivity, ρ_T which is also complex and the inverse of the total complex conductivity is given as:

$$\rho_T = \rho_T' - i\rho_T'' = (\sigma_T' + i\sigma_T'')^{-1}$$

It is convenient in determining material properties to relate the electrical response to equivalent electrical circuits. The two components, the loss and storage components, can be determined either in terms of a series RC cicuit or a parallel RC circuit.

In the series mode, in which case the material response is equated to that of a series RC circuit (Figure 1.1a), the complex impedance, Z, is measured:

$$Z = R_s - iX_s$$

where R_s is the loss component and $X_s = \frac{1}{\omega C_s}$, the reactance, is the storage

a)

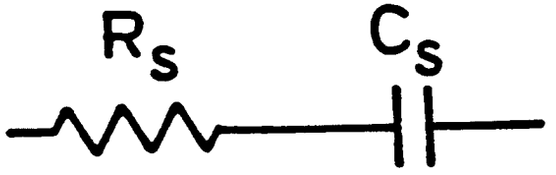

b)

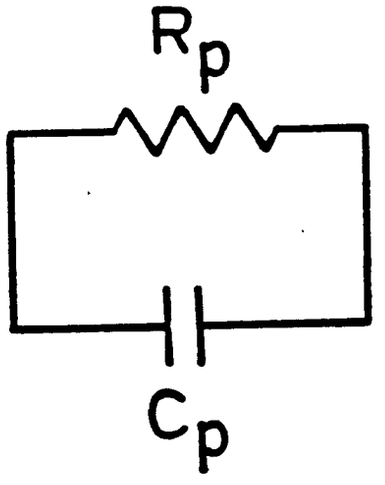

Figure 1.1 a) Series RC circuit. b) Parallel RC circuit. Subscript denotes circuit arrangement (S=series, P=parallel).

component.

In the parallel mode, in which case the material response is equated to that of a parallel RC circuit (Figure 1.1b), the admittance Y is measured:

$$Y = G_p + iB_p$$

where $G_p = \frac{1}{R_p}$, the conductance, is the loss component and $B_p = \omega C_p$, the susceptance, is the storage component.

The dissipation factor, D, the ratio between energy loss and energy storage, is determined by the relative magnitudes of the in-phase and quadrature components in either the series or parallel mode:

$$D = \frac{G_p}{B_p} = \frac{R_s}{X_s}$$

D is equivalent to the loss tangent of the system (tan δ) where δ is the phase angle - the angle between the in-phase and quadrature components.

In defining sample properties it is common practice to assume that the electrical response of the material can be represented by a parallel RC circuit. The resistivity (ρ) is given by

$$\rho = A\frac{R_p}{d}$$

and the dielectric constant is given by

$$\varepsilon = d\frac{C_p}{A\varepsilon_0}$$

where A is the cross-sectional area of the sample, d is the thickness, and ε_0 is the permittivity of free space; $\varepsilon_0 = 8.85 \times 10^{-14}$ F/cm.

It is also possible to express the resistivity and the dielectric constant in terms of free carrier conduction and dielectric displacement. Starting with a parallel RC circuit:

$$G_p + i\omega C_p = \sigma_T' + i\sigma_T'' = (\sigma' + \omega\varepsilon'') + i\omega(\varepsilon' + \sigma''/\omega)$$

This yields the following expressions for the resistivity and the dielectric

constant:

$$\rho = \frac{A}{dG_p} = \frac{A}{t(\sigma' + \omega\varepsilon'')}$$

$$\varepsilon = \frac{C_p A}{t\varepsilon_o} = \frac{(\varepsilon' + \sigma''/\omega)A}{t\varepsilon_o}$$

$\frac{\sigma''}{\omega}$ in most dielectrics is equal to 0 (Olhoeft, 1979).

The dissipation factor as defined above is for the total electrical response. In order to discuss purely dielectric mechanisms it is necessary to isolate D for the dielectric component. As the imaginary part of the dielectric constant includes free carrier conduction along with dielectric loss, it is necessary to subtract the contribution from the free carrier conduction in order to consider the dielectric mechanisms. In rocks the free carrier conduction corresponds to the ionic conduction; this can be removed by subtracting the d.c. conduction. It is important to note that while this removes the d.c. ionic conduction it is impossible to remove a.c. ionic conduction should it be present.

Expressing D in terms of free carrier conduction and dielectric displacement yields:

$$D = = \frac{\rho_T'}{\rho_T''} = \frac{\sigma_T'}{\sigma_T''} = \frac{\sigma' + \omega\varepsilon''}{\sigma'' + \omega\varepsilon'}$$

Subtracting σ' from the imaginary part of the dielectric constant, we obtain

$$D = \frac{\varepsilon''}{\varepsilon'}$$

In terms of the parallel RC circuit the resistivity is a measure of the conduction or loss in the system (R_p) and the dielectric constant is a measure of the capacitance or storage in a system (C_p). This will be true for any material that responds to an applied electric field like a parallel RC circuit. This will not be true however if the material response is not like that of a parallel RC circuit. For example, if the actual material response is that of a series RC circuit yet

measurements are made in the parallel mode, the measured resistance and capacitance of the material are given by the following expressions:

$$R_p = \frac{\omega C_s R_s^2 + 1}{\omega C_s R_s}$$

$$C_p = \frac{C_s}{\omega^2 R_s^2 C_s^2 + 1}$$

The measured resistance would contain contributions from the capacitance of the circuit and the measured capacitance would contain contributions from the resistance of the system. In this example therefore, the dielectric constant which is calculated from the parallel capacitance would not be a measure of simply capacitive or polarizing mechanisms in the rock, but would contain a contribution from the conductive mechanisms. As the equivalent electrical circuit for a material becomes more complex, it can be seen that assuming an incorrect equivalent circuit will produce very misleading measurements.

The dielectric constant is calculated from the assumed parallel capacitance, yet it is found that the electrical response of the rock samples is not that of a parallel RC circuit. The dielectric constant cannot therefore be assessed simply in terms of a capacitive mechanism . A major part of this study is concerned with determining an equivalent electrical circuit that accurately models the response of the rock samples. Having determined the appropriate equivalent circuit it is then possible to separate the various contributions to the observed dependence of the dielectric constant on frequency, sample, and fluid properties.

CHAPTER 2

SAMPLE DESCRIPTION AND EXPERIMENTAL PROCEDURE

Introduction

A variety of sandstones was used in this study representing a range in porosity from 6% to 28%, in permeability from microdarcies to millidarcies, and in clay content from 0% to 18%. The same procedure was followed for each sample in preparation, cleaning and measurement. This procedure evolved over time, parts of it for scientific reasons, parts simply to ensure consistency.

Petrographic Descriptions

Detailed petrographic descriptions of each sandstone sample are given in Table 2.1 (Stanford Rock Physics Data Base). The sandstone samples can be divided into two categories- high porosity sandstones and tight gas sands. Included in the high porosity sandstones are the following samples: Berea 100, Berea 200, Berea 400, Berea 500, St. Peter's, Indiana Light, Indiana Dark, Massillon, and Boise. Berea Sandstone is a quartzose sandstone; the various samples of Berea Sandstone vary mainly in permeability, with the number after "Berea" in the sample name referring to the approximate permeability of the sample in millidarcies. St. Peter's Sandstone is a medium-grained, well-sorted orthoquartzite with trace, if any, clays. Indiana Light is a fine-grained, well-sorted subarkose with clay cement. Indiana Dark is petrographically identical to Indiana Light, but contains 22% iron oxides and hydroxides, possibly mixed with clay. Massillon Sandstone is a medium-grained, well-sorted quartz arenite with iron oxide, clay, quartz overgrowths and chert cement. Boise Sandstone is a fine to medium-grained arkose with minor carbonate-clay cement. The tight gas sandstones from the Spirit River Formation in the Alberta Basin (samples

TABLE 2.1
SAMPLE DESCRIPTION

Sample	φ	k	Petrographic description (as % total) Framework Grains				Cements			
			qtz	cht	fldsp	lithics	qtz	clay	Fe ox	carb
Berea 100	.197	84 md	53	2	3	8	11	7(c)	-	7
Berea 200	.209	372 md	58	1	7	8	10	3	-	1
Berea 400	.219	397 md	61	2	6	2	8	1(c)	-	1
Berea 500	.204	555 md	66	1	1	1	5	1	8	-
CH58-79	.069	10.30 μD(a)	30	12	-	6	-	18	-	18
CH60-79	.074	-	36	11	-	10(b)	15	4	-	16
CH61-79	.070	7.18 μD(a)	38	16	1	4(b)	16	3	-	15
CH66-79	.065	2.38 μD(a)	30	12	-	6(b)	8	18	-	24
St. Peter's	.173	944 mD	77	-	-	-	8	-	-	-
Indiana Light	.246	120.1 mD	55	2	10	1	-	10	-	-
Indiana Dark	.275	30.2 mD	57	-	7	-	-	5	22	-
Massillon	.170	50 mD	55	2	10	1(b)	-	-	27	-
Boise	.256	912 mD	28	-	44	1(b)	6	-	-	3

φ = porosity; k = permeability; qtz = quartz; cht = chert; fldsp = feldspar; Fe ox = iron oxides; carb = carbonate

(a) in-situ conditions

(b) argillaceous

(c) clay percentage includes minor chlorite and/or sericite

are: CH58-79, CH60-79, CH61-79, CH66-79) are fine-grained litharenites, very well-sorted, with very low porosity and a clay content that varies from 7% to 15%.

Determination of Surface Area to Volume Ratios

As a means of further characterizing the samples, I determined the surface area to volume ratios of the internal pore space of five of the samples. The surface areas were obtained from nitrogen adsorption isotherms by using the Brunauer-Emmett-Teller equation (Brunauer et al., 1938). It was necessary to break the samples into pieces that could fit through a funnel 4mm. in diameter. Care was taken to avoid totally crushing the sample, so that the geometry of the pore space could be preserved. Rock surface areas are largely controlled by the presence of high surface area material such as clays, sericite, iron oxides and hydroxides (Clark, 1980). Other contributing factors are crack-like pores, which, as seen in scanning electron microscope photographs, are important in the tight gas sands.

The values obtained for the five samples are in the range and in the order expected given what was previously known about the petrography. St. Peter's Sandstone, a clean orthoquartzite, has the lowest surface area of 0.124 m^2/gm. Amongst the samples, Berea 200 with 3% clay, and Berea 100 with 7% clay, have surface areas of 0.84 m^2/gm and 1.234 m^2/gm. The surface area of the tight gas sand, CH60-79, was found to be 2.86 m^2/gm. This is in line with the clay content and pore geometry of this sample and can probably be considered as a representative value for the tight gas sands. Indiana Dark with 22% iron oxides and hydroxides, which is clearly associated with large surface area, has the highest surface area of 5.00 m^2/gm.

Surface area is measured as m^2 of surface area per gram of sample. To convert this to surface area per unit volume of pore space:

$$\frac{\text{surface area}}{\text{volume}}(cm^{-1}) = \frac{\text{surface area}}{\text{mass}}\left[\frac{m^2}{gm}\right] \times 2.64\left[\frac{gm}{cc}\right] \times \left[\frac{1-\varphi}{\varphi}\right] \times 10^4 \frac{cm^2}{m^2}$$

where φ is porosity and a value of 2.64 is assumed to be the density of the rock.

The tight gas sand, with relatively high surface area and low porosity, has a surface area to volume ratio of 9.45×10^5 cm^{-1}. St. Peter's, by comparison, with very low surface area and high porosity has a surface area to volume ratio of 1.57×10^4 cm^{-1}. Berea 100 and 200 have surface area to volume ratios of 1.33×10^5 cm^{-1} and 8.40×10^4 cm^{-1} respectively. Indiana Dark, while being the sample with the highest surface area, also has the highest porosity, resulting in a surface area to volume ratio which is less than that of the tight gas sand, and equal to 3.48×10^5cm^{-1}.

Preparation of Samples

The samples were prepared as thin disks with a diameter of two inches and a diameter to thickness ratio of greater that 10:1. This geometry was chosen to reduce errors due to stray capacitance (Scott and Curtis, 1939). The samples were surface ground to a smoothness varying less than .001".

One major interest in this study was the effect of contained pore fluids on the electrical response of a sample. Because the samples had often been previously saturated in their natural environment with a pore fluid of some salinity, there would have been residual salts left in the pores of the rock. In order to be able to saturate a rock and know the salinity of the fluid in the pores, it was necessary to remove any salts. This was done by soaking the sample in deionized water for a period of time, usually a couple of weeks, until the sample was "salt-free". As both the resistivity and the dielectric constant of a sample are sensitive to the salinity of the pore fluid, the samples were repeatedly dried, partially saturated with deionized water and the resistivity and dielectric constant measured until it was found that these parameters were no

longer changing. At this point the sample was classified as "salt-free"; it was assumed that all residual salts had been removed so that when deionized water was put into the rock, the salinity of the water remained that of deionized, resulting in a consistent measurement of both the resistivity and the dielectric constant.

Electrodes

There is much discussion in the literature of the techniques and problems in measuring the electrical properties of rock samples (Tarkhov, 1948; Madden and Marshall, 1958; Collett, 1959; Keller and Licastro, 1959; Scott et al., 1967; Collett and Katsube, 1973). There are choices to be made in terms of the electrode material, electrode application, and electrode configuration. No combination is perfect; each has its advantages and disadvantages. I will briefly review some of the various options as I describe the technique used in this study.

The two end members in terms of electrode materials are blocking electrodes and reversible electrodes (Hu, 1980). An electrode is blocking if the mode of conduction in the electrode is different from that in the sample. A metallic electrode used on a rock sample for example, is a blocking electrode; rocks are ionic conductors, while metal electrodes are electronic conductors. This results in a build-up of ions where the current flows across the rock/metal interface.

In a reversible electrode an electrochemical reaction occurs such that there is an exchange of charge carriers across the interface, preventing a build-up of ions and /or electrons. One example of such an electrode that has been used with rock samples is the silver-silver chloride electrode (Scott et al., 1967). In using this electrode, it is assumed that the ionic conductor in the rock is the chloride ion; when this ion reaches the electrode the chloride reacts with

the free silver to form silver chloride, thus allowing the ions to cross the sample/electrode boundary.

The choice of electrode material depends entirely upon the type of material under investigation. I feel that while reversible electrodes may be very useful in some simple systems, there are two major problems in their use with rock samples. One problem is the necessary assumption that the current is totally carried by one ionic species and that this ionic species has been correctly identified. While a silver-silver chloride electrode for example, is electrochemically reversible with respect to a chloride ion, the electrode will obviously still be blocking to any other ion. Another problem with this method is in obtaining good contact between the sample and electrode. The reversible electrodes are usually made by soaking a blotter in a solution of the desired chemical composition. Ensuring good and even contact between a blotter and the sample surface is not simple and may well introduce an air gap between the sample and the electrode. An air gap error can introduce a capacitance of the same order of magnitude as the sample itself making it very difficult to recognize and correct for (Scott et al., 1967).

The electrodes in this study were sputtered platinum. 1000 Å were applied by sputtering onto the two flat faces of each disc-shaped sample. Platinum is a relatively inert material (Scott et al., 1967) and sputtering is the best possible way I have found to contact a sample. Platinum however is a blocking electrode, so there was a charge build-up at the sample/electrode interface which can contribute to the measured electrical response at low frequencies (Scott et al., 1967).

Figure 2.1 shows two standard electrode configurations, a two-electrode and a four-electrode setup. The usual procedure in determining sample properties is to measure the change in magnitude and phase of the voltage across the

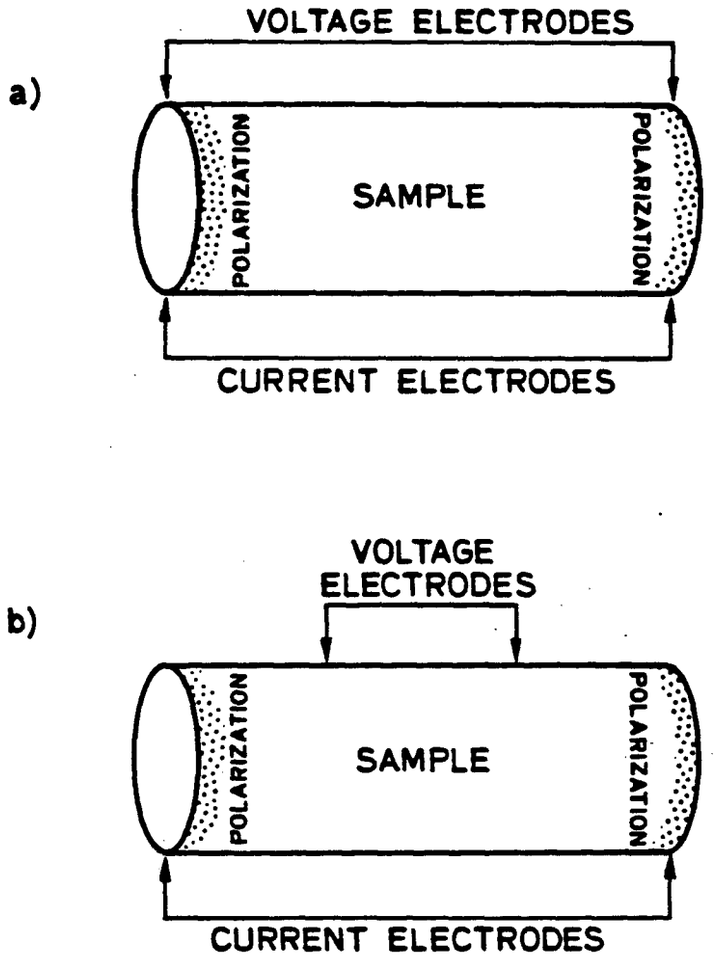

Figure 2.1 a) Two electrode set-up. Polarization at the current electrodes introduces an error in the measured voltage. b) Four electrode set-up. Voltage electrodes are positioned outside the region of polarization at the current electrodes thereby avoiding the error in the measurements due to this polarization.

sample. In a two-electrode set-up the ions build up where the current passes, ie. at the current electrodes. As the current electrodes in this set-up are also the voltage electrodes, this results in polarization at the voltage electrodes, introducing an error into the measurement.

Using a four-electrode method the electrode problem can be greatly reduced because the voltage electrodes are separated from the zone of polarization at the current electrodes. As the voltage electrodes themselves have a high impedance, they will draw very little current, so that essentially no polarization will occur at the voltage electrodes. Consequently, it is possible to make a measurement that will be unaffected by polarization at the sample/electrode interface.

Despite this advantage there are disadvantages that made the four-electrode system unsuitable for use in this study. Cylindrical shaped samples are required unless the sample is fully saturated, in which case a spacer saturated with the pore fluid can be used to separate the current electrodes from the sample. In the kHz and MHz frequency range cylindrical samples will definitely introduce problems due to edge effects which are essentially removed by using very thin disks. As the effect of varying saturation was one of the interests of this study an electrode arrangement suited only for measurements on fully saturated samples was not useful. Besides these problems with the sample geometry and saturation, there were serious instrumentation problems that made four-electrode measurements extremely difficult.

In summary then, I used disc shaped samples, which eliminates stray capacitance; two electrodes, which allows this geometry and measurement of varying saturation; sputtered platinum, which ensures excellent contact between the sample and electrode. The one problem with this set-up is polarization at the sample/electrode interface at low frequencies. The extent of

this polarization is discussed in the next chapter.

Measurement Technique

Measurements were made with an HP 4192A LF Impedance Analyzer interfaced with an HP 9845A desktop computer and displayed with an HP 4172 plotter. The parallel capacitance, C_p, parallel conductance, G_p, series resistance, R_s, and reactance, X_s, were measured over a frequency range of 5 Hz to 13 MHz with 50 measurements made through each logarithmic sweep of this interval. The oscillation amplitude was set at 1 volt. The HP 4192A has a "zero-offset" option which corrects for the impedance of the sample holder and cables. This correction was made before starting any measurements. To test the accuracy of the experimental set-up, a sample was prepared in the same geometry as the samples from a material of known dielectric constant. The material is STYCAST HiK, manufactured by Emerson and Cuming, described in technical bulletin 5-2-2, and has a dielectric constant of 15. The dielectric constant of this standard was always measured prior to any series of measurements. From this procedure the accuracy of the measurement was determined to be within 2%.

Method of Varying Saturation

To study the effect of water saturation on the electrical properties, a sample was first fully saturated with deionized water and then allowed to dry gradually. A sample was fully saturated by initially evacuating it in a pressure vessel, then allowing degassed deionized water to flow into the sample vessel, thus saturating the sample under a confining pressure of 1600 psi for at least 12 hours. Measurements on the fully saturated sample were made immediately upon removal from the pressure vessel. Subsequent measurements were made as the sample dried, its weight being monitored to determine the level of water

saturation. These drying experiments were done only for deionized water in the pores. As the rock had been previously cleaned it could be assumed that although the rock and water may come to some equilibrium by cation exchange, there would be no salts added to the pore fluid, so as the rock dried the salinity would remain constant. It was obviously impossible to do such drying experiments with saline solutions in the pores of the rock, as during drying the water would evaporate and the salt would remain, resulting in an increasing salinity.

Varying Samples and Pore Fluid Salinity

In order to compare the electrical response of different rock types it is necessary to have the same level of water saturation. As it is essentially impossible to always obtain the same level of saturation while drying different samples, the samples were all partially saturated to a selected standard saturation level, S_w = 0.36, by soaking in a beaker of fluid. To also be able to compare the effect of salinity, the samples were saturated to Sw=.36 with solutions of salinity varying from deionized to 1.0 M NaCl.

Initial Time Dependence in Measured Properties

It was found that the measured electrical properties of a saturated sample changed rapidly over the first few minutes after application of a voltage. Specifically the resistance decreased rapidly while the capacitance increased. This brings up the interesting question raised by Shi (1972) in reference to d.c. measurements as to which measured conductivity should be used- an initial measurement made at the moment the potential is first applied, or a type of steady state measurement, made some arbitrary time after the potential was applied. In this study, as a standard procedure, a sample was placed in the sample holder with an applied electric field and then left for 20 minutes until

making a measurement. The time taken to complete the measurements was about 2 minutes; the sample was then immediately removed and weighed and the saturation level for that set of measurements determined from that weight.

CHAPTER 3

COMPLEX PLANE ANALYSIS OF THE DATA

Introduction

Before considering the measured dielectric constant it is necessary to develop some understanding of the total electrical response, including both conductive and capacitive mechanisms, and determine an appropriate equivalent electrical circuit. It has been shown in Chapter 1 that this is essential in separating the various contributions to the dielectric constant. One method of data analysis and presentation in the study of the electrical response of materials is the use of complex plane plots. This method involves plotting the real versus the imaginary part of some complex electrical quantity for a wide range of frequencies. The complex planes most commonly used are the complex dielectric constant, ε^*, the complex admittance, Y^*, and the complex impedance, Z^*, planes. The resulting plot, in any of these planes, is some combination and variation of semicircles and straight lines. Components of the curve shape can be related to electrical circuit elements, thereby making it possible to determine an equivalent electrical circuit to model the frequency response of the material under investigation. The ε^* plot was used by Cole and Cole (1941) in studying polar liquids and is often referred to as a Cole-Cole plot. Bauerle (1969) first demonstrated the success of applying this method to solids with his measurements on the solid electrolyte, zirconia-yttria. I have found the method of complex plane analysis to work very well when applied to porous rocks containing pore fluids. The presentation of data in this form clearly shows the various components in the frequency response providing a good basis with which to undertake further interpretation and study of the electrical properties.

Representation in the Complex Impedance Plane

The choice of complex plane to be used depends upon the physical nature of the system. Jonscher (1975) suggests the use of the complex dielectric constant plane for a homogeneous material as this form of representation is most closely linked to the physical interpretation of the system; the use of the complex impedance plane when considering an inhomogeneous system consisting of a relatively conducting bulk layer in series with a relatively insulating barrier layer; and the use of the complex admittance plane when a parallel leakage conductance is present with a perfect capacitance with negligible series resistance.

The rock system investigated here consists, on a gross scale, of a conductive medium, the rock sample, with blocking electrodes. The appropriate type of complex plane plot to use, therefore, is a complex impedance (Z^*) plot. Impedance can be given by the following expression:

$$Z = R_s - iX_s$$

where R_s is the series resistance and X_s is the reactance. In a complex impedance plot, the imaginary part of the impedance, $-X_s$, is plotted against the real part, R_s.

Figure 3.1 shows the electrical response of two simple circuits presented in the complex impedance plane. In Figure 3.1a is shown a series RC circuit with its corresponding complex impedance plot. In the complex impedance plane the frequency response of a series RC circuit produces a straight line which is perpendicular to the real axis with frequency increasing towards the real axis. In Figure 3.1b is shown a parallel RC circuit with its corresponding complex impedance plot. The impedance written in terms of the parallel resistance and capacitance is given by the following expression:

$$Z = \frac{R_p}{(\omega R_p C_p)^2 + 1} + \frac{i\omega C_p R_p^2}{(\omega R_p C_p)^2 + 1}$$

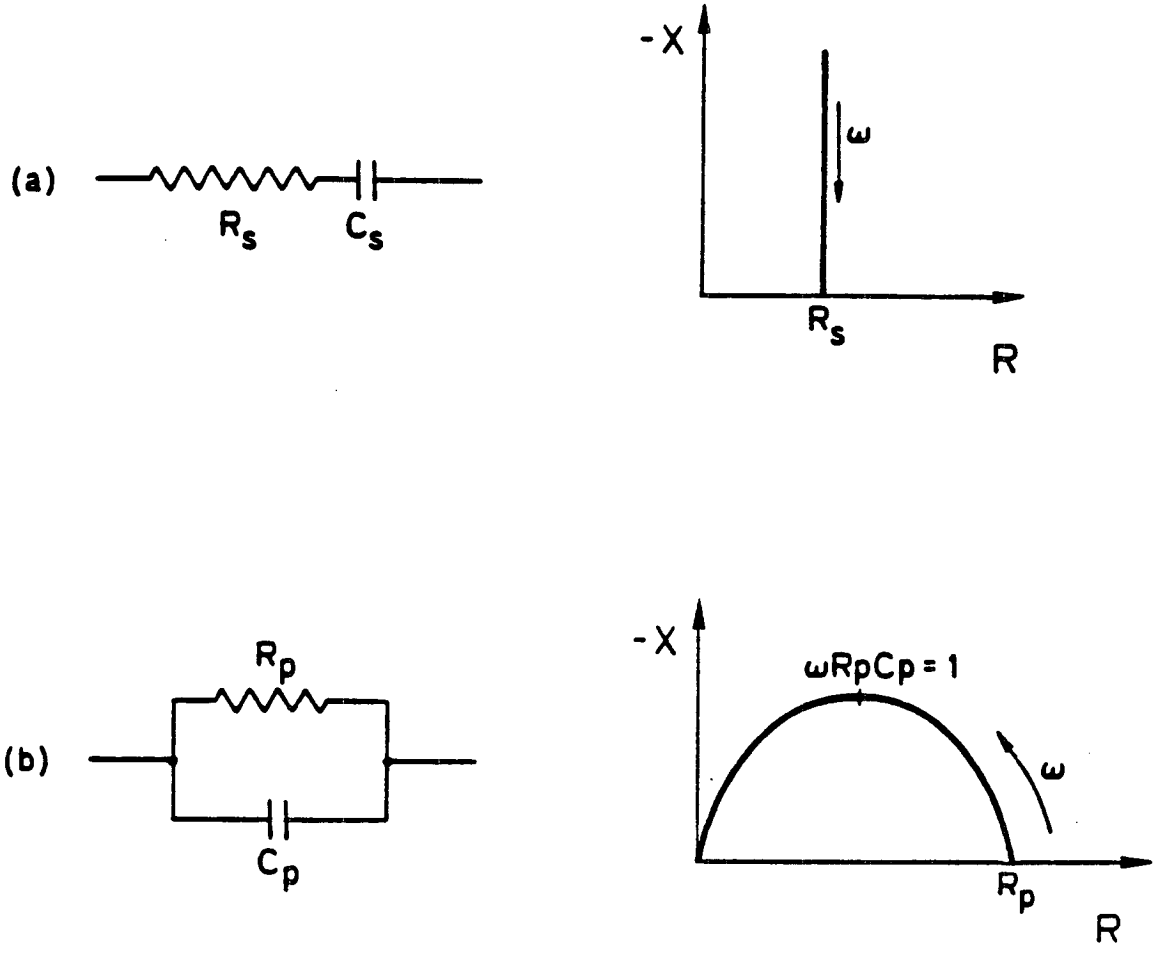

Figure 3.1 a) Series RC circuit and corresponding complex impedance plot. The plot of -X versus R for this circuit as a function of frequency is a line intersecting the real axis at Rs. b) Parallel RC circuit and corresponding complex impedance plot. The plot of -X versus R for this circuit is a semicircle intersecting the real axis at Rp.

where R_p is the parallel resistance and C_p is the parallel capacitance. The frequency response of a parallel RC circuit produces a semicircle in the complex impedance plane with the center of the semicircle positioned on the real axis and frequency increasing in a counter clockwise direction.

The data from a partially saturated sample of Berea Sandstone, when presented in the form of a Z^* plot (Figure 3.2), comprise a "depressed" semicircular arc, with the center of the semicircle below the real axis, and an inclined straight line. Frequency increases, as shown in the figure, down the line and counter clockwise along the semicircle. I will define as f_0 the frequency at the lowest point on the complex impedance plot which separates the linear lower frequency region from the semicircular higher frequency region. Essentially the same form of complex impedance plot has been found for all samples.

Modelling With the Debye Circuit

The total frequency response of any rock sample can be modelled as a first approximation with a Debye circuit. The basic Debye model in which dielectric loss can be characterized by a single relaxation time, is modelled by a series RC circuit. The Debye circuit which is frequently used in the interpretation of dielectric losses (Hu,1980), is the series RC circuit with an additional parallel capacitance which represents the high frequency geometrical effect of a material with a finite dielectric constant between two planar electrodes. A Debye circuit and the corresponding complex impedance plot is shown in Figure 3.3 (from Ho, 1980). R_2 corresponds to the d.c. resistance. C_1 and C_2 are capacitors with C_2 greater than C_1. The comparative values of C_1 and C_2 determine T, a measure of the degree of separation between the semicircular and linear portions of the complex impedance plot.

It has been possible to recognise in the complex impedance plots of the data, two regions in the frequency response; the region at frequencies less than

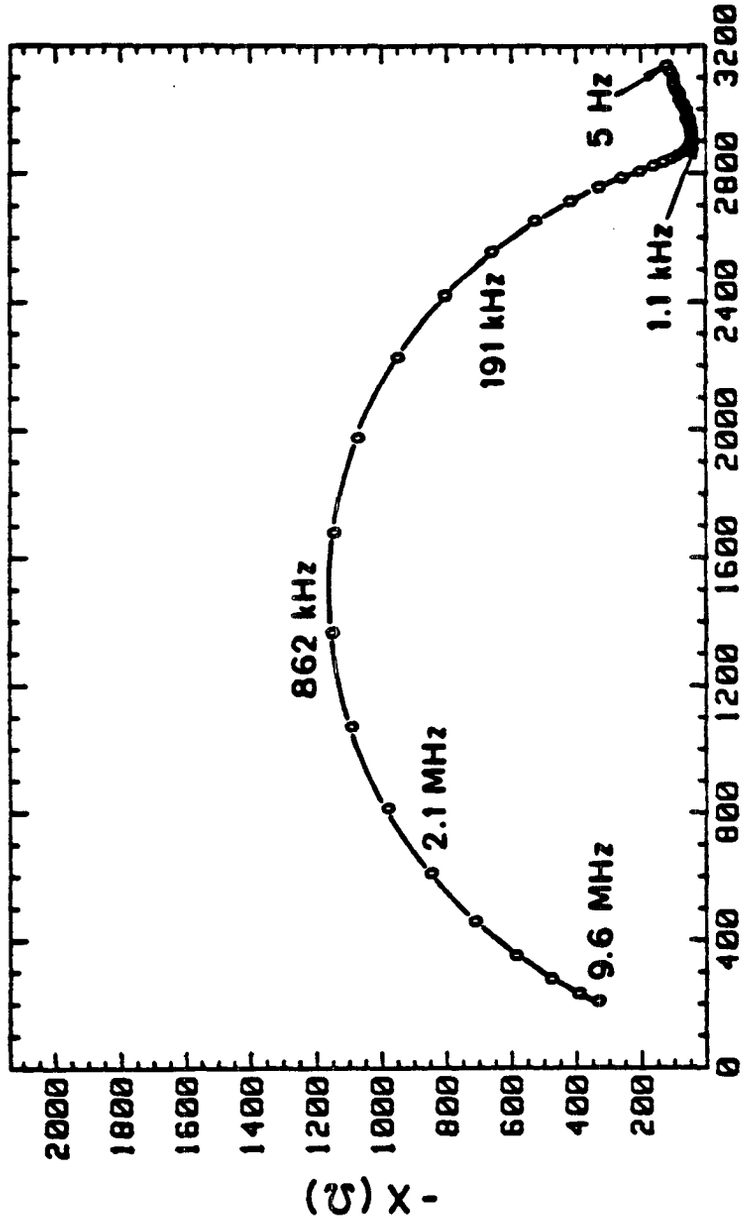

Figure 3.2 Complex impedance plot of data for a partially saturated sample of Berea 100, frequency 5 Hz to 9.6 MHz. Note the two regions in the plot, linear and semicircular. fo corresponds to the frequency separating these two regions; fo = 1.1 kHz.

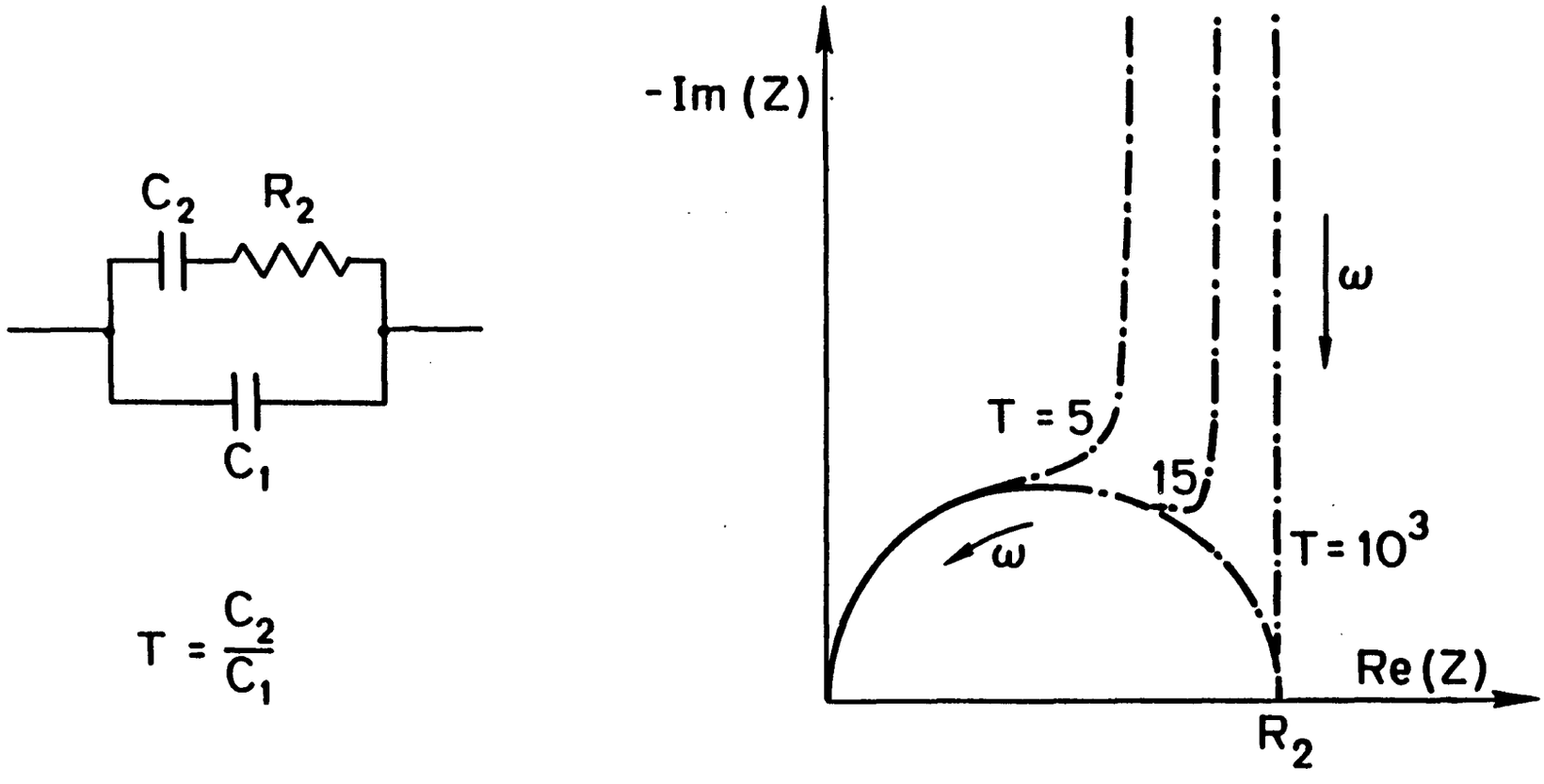

Figure 3.3 Debye circuit and corresponding complex impedance plot for various values of T.

f_0 which appears as a line in the plot will be referred to as the "low frequency response"; the region at frequencies greater that f_0 which appears as a semicircular arc will be referred to as the "high frequency response". Taking the Debye circuit as the equivalent electrical circuit to model the total electrical response, it is possible to determine an approximate equivalent electrical circuit for each of the two frequency regions of the response.

Considering the Debye circuit in Figure 3.3, it is obvious from the good separation seen between the linear and semicircular regions in the complex impedance plots for the rock samples (Figure 3.2) that $C_2 \gg C_1$. The impedance due to a capacitor, which is the reactance (X_c), is given by:

$$X = \frac{1}{\omega C}$$

which means that the impedance of the two capacitors, C_1 and C_2 is very different at any given frequency. At low frequencies the impedance of C_1 will be very high such that no current will flow through that portion of the circuit; the circuit is effectively a series RC circuit (R_2 in series with C_2) at low frequencies. (See Figure 3.4.) Thus the linear low frequency portion of the complex impedance plot for the Debye circuit corresponds to a series RC circuit. As shown in Figure 3.1a, a series RC circuit does produce a line in the complex impedance plane. A series RC circuit is therefore a good equivalent circuit with which to start in modelling the low frequency response. At high frequency, the impedance of both C_1 and C_2 decreases. The impedance of C_1 decreases to the point where current will flow through that part of the circuit; the impedance of C_2 decreases to essentially zero, leaving a parallel RC circuit (R_2 in parallel with C_1). (See Figure 3.4) A parallel RC circuit, as seen in Figure 3.1b, does produce a semicircle in the complex impedance plane, so can be used as the equivalent circuit with which to start in modelling the high frequency response.

a) At low frequency:

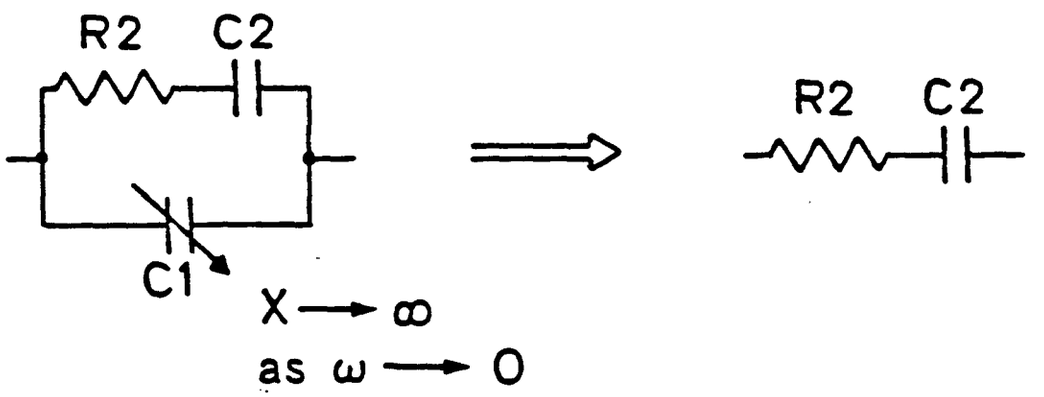

b) At high frequency:

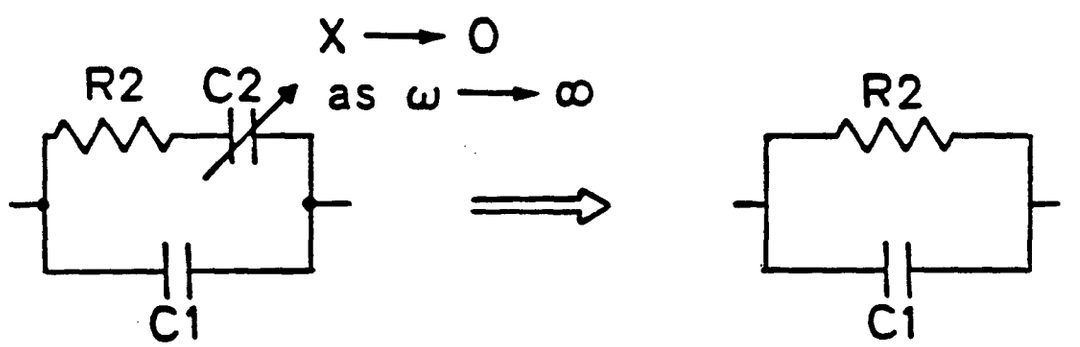

Figure 3.4 a) At low frequency the Debye circuit reduces to a series RC circuit as the impedance of C1 goes to infinity.
b) At high frequency the Debye circuit reduces to a parallel RC circuit as the impedance of C2 goes to zero.

A number of features of the electrical response of the Debye circuit are illustrated in the complex impedance plot. The angular frequency separating the two regions, ω_0, can be given by the following expression:

$$\omega_0 = (R^2 C_1 C_2)^{-1/2}$$

(Raistrick and Huggins, 1976). The response at this frequency is totally real, plotting on the real axis, the imaginary component having gone to 0. The value of R_s at this point is R_2, the d.c. resistance of the system.

Both a series RC circuit and a parallel RC circuit have a characteristic relaxation time (τ) where,

$$\tau = RC$$

The relaxation frequency for the high frequency response which corresponds to the parallel RC circuit, is the frequency at the top of the semicircle, where $-X_s$ reaches a maximum value. The relaxation frequency for the low frequency response, given that $C_2 >> C_1$ is at much lower frequency. The good separation between the two regions in the complex impedance plot is due to the fact that the relaxation times of the two are significantly different so act as distinct mechanisms.

Defining Two Regions in the Frequency Response

The complex impedance plots obtained for the rock samples always show very clearly either one or both of the two regions in the frequency response. Differences are found however in the frequency distribution of the data points when the sample, the level of water saturation, and/or the salinity of the pore fluid are changed; i.e. f_0 depends upon sample and fluid properties as predicted by the expression for ω_0 given above. Specifically f_0 is found to be inversely proportional to the d.c. resistance of the sample.

The d.c. resistance is by definition the value of R_s at the point where the semicircle intersects the real axis with decreasing frequency; this frequency

corresponds to f_0. Referring back to Figure 3.2, the d.c. resistance of the sample is taken to be the value of R_s at 1.1 kHz, that is 2860 Ohms. The d.c. resistance should be determined ideally at the lowest frequency where the impedance is entirely real, the imaginary part having gone to 0; this corresponds to the point in the complex plane where the impedance plots on the real axis. In Figure 3.2 it can be seen that the imaginary part still contributes to the impedance at 1.1 kHz, but this is the best value for the d.c. resistance that can be determined from this form of presentation of the data.

As the level of water saturation in a sample is increased, the resistance decreases, and f_0 moves to higher frequencies. In Figure 3.5 are shown examples of the complex impedance plots for Berea Sandstone at various levels of water saturation with the corresponding values of f_0 and d.c. resistance given in Table 3.1. When Berea 100 is 90% saturated two regions in the complex impedance plot are apparent, the lower frequency linear region extending from 5 Hz to f_0=1.5 kHz. At 20% saturation, f_0 has dropped to 460 Hz. For the dry sample, the low frequency portion of the response is not seen, f_0 being less than 5 Hz (the lowest measured frequency). These data suggest that while the lower frequency response will affect the electrical response up to 460 Hz in a 20% saturated sample, it will affect the response up to 1.5 kHz in a 90% saturated sample, and is not seen at all in the frequency range of this study in a dry sample.

In Figure 3.6 the relationship between f_0 and S_w is illustrated. The overall trend suggests that f_0 increases with decreasing resistance and increasing saturation.

The same trend is observed in the data from all other samples. Data from a tight gas sand (CH61-79) are presented in Figure 3.7, the values of f_0 given in Table 3.2 and the change with saturation plotted in Figure 3.8.

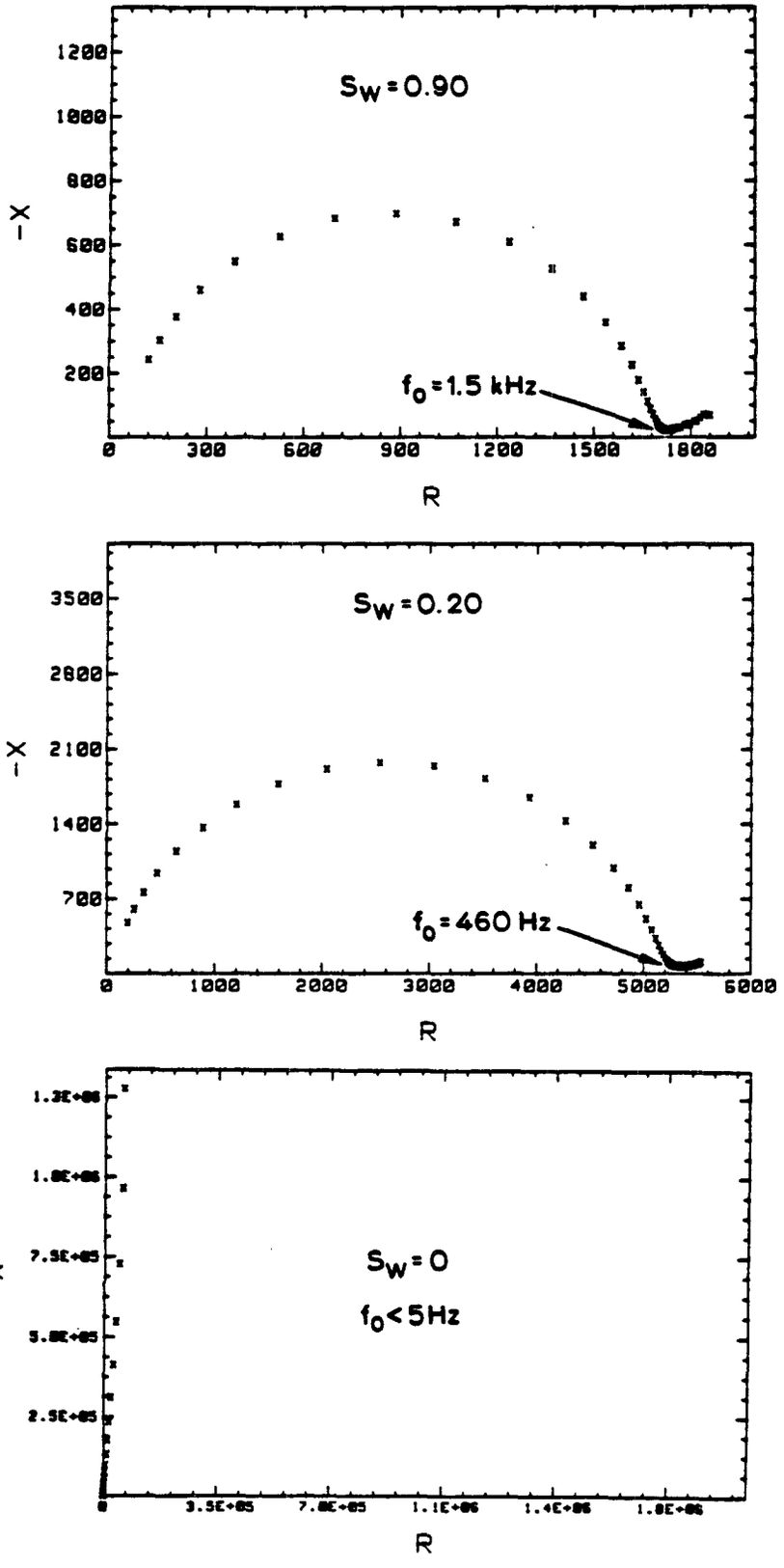

Figure 3.5 Complex impedance plots for Berea 100 at various levels of saturation (Sw). fo decreases with decreasing saturation.

Table 3.1
Berea 100: Effect of changing saturation on f_o

S_w	$R_{d.c}$ (kilohms)	f_o (Hz)
.9	1.74	1536
.8	1.82	1536
.7	1.88	1536
.6	2.05	841
.5	2.29	622
.4	2.79	622
.3	3.68	622
.2	5.33	460
.11	8.65	102
.001	(1)	(2)

(1) $R_{d.c}$ exceeds instrument limit of 2 megohms
(2) f_o is less than 5 Hz.

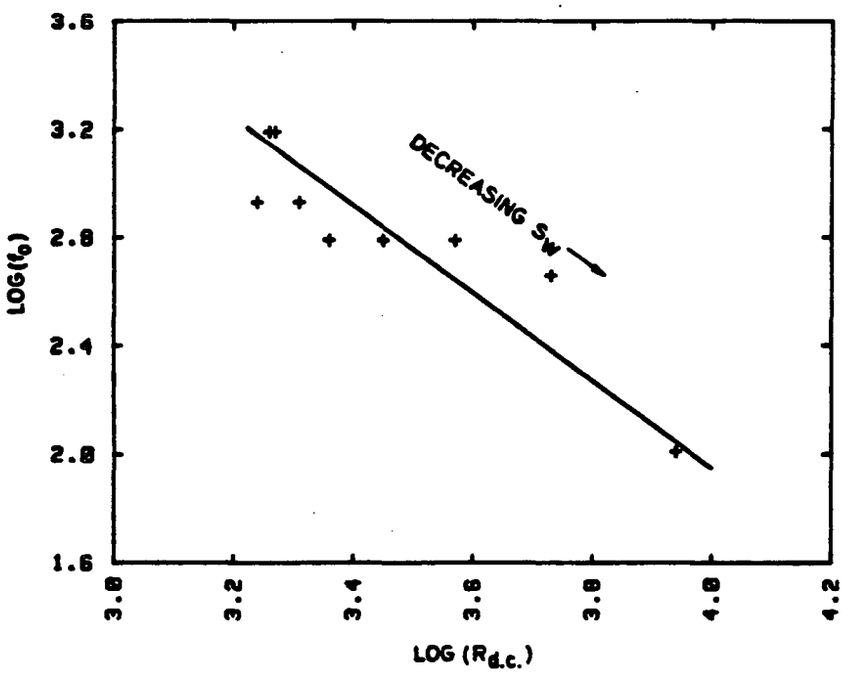

Figure 3.6 Logarithm of fo versus logarithm of d.c. resistance for Berea 100 at various levels of saturation (values plotted given in Table 3.1). fo decreases with increasing resistance and decreasing saturation.

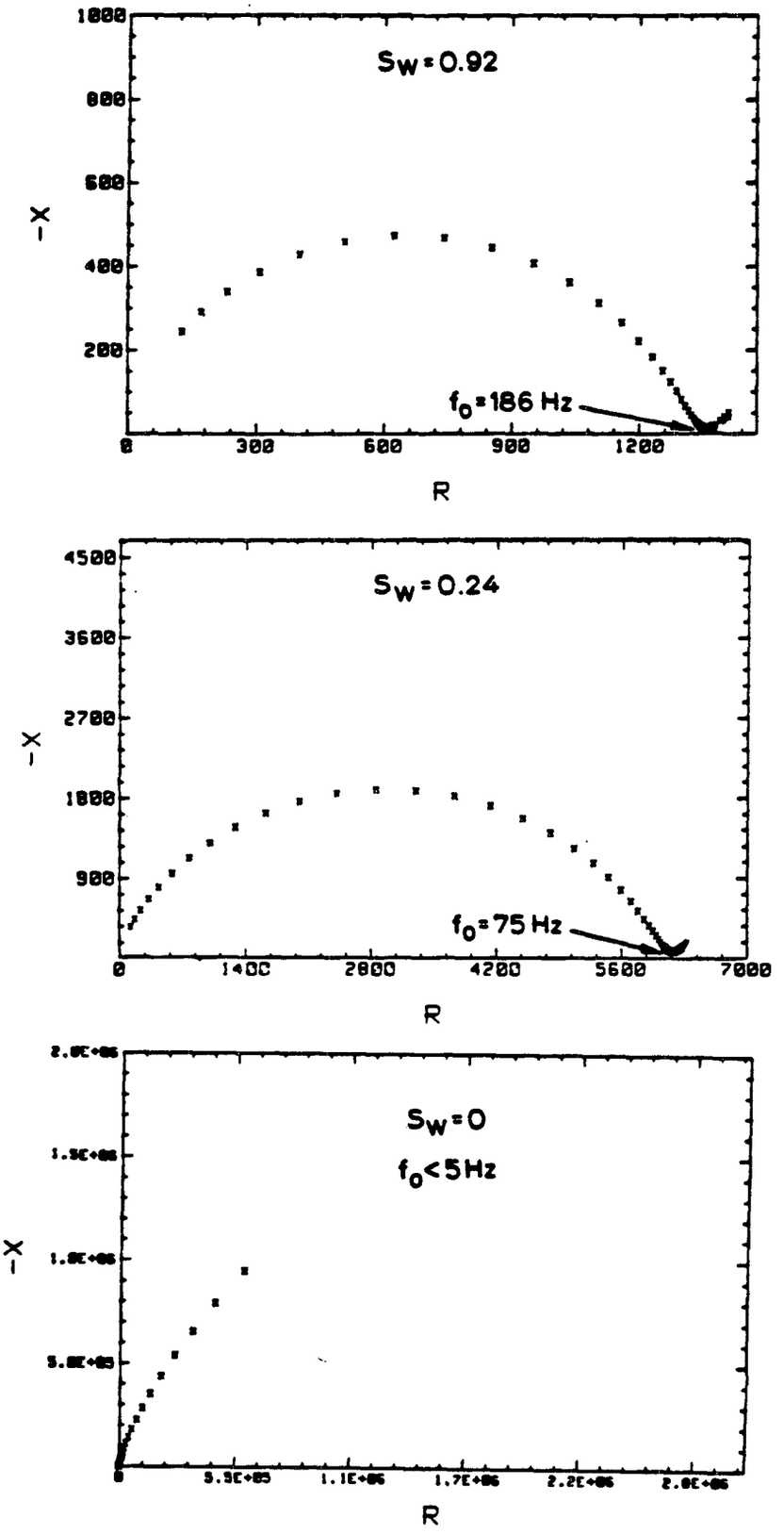

Figure 3.7 Complex impedance plots for CH66-79 at various levels of saturation (Sw). fo decreases with decreasing saturation.

Table 3.2
CH66-79: Effect of Changing Saturation on f_o

S_w	$R_{d.c}$ (kilohms)	f_o (Hz)
.92	1.40	186.2
.84	1.40	340.3
.76	1.42	340.3
.73	1.51	460.0
.62	1.77	460.0
.51	2.11	460.0
.38	2.94	460.0
.24	6.19	75.4
.16	20.00	6.6
.08	(1)	(2)
.016	(1)	(2)
.004	(1)	(2)

(1) $R_{d.c}$ exceeds instrument limit of 2 megohms
(2) f_o is less than 5 Hz.

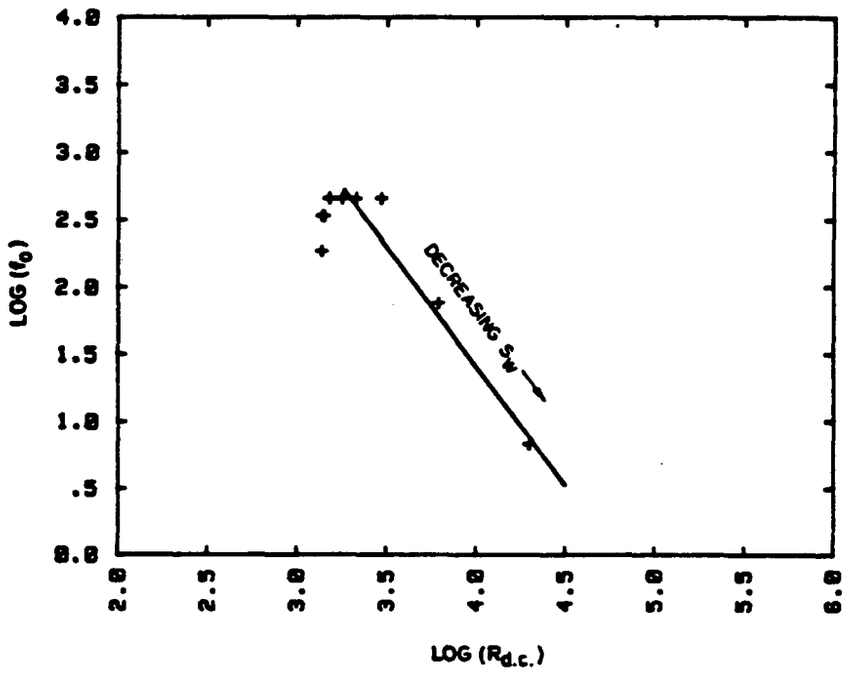

Figure 3.8 Logarithm of fo versus logarithm of d.c. resistance for CH66-79 at various levels of saturation. fo decreases with increasing resistance and decreasing saturation.

Changing the salinity of the pore fluid affects f_0 through the d.c. resistance in the same way. In Figure 3.9 are shown the data for Berea 100, 38% saturated with fluids of varying salinity with f_0 changing from 622 Hz when the sample is saturated with deionized water to 13 kHZ when saturated with .5 M NaCl solution. The change in f_0 with the change in d.c. resistance for the various salinities is plotted in Figure 3.10 and the values given in Table 3.3. The same general trend is found for all the samples.

Besides the change in f_0 with saturation and salinity in any one sample, f_0 also changes between samples, with the parameter that seemingly determines the value of f_0 being the d.c. resistance of the sample. The expression given above for ω_0 shows a dependence on the values of R_2, C_1, and C_2. As the change in R_2 is by far the largest, being on the order of kilohms while C_2 and C_1 are usually on the order of 10^{-6} and 10^{-12} Farads respectively, f_0 will be inversely proportional to R_2, as observed.

This has important implications in interpreting measurements of the d.c. resistance of different samples with different pore fluids when these measurements are all made at some constant and predetermined frequency. This has been discussed by Raistrick and Huggins (1976) with respect to measurements of d.c. conductivity of solid electrolytes. The results here suggest that the resistance of a rock sample should be measured at f_0, the value of which is dependent upon the d.c. resistance of the sample. Therefore, instead of choosing some frequency and consistantly measuring at that frequency, a more accurate and meaningful method of measuring d.c. resistance is with a frequency sweep measurement of the complex impedance. f_0 can be determined as corresponding to the minimum in the imaginary part and the real part at that frequency taken as the d.c. resistance. The measured resistance is equal to the d.c. resistance only when the frequency of

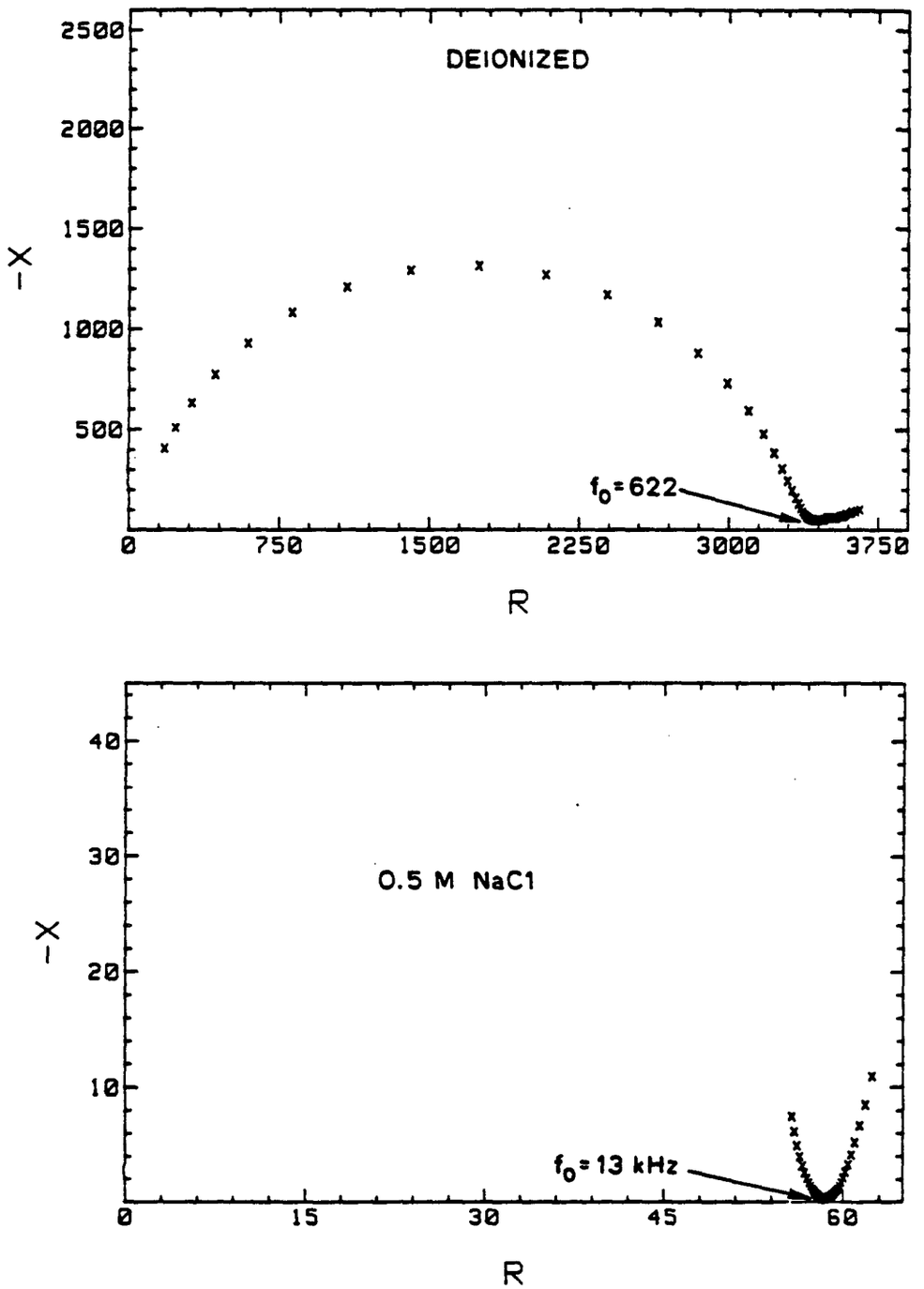

Figure 3.9 Complex impedance plots for Berea 100 partially saturated with deionized water and 0.5 M NaCl. fo increases with increasing salinity of pore fluid.

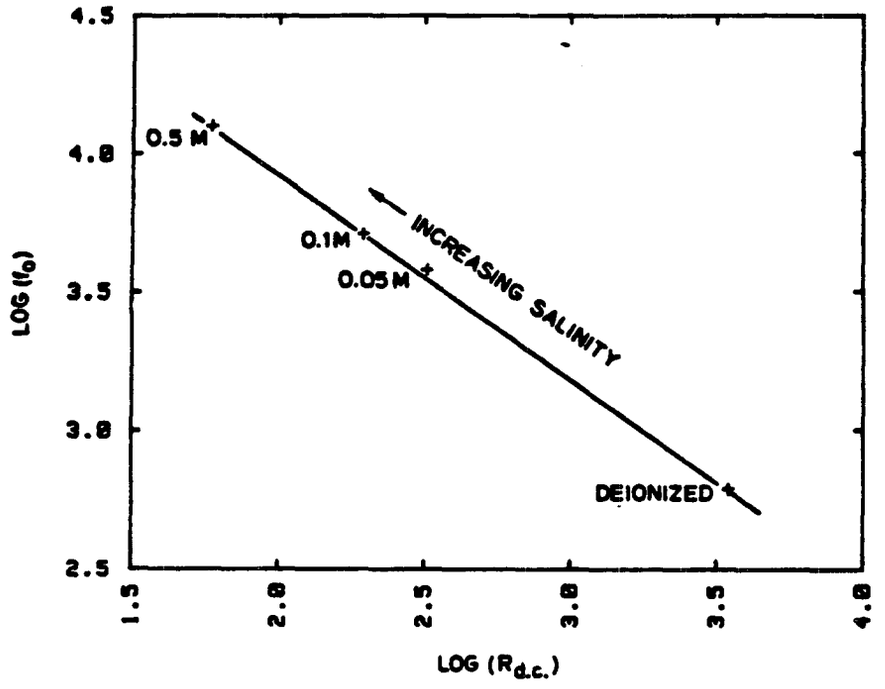

Figure 3.10 Logarithm of fo versus logarithm of d.c. resistance for Berea 100 36% saturated with solutions of varying salinity, from deionized to .5M NaCl. fo decreases with increasing resistance and decreasing salinity of pore fluid.

Table 3.3
Berea 100: Effect of Changing Salinity on f_e

Salinity (MNaCl)	$R_{d.c}$ (ohms)	f_e (Hz)
deionized water	3459.0	622
.05	322.5	3797
.1	194.2	5130
.5	58.4	12,671

measurement is equal to f_0; this is shown schematically in Figure 3.11.

Deviations From Debye Behavior

The electrical response of rocks has been modelled with a Debye circuit as a good first approximation to the equivalent circuit. There are however some significant differences between the response of the rocks and the Debye circuit. The complex impedance plot for the Debye circuit is composed of a vertical straight line and a semicircle centered on the real axis, while in a complex impedance plot for a rock sample, the line is inclined with respect to the real axis and the semicircular arc shows some asymmetry in the angles in which the arc intersects the real axis and is centered below the real axis. The Debye circuit shows the sort of ideal behavior in the complex impedance plane that would be exhibited by any electrical circuit composed of frequency independent resistors and capacitors.

The non-ideal form of complex plane plot found for the rock samples is not uncommon. In fact it is very rarely that real materials are found to produce ideal plots composed of exact semicircles and vertical lines (Jonscher, 1975). To model this non-ideal behavior with an equivalent electrical circuit, frequency dependent circuit components are needed (Cole and Cole, 1941; Raistrick et al., 1976), such as frequency dependent resistors and capacitors. A review of the data in Chapter 4 reveals a frequency dependence in the measured properties of rocks that is totally lacking in the Debye circuit. A more complicated equivalent electrical circuit is required.

Summary

Representation of data in the complex impedance plane. is a useful technique to employ in the study of the electrical response of rocks. With a complex impedance plot it is very easy to identify the various components of the

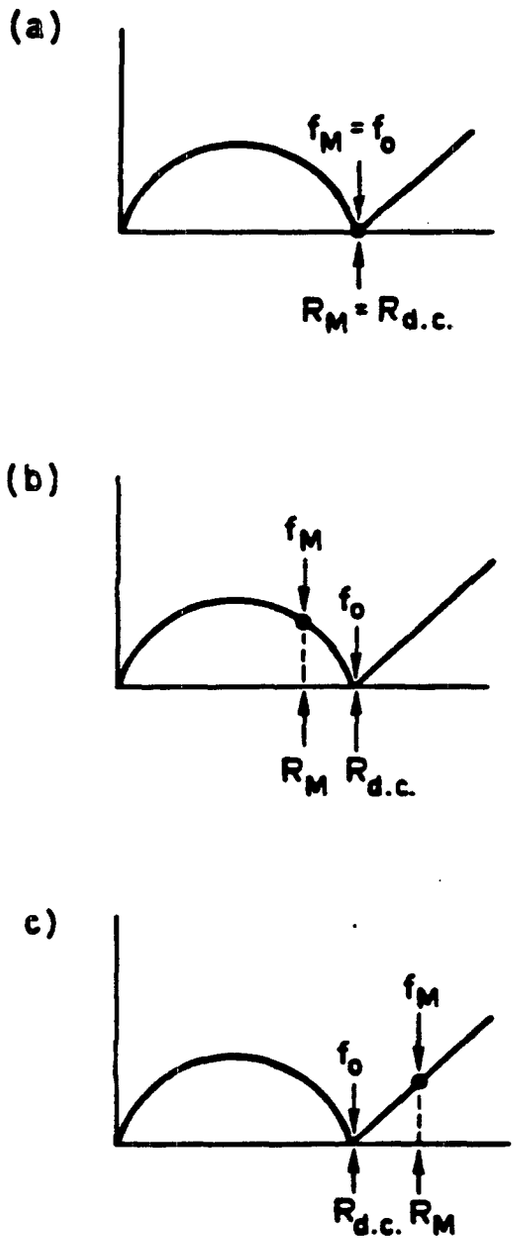

Figure 3.11 a) If the frequency of measurement (fM) is equal to fo, then the measured resistance (RM) is equal to the d.c. resistance (Rd.c.). b) If the frequency of measurement is greater than fo, then the measured resistance is less than the d.c. resistance. c) If the frequency of measurement is less than fo, then the measured resistance is greater than the d.c. resistance.

frequency response. The data from the rock samples studied here show very clearly two regions in the frequency response, a low frequency linear region and a high frequency semicircular region. I interpret there to be a distinct mechanism governing the electrical response in each of these two regions and will consider these regions separately; the frequency dividing the two regions, f_0, is dependent upon the d.c. resistance of the sample.

An accurate understanding of measured electrical properties is only possible after an appropriate equivalent circuit is determined so that the contributions to the capacitance and conduction in the rock can be separated. As a first approximation a Debye circuit has been used to model the data; the low frequency response can be best modelled by a series RC circuit and the high frequency response by a parallel RC circuit. There is an observed frequency dependence in the electrical response of the rock samples however that cannot be modelled with a Debye circuit, indicating a need for an improved circuit that can accommodate this frequency dependence.

CHAPTER 4

THE LOW FREQUENCY RESPONSE: INTERFACIAL POLARIZATION

Introduction

There appear to be two distinct mechanisms governing the electrical response of fully and partially saturated sandstone samples within the frequency range of this study. The low frequency electrical response is readily recognizable as a linear region in the complex impedance plot. As a two electrode set-up is used, there is undoubtedly polarization at the sample/electrode interface at these low frequencies (Scott et al., 1967). It is necessary to determine the extent and effect of this polarization and correct for that portion of the frequency response before a study of the electrical response of the rock itself is possible.

Polarization at the Sample/Electrode Interface

Ho (1980), in a study of solid electrolytes using a two electrode set-up, varied the electrode composition and application and determined that the low frequency linear response of his data in the complex impedance plane (Figure 4.1) was that of a platinum electrode. The material studied by Ho (1980) was an ionic conductor with platinum electrodes. As rocks are also ionic conductors and studied here with the same electrode material it is reasonable to expect a similar electrical response.

I used an approach described by Scott et al. (1967) to assess the effect of polarization at the sample/electrode interface. Scott et al. (1967) made measurements on the same sample at two different thicknesses to quantify the amount of polarization occurring at the sample/electrode interface. They assumed that the polarization acts as a capacitance in series with the sample

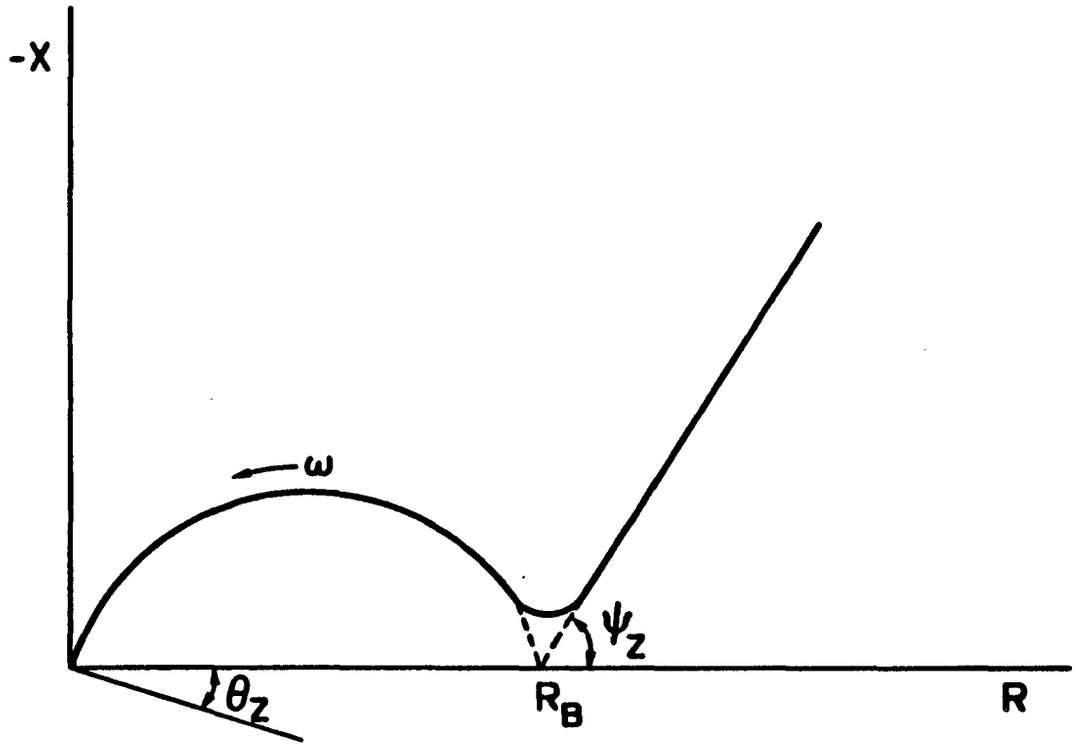

Figure 4.1 Schematic representation of the complex impedance of solid electrolye/blocking electrode system (from Ho, 1980).

and that this polarization capacitance is dependent upon the surface area of the sample/electrode interface, while the capacitance of the sample itself depends upon the volume of the sample. Varying the thickness therefore keeps the electrode polarization capacitance constant but changes the sample capacitance, so by subtracting the total capacitances one can remove the contribution of the electrode polarization capacitance from the total measured capacitance.

I used this approach with slight modification assuming that the polarization at the sample/electrode interface, which is in series with the sample, acts as an impedance with both resistive and capacitive elements. Given that the sample impedance per unit thickness and the impedance at the sample/electrode interface are both independent of the thickness of the sample, the correct impedance Z can be found:

$$Z = \frac{t_1(Z_2 - Z_1)}{t_2 - t_1}$$

where Z_1 is the impedance of the thinner sample; t_1 is the thickness of the thinner sample; Z_2 is the impedance of the thicker sample; t_2 is the thickness of the thicker sample.

This is a very tedious and time-consuming process, so was carefully done for only two samples, Berea 100 and CH60-79. Data for Berea 100 at Sw=.30 are presented in Figures 4.2a and 4.2b. The data presented in the complex impedance plane in Figure 4.2a includes polarization at the sample/electrode interface. The sample response with the polarization at the interface removed is shown in Figure 4.2b. The result of removing the electrode polarization is to flatten the linear part of the curve and shift the entire curve by some resistance. This corrects for both the capacitive and resistive elements associated with the electrode polarization. The low frequency response

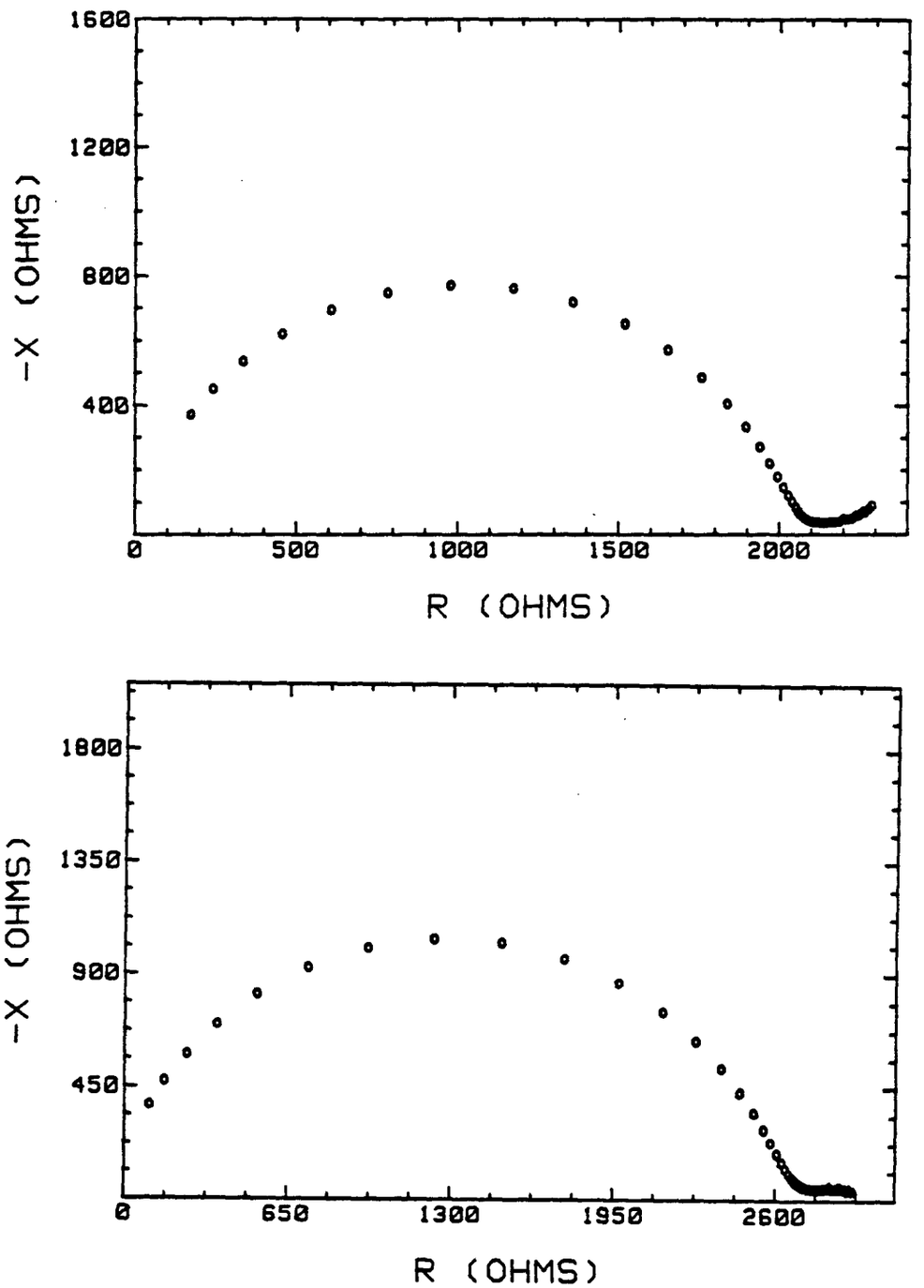

Figure 4.2 a) upper figure: Data for Berea 100, Sw=.30, with no correction made for polarization at the sample/electrode interface. b) lower figure: Data for Berea 100, Sw=.30, having removed the impedance due to polarization at the sample/electrode interface. Note how this correction has affected the low frequency linear portion of the plot.

remaining is polarization within the rock itself.

Figure 4.3 shows the effect of the polarization at the sample/electrode interface on the measured dielectric constant. The error due to the electrode polarization causes an enhancement of the correct value of the dielectric constant by a factor of four at low frequencies. This error decreases with increasing frequency such that above f_0 the error, if any, is less than 10%.

The low frequency data obtained from saturated sandstones does appear to be dominated by polarization at the platinum electrode. As the low frequency response is most like that of a series RC circuit, the electrode polarization capacitance is equal to the measured series capacitance. A plot of the electrode polarization capacitance (C_s) as a function of frequency within the low frequency region for different samples at different levels of water saturation is given in Figure 4.4. The polarization capacitance in all cases shows a power law dependence upon frequency:

$$C_s = A\omega^{-\alpha}$$

where ω is angular frequency, A and α are constants; α is equal to approximately 0.8.

The capacitance due to polarization at a sample/electrode interface has often been described in the literature by a power law dependence upon frequency (Grahame, 1952; Schwan, 1968; Scheider, 1975) with the specific value of the power law exponent dependent upon the material. In dilute electrolytes, α is usually constant over most of the frequency range where the polarization capacitance is measureable, and has a value between 0 and 0.5 (Scheider, 1975). In very concentrated electrolytes α may change gradually with frequency, as seen by Schwan (1968) and Wolff (1936). In the samples from this study, α is obviously constant over a large frequency range, although the value of α is larger than that reported in other materials.

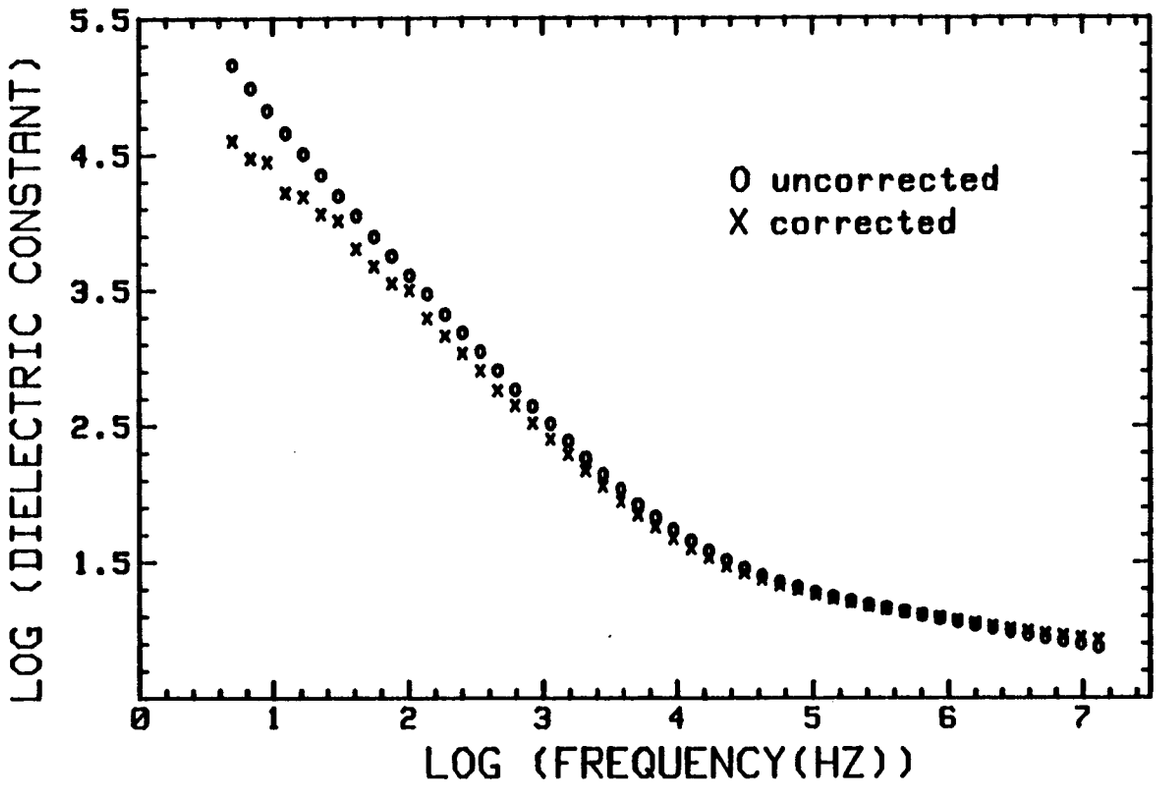

Figure 4.3 The logarithm of the dielectric constant versus the logarithm of frequency for Berea 100, Sw=.30. Two data sets are shown, one corrected for the electrode polarization and one uncorrected for the electrode polarization. Electrode polarization causes an enhancement of the dielectric constant at low frequency.

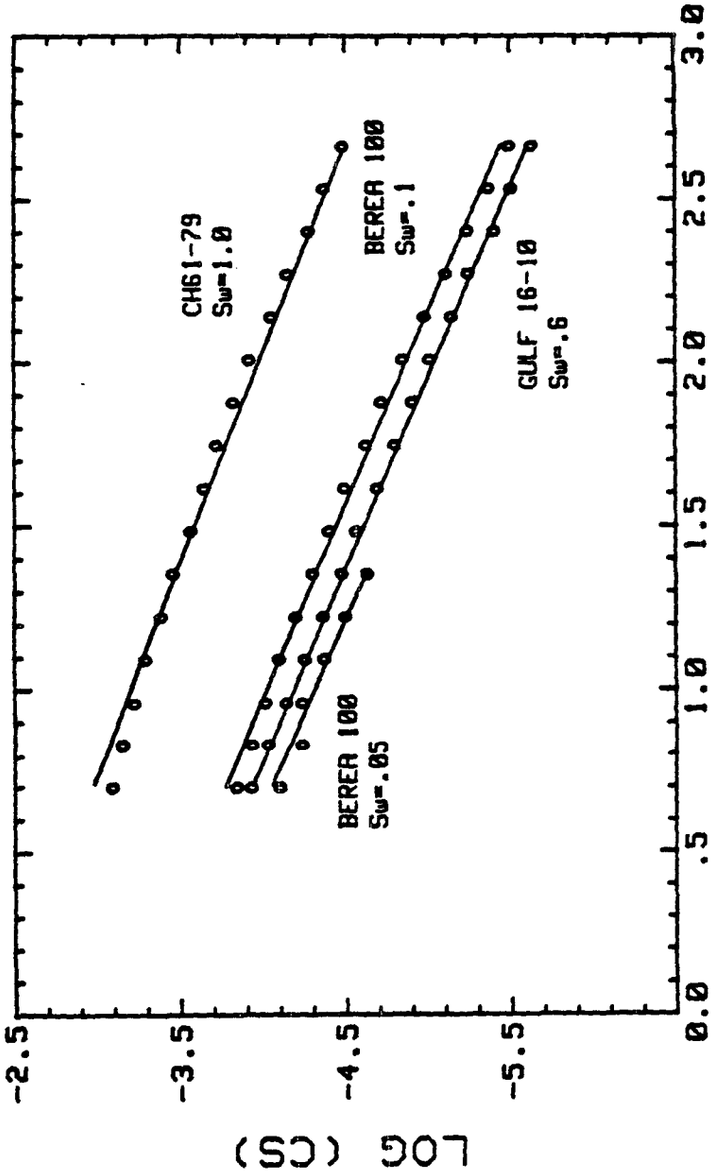

Figure 4.4 The logarithm of the series capacitance versus the logarithm of frequency for the low frequency (less than fo) response of three rocks at various levels of saturation. Cs shows a power law dependence upon frequency.

A consistent relationship is found between the electrode polarization capacitance at any frequency in the low frequency region and the d.c. conductance of the sample. Scheider (1975) in looking at the polarization at the interface between an electrode and electrolytic solutions showed that the polarization capacitance at any given frequency is directly proportional to the conductivity of the solution. I have found the same linear relationship for each rock sample shown in Figure 4.5 where the capacitance at 32 Hz is proportional to the d.c. conductance of the sample. While 32 Hz has been used here, this relationship holds for any frequency within the low frequency region. The plot includes examples from three different rock samples at various levels of saturation; the proportionality constant varies from sample to sample. The values used for d.c. conductance are $1/R_{d.c.}$ where $R_{d.c.}$ is the value of R_s at f_0 as discussed in the previous chapter.

From this study of the low frequency data I have concluded that the low frequency linear response is dominated by the response of the polarization at the sample/electrode interface. This polarization only affects the measured data in the low frequency region, i.e. data above f_0 are unaffected by the electrode polarization.

Polarization at Interfaces Within the Rock

The process in the low frequency region has been shown to be predominantly that of diffusion of ions to and polarization at the electrode interface. It is reasonable to assume however that other types of interfacial polarization are present in the sandstones and contribute to this low frequency response, for example polarization at microscopic interfaces in the rock such as the membrane polarization associated with clays (Fuller and Ward, 1970). When the method of varying the thickness of the sample was used to subtract the impedance of the electrode from the total measured impedance, the

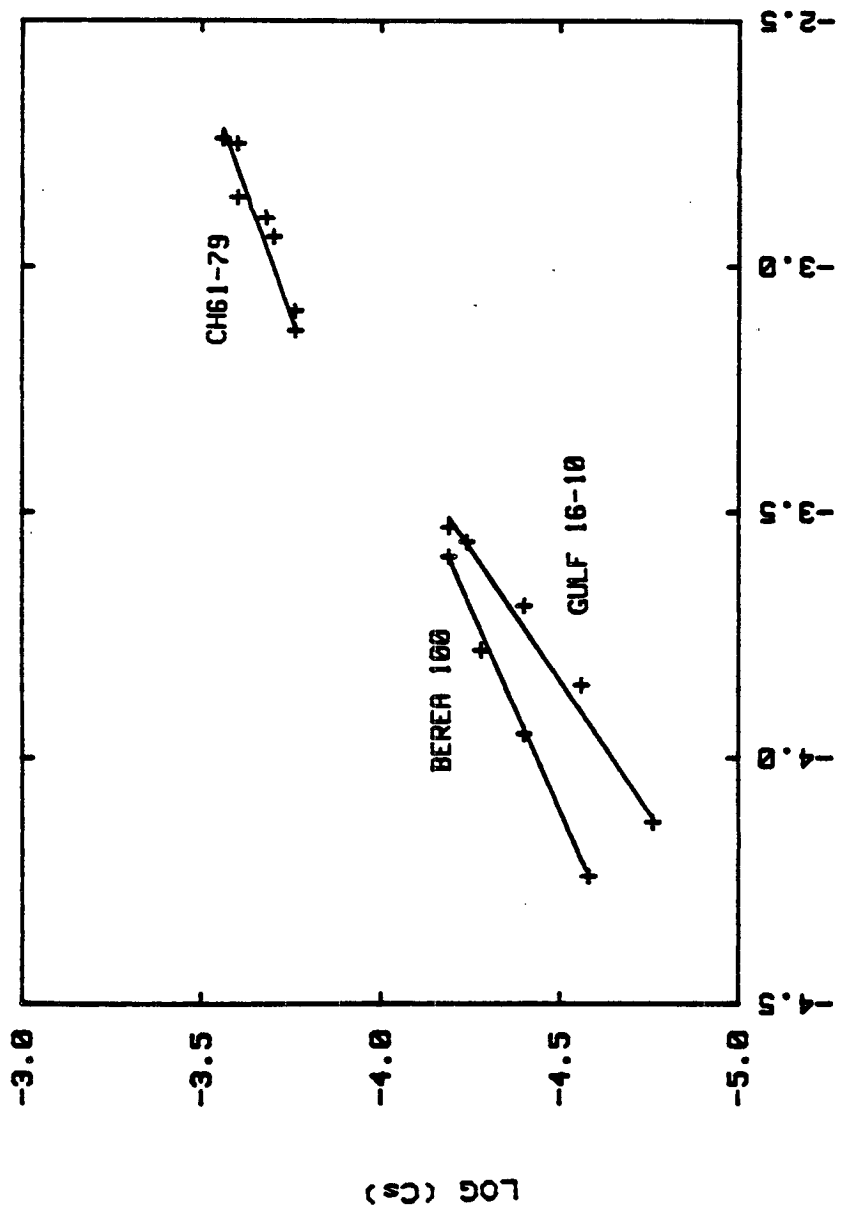

Figure 4.5 The logarithm of the series capacitance at 32 Hz versus the logarithm of the d.c. conductance for three rocks at various levels of saturation.

polarization of the rock itself at low frequencies could be seen in the complex impedance plot as a line with very small phase angle (Figure 4.2b).

The technique of varying thickness is by no means an ideal method by which to obtain low frequency data, as is evidenced by some scatter in the data. It is possible however, to make some observations about the electrical response in this frequency range. As the low frequency response can be approximately modelled by a series RC circuit, C_s is a measure of the low frequency polarization in the sample. Data for Berea 100, S_w=.30, with the electrode polarization removed, are shown in Figure 4.6. C_s shows a power law dependence upon frequency with a power law exponent equal to -1. This same power law dependence has been recently reported by Vinegar and Waxman (1984).

A power law dependence of capacitance upon frequency in the low frequency data for the rock itself is not an unexpected find. The well documented existence of a power law dependence in the capacitance due to polarization at an electrode interface (Scheider, 1975) I feel suggests a power law dependence in the capacitance due to polarization at any interface. In both cases the mechanism involved is diffusion to and polarization at an interface or interfaces, be it the electrode or microscopic "barriers" in the rock, such as clays or at pore throats.

One very interesting aspect of this low frequency response of the rock is that the dissipation factor, which is the ratio of electrical energy dissipated to the electrical energy stored per cycle is approximately constant (Figure 4.7). This follows very simply from consideration of the complex impedance plot of this diffusion and polarization process; the signature of this process in the complex impedance plot shows a linear relationship between the real and imaginary parts of the impedance, where the phase angle (δ) remains constant.

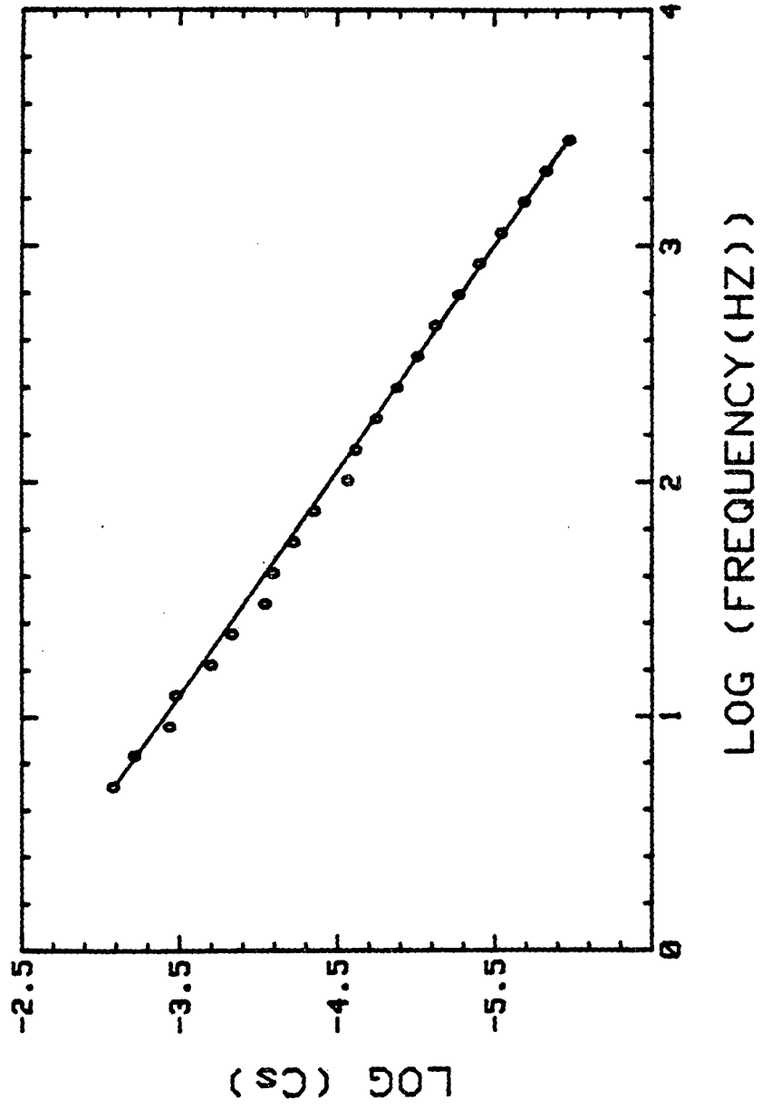

Figure 4.6 The logarithm of the series capacitance versus the logarithm of frequency in the low frequency (less than fo) region for Berea 100, Sw=.30. Cs shows a power law dependence upon frequency.

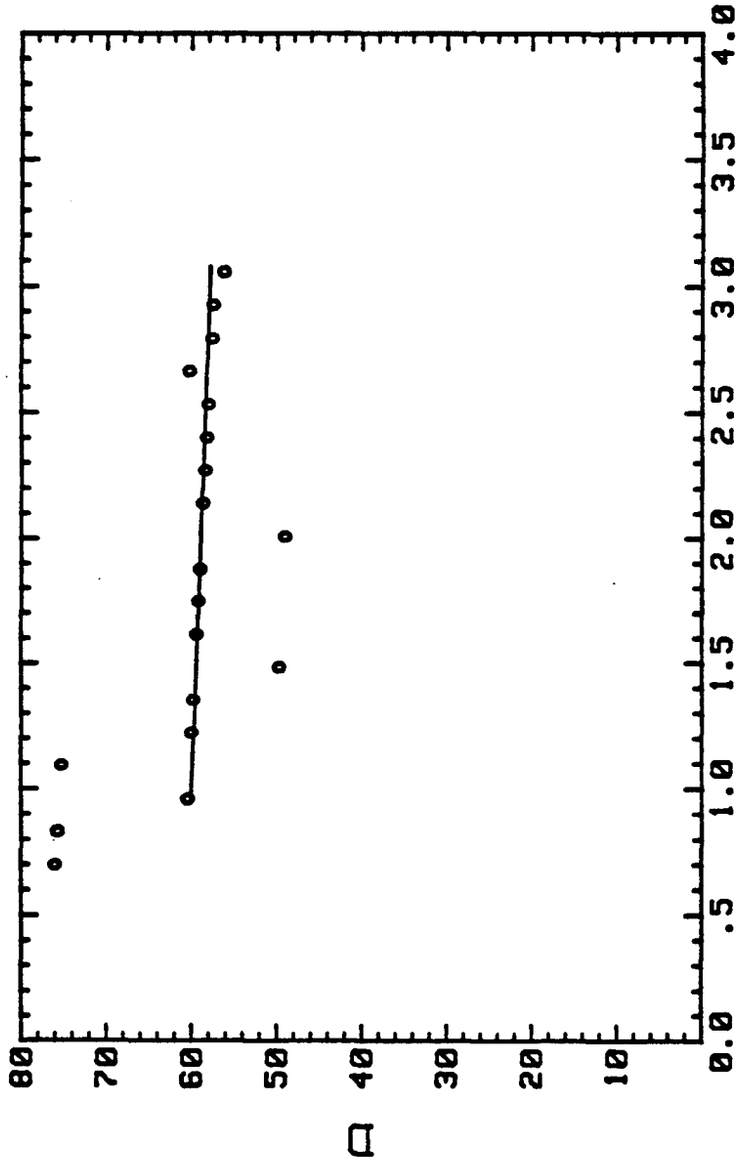

Figure 4.7 The dissipation factor versus the logarithm of frequency in the low frequency (less than fo) region for Berea 100, Sw=.30. D is approximately constant with respect to frequency.

As the dissipation factor is calculated as tan δ or as the real part of the impedance divided by the imaginary part, the dissipation factor for any mechanism that can be represented by a line in the complex impedance plane (except where parallel or perpendicular to the real axis), will be constant with respect to frequency. Scheider (1975) notes that the constant phase was observed by Fricke (1932) and constant D noted by Cole and Cole (1941) and comments: "This fundamental insight may yet turn out to be central to polarization dispersion, but in 30 years since it was pointed out, no one has developed it further." Constant D is found elsewhere in the electrical response of the rocks and will be fully discussed in a later chapter.

Summary

The linear portion of the complex impedance plot is the response dominated by polarization at the sample/electrode interface. It has been shown that electrode polarization effects are restricted to these frequencies, less than f_0, so all data at frequencies above f_0 are the true sample response. This provides a very useful way of recognizing electrode polarization in experimental data; it can be easily separated in the complex impedance plane and f_0, the upper limit of polarization, determined from the complex impedance measurements.

When the polarization at the sample/electrode interface is removed, interfacial polarization within the rock itself can be detected. This polarization shows a power law dependence upon frequency, and a dissipation factor that is constant with respect to frequency.

CHAPTER 5

FREQUENCY DEPENDENCE: REVIEW OF THE DATA

Introduction

A comparison with the complex impedance plot of the Debye circuit indicates an anomalous frequency dependence in the electrical response of rocks. It is informative at this point to review the data and summarize the form of this frequency dependence with respect to sample and fluid properties.

Frequency Dependent Capacitance

It has been shown (Chapter 3) that the Debye circuit acts as a series RC circuit at frequencies less than f_0 and as a parallel RC circuit at frequencies above f_0. In Figure 5.1 is shown the frequency response of both C_p and C_s of the Debye circuit. I have given values to the circuit elements as follows: C_1 = 2.5 x 10^{-11} Farads, C_2= 1 x 10^{-3} Farads, R = 2.7 kilohms. At low frequencies, where the Debye circuit acts as a circuit with C_2 in series with R_2, C_s is a constant value equal to C_2, until a point at which C_s starts to drop. This is not due to a change in the value of C_2, which is fixed, but reflecting the transition from a low frequency response dominated by the C_2-R_2 series circuit to a response dominated by the C_1-R_2 parallel circuit. The frequency at this transition point is equal to f_0. Above f_0, C_p has a constant value equal to C_1. It is obvious from this example that if a sample response can be modelled by a Debye circuit the value of the low frequency capacitance, C_2, can be obtained from the measured C_s at frequencies less than f_0, and the value of the high frequency capacitance, C_2, can be obtained from the measured C_p at frequencies greater than f_0. It is important to note that each capacitance has a constant value, independent of frequency, throughout the frequency range in which it dominates the frequency

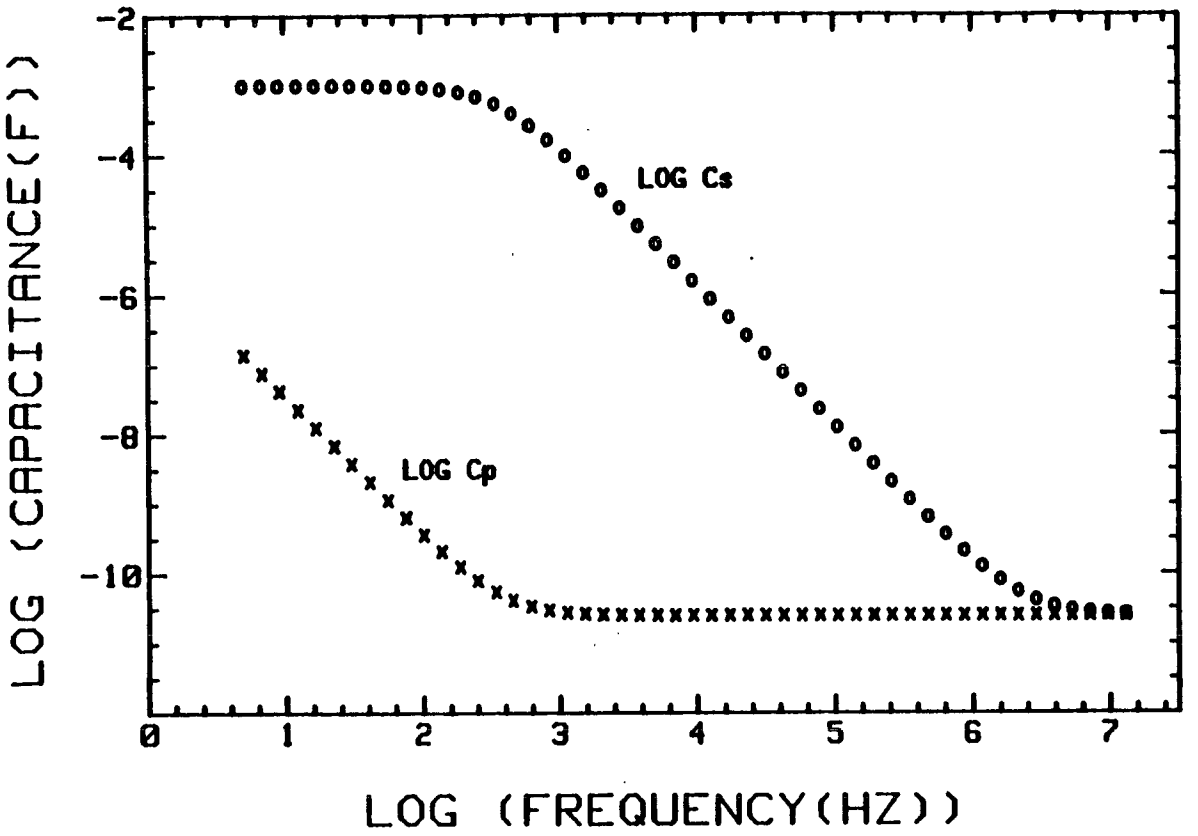

Figure 5.1 The logarithm of capacitance, series and parallel, versus the logarithm of frequency for a Debye circuit with R2 = 2.7 kilohms, C2 = 1 x 10^{-3} Farads, C1 = 2.5 x 10^{-11} Farads.

response.

C_p is the parameter from which the dielectric constant of a material is calculated. For a material exhibiting a Debye response, C_s in the low frequency region is constant but C_p, given by the following expression,

$$C_p = \frac{C_s}{\omega^2 R_s^2 C_s^2 + 1}$$

goes as $1/\ \omega^2$. The dielectric constant, calculated from C_p, has a frequency dependence simply due to the fact that the equivalent circuit for the material contains two capacitors significantly different in value, one of which acts in series with the d.c. resistance of the sample, the other of which acts in parallel.

In Figure 5.2 is shown the frequency dependence of C_p and C_s for a 30 % saturated sample of Berea 100; these data have been corrected for polarization at the sample/electrode interface. The general form of the frequency dependence is very similar to that of a Debye circuit. There is however an anomalous frequency dependence that can be clearly seen in looking at the capacitive response of the rocks compared to that of a Debye circuit. In Figure 5.3 I have shown the frequency dependence of C_p and C_s of a Debye circuit and that of the 30% saturated sample of Berea Sandstone. The low frequency capacitance measured in the rock (C_s) corresponds to the low frequency capacitance in the Debye circuit, C_2, and C_p measured at high frequency in the rock corresponds to the high frequency capacitance, C_1, in the Debye circuit. Yet it is obvious from Figure 5.3 that the capacitance in a rock sample shows a frequency dependence that is totally lacking in the Debye circuit. In the low frequency region, C_s is not constant, but shows a power law dependence upon frequency; in the high frequency region, C_p is not constant, but shows a power law dependence upon frequency.

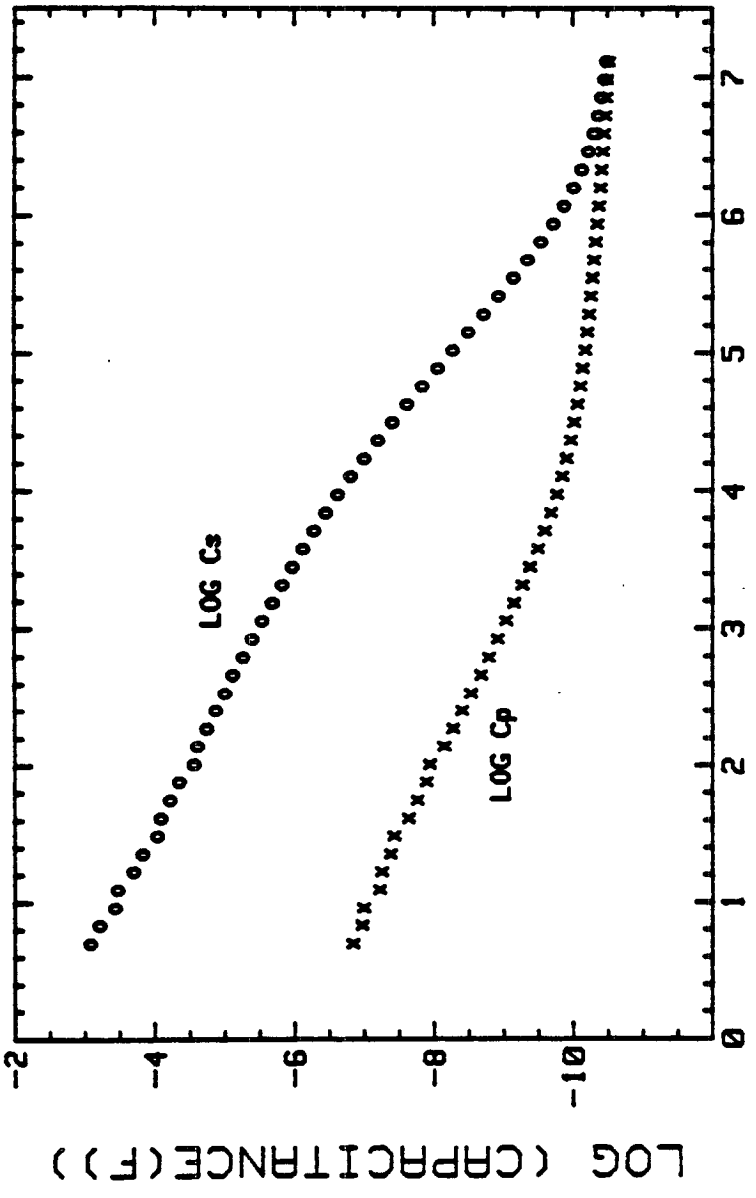

Figure 5.2 The logarithm of capacitance, series and parallel, versus the logarithm of frequency for Berea 100, Sw=.30.

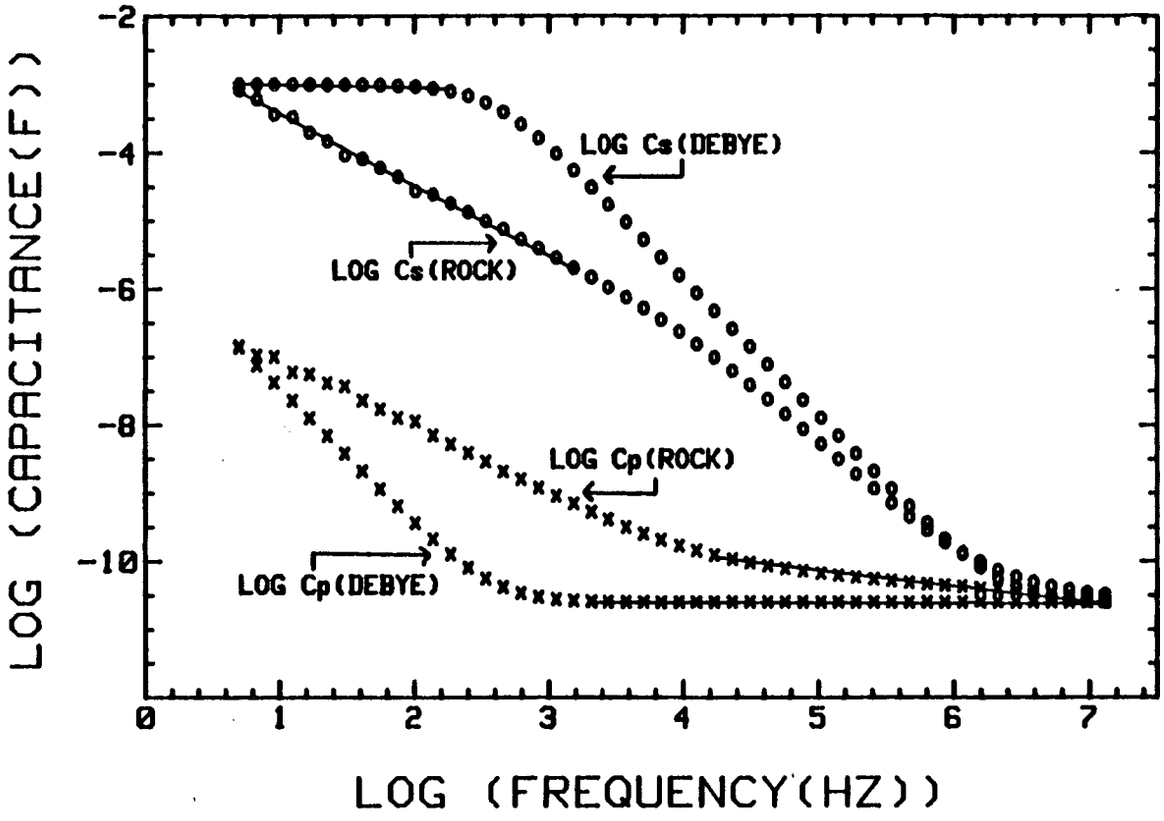

Figure 5.3 The logarithm of capacitance, series and parallel, of the Debye circuit and Berea 100, Sw=.30, versus the logarithm of frequency. At low frequency, where Cs of the Debye circuit is constant with respect to frequency, Cs of Berea 100 shows a power law dependence upon frequency. At high frequency, where Cp of the Debye circuit is constant, Cp of Berea shows a power law dependence.

It has been shown that at low frequencies C_s is a measure of the capacitance of the system and at high frequencies C_p is a measure of the capacitance. Thus the purely capacitive element of the rock sample shows the trend with frequency as shown in Figure 5.4 - equal to C_s up to f_0 and then dropping rapidly to become equal to C_p at high frequencies. It can be seen that the capacitance C_2 is approximately approximately equal to 10^{-9} Farads and the capacitance C_1 is approximately equal to 10^{-11} Farads. The assumption that $C_2 >> C_1$ is obviously true. This is the capacitance in the rock. The dielectric constant however, cannot be considered as the capacitance in the rock for all frequencies; the dielectric constant is calculated from C_p, the frequency dependence of which will now be examined more closely.

Figure 5.5 is a plot of log Cp versus log frequency for a 30% saturated sample of Berea Sandstone across the frequency range of 5 Hz to 13 MHz, the data having been corrected for the electrode polarization. There are clearly two linear regions in the plot, each of which can be described by a power law dependence of the capacitance upon frequency:

$$C_p = A\omega^{-\alpha}$$

where α is always greater in the low frequency ($<f_0$) than in the high frequency ($>f_0$) region. A power law dependence in these two frequency regions was found for all samples at all levels of saturation.

In Figure 5.6 is plotted log C_p versus log frequency for Berea 100 in the high frequency region for S_w=.90 to 0. There is obviously a dependence on S_w, the topic of a later chapter, but of greatest importance here is the consistent power law dependence with a systematic variation of the power law exponent, α, with saturation. α as a function of saturation is given in Figure 5.7. As the saturation decreases, α increases until some critical saturation at low saturations where α drops rapidly. This same relationship is found for all seven samples for which

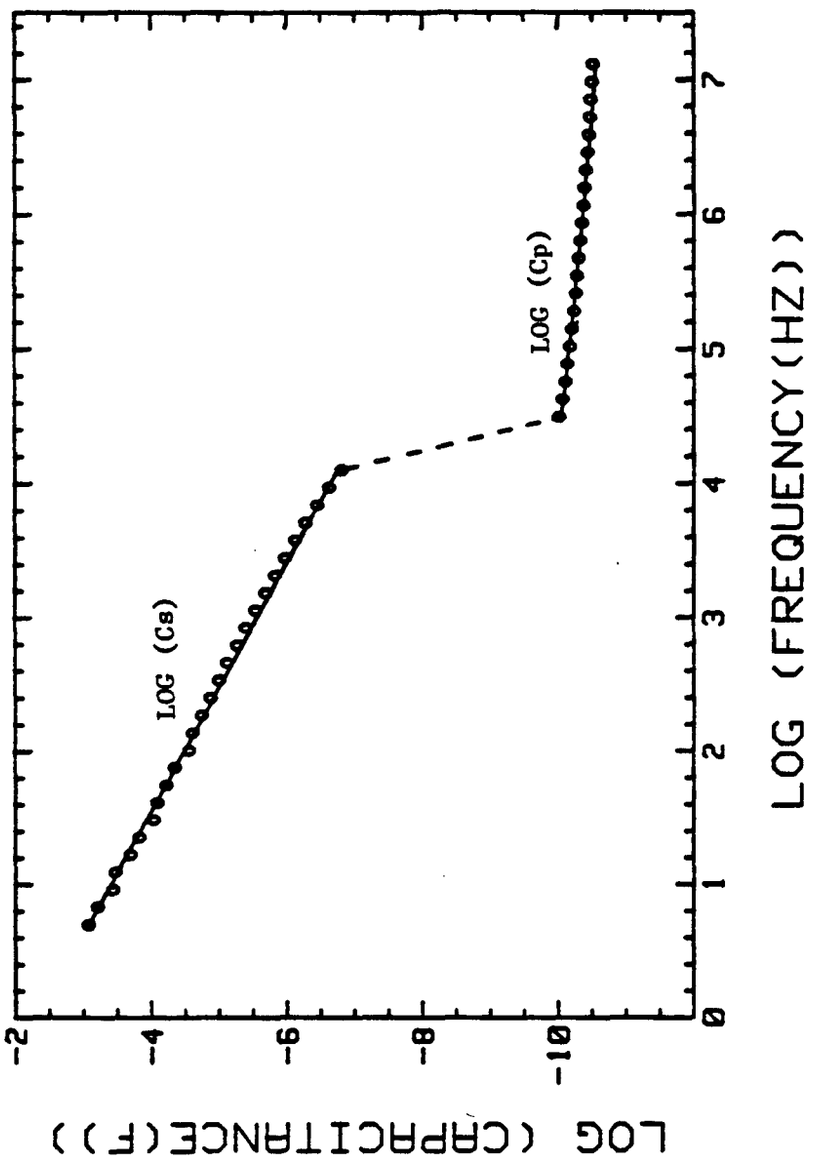

Figure 5.4 The logarithm of the capacitance of Berea 100, Sw=.30, as a function of frequency. Cs is a measure of the capacitance at frequencies less than fo; Cp is a measure of the capacitance at frequencies greater than fo.

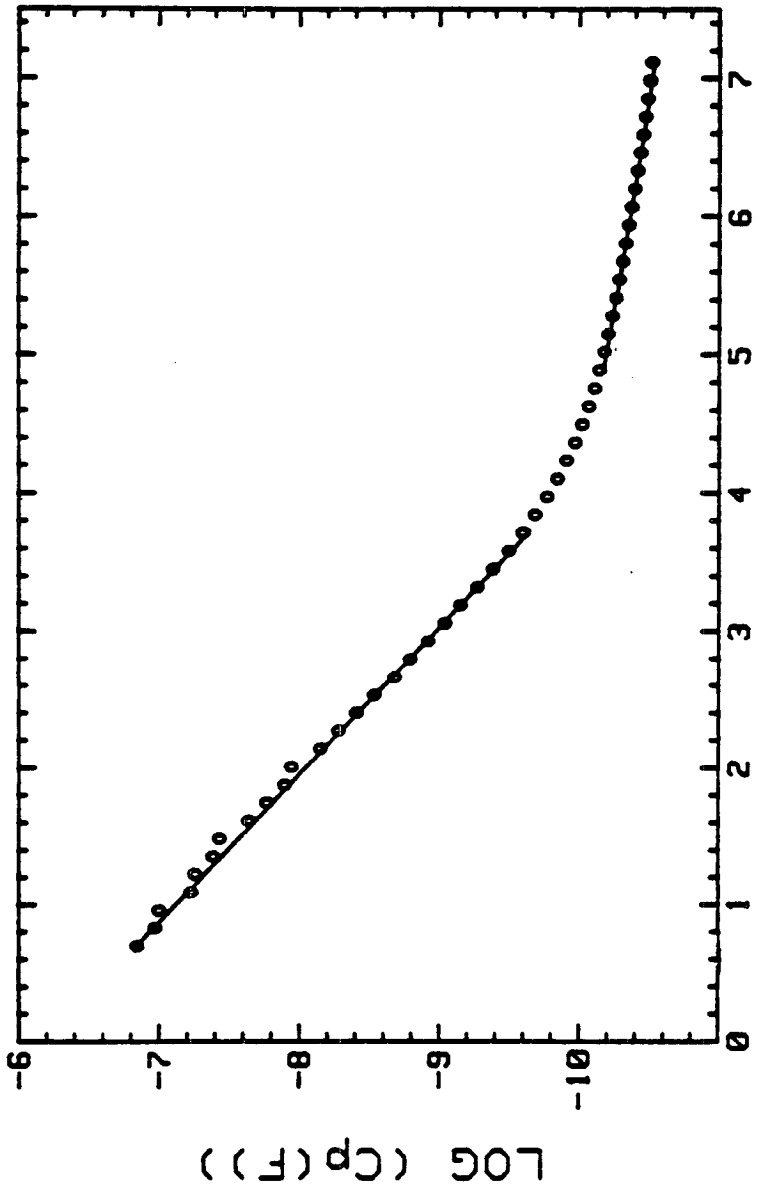

Figure 5.5 The logarithm of the parallel capacitance of Berea 100, Sw=.30, versus the logarithm of frequency. Note the power law dependence upon frequency in both the low frequency and high frequency regions.

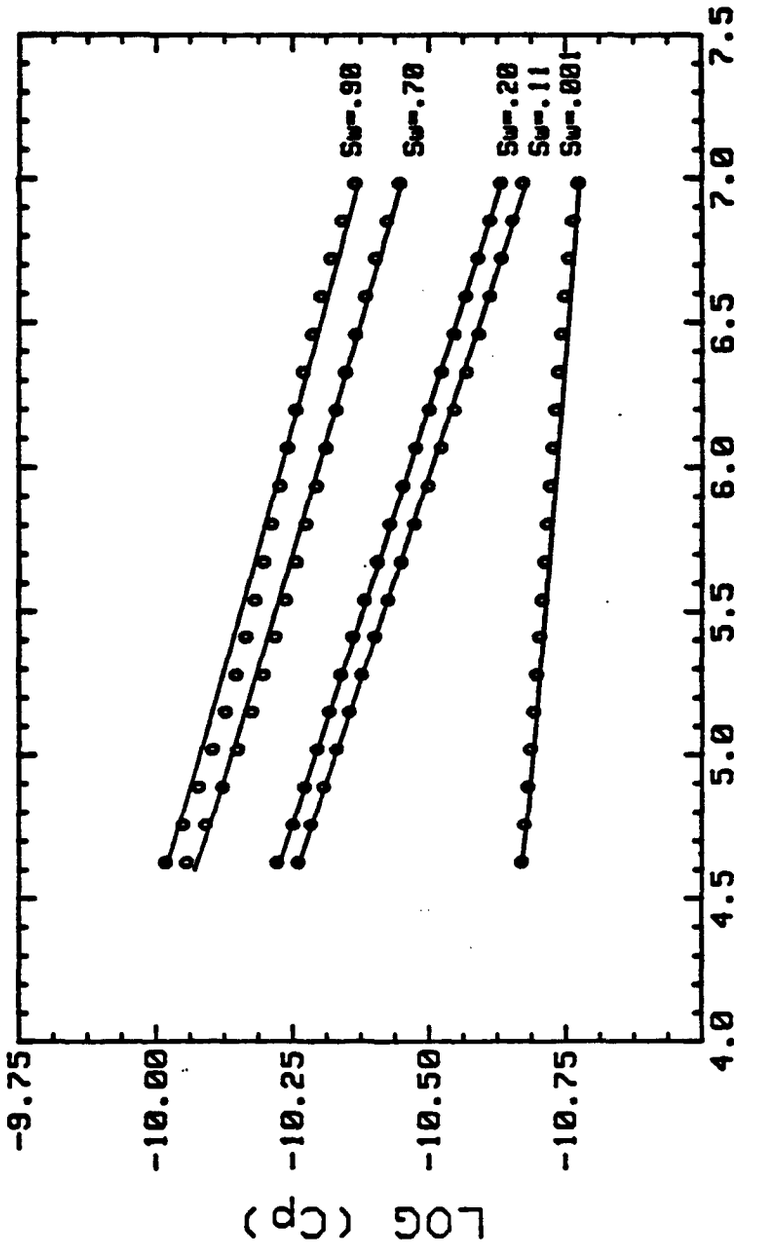

Figure 5.6 The logarithm of parallel capacitance versus the logarithm of frequency for Berea 100 at various levels of saturation.

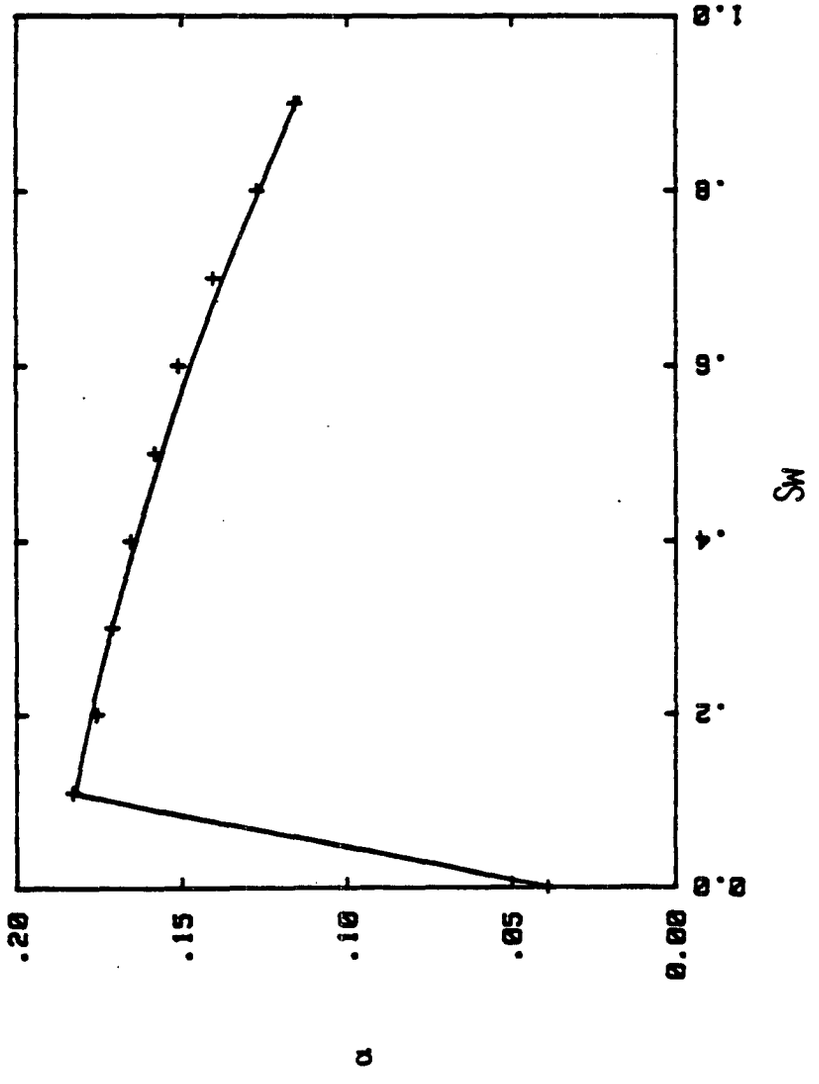

Figure 5.7 The negative power law exponent (α) as a function of saturation for Berea 100.

measurements were made as a continuous function of saturation. The frequency dependence is systematically affected by the changing saturation (Figure 5.8).

When the salinity of the pore fluid is changed, C_p still shows a power law dependence upon frequency. Data for CH66-79 for Sw=0.36 with pore fluid salinity varying from from 0.005 M NaCl to 0.2 M NaCl are shown in Figure 5.9. Here there is a general increase in α with salinity. This eliminates the possibility that α depends on the resistivity of the system as the trend with changing resistivity for varying salinity is opposite to that found with changing resistivity for varying Sw.

Frequency Dependent Resistance

At low frequencies, when the sample responds more like a series RC circuit, C_p and thus the dielectric constant contains a contribution from the resistance. It is therefore important to examine the frequency dependence in the resistance, both in the series and the parallel mode.

First considering the parallel mode, in Figure 5.10 is shown the response for the Debye circuit. R_p is constant with respect to frequency. In Figure 5.11 are the data for Berea 100 at various levels of saturation. R_p is essentially independent of frequency up to some frequency at which point there is a rapid decrease. As the sample becomes drier, this frequency dependence extends to lower frequencies.

In the series mode, R_s of the Debye circuit varies with frequency as shown in Figure 5.12. R_s as a function of frequency for Berea 100, Sw=.30, is plotted in Figure 5.13. As for the Debye circuit, R_s is essentially independent of frequency up to a point and then drops rapidly.

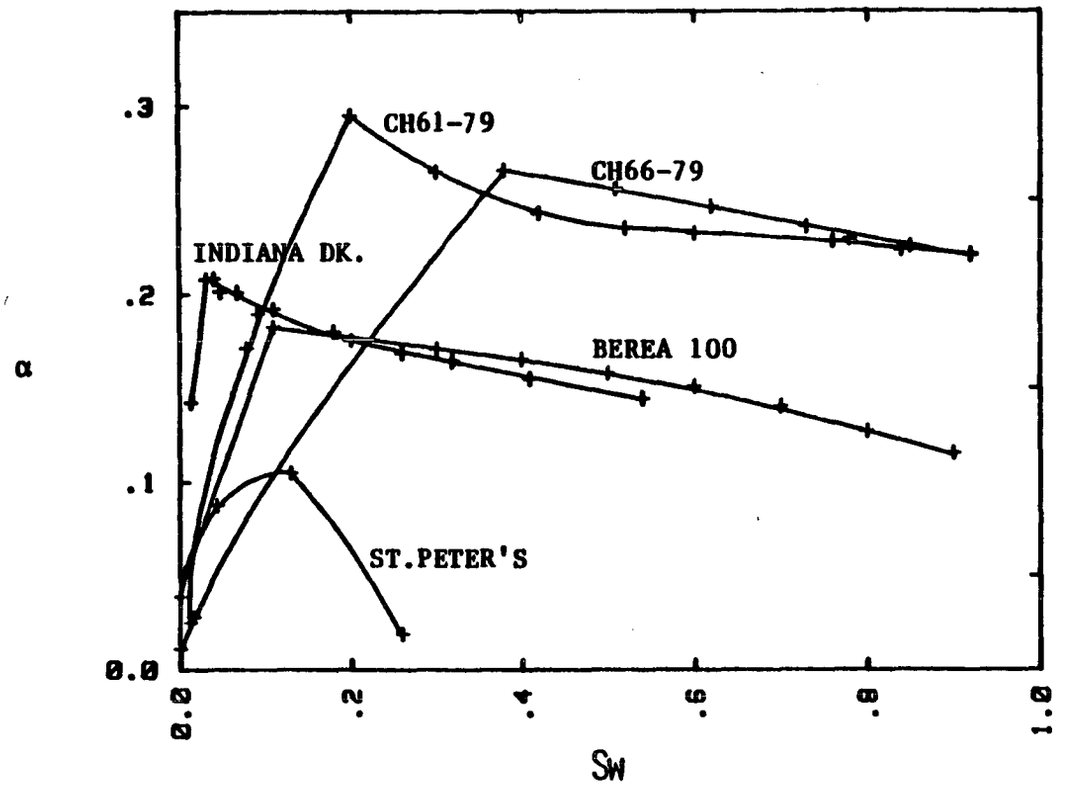

Figure 5.8 The negative power law exponent (α) as a function of saturation for five different sandstones.

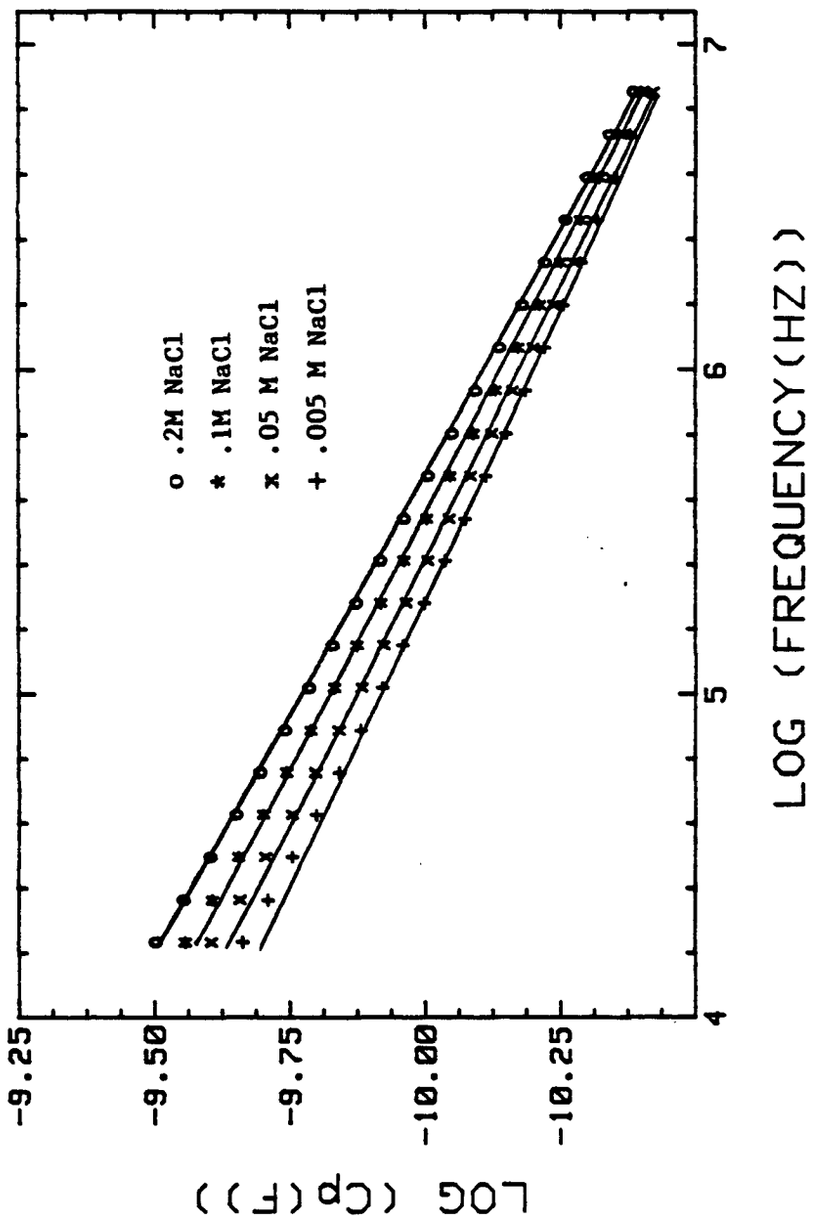

Figure 5.9 The logarithm of parallel capacitance versus the logarithm of frequency for Ch66-79, 36% saturated with pore fluids of various salinities.

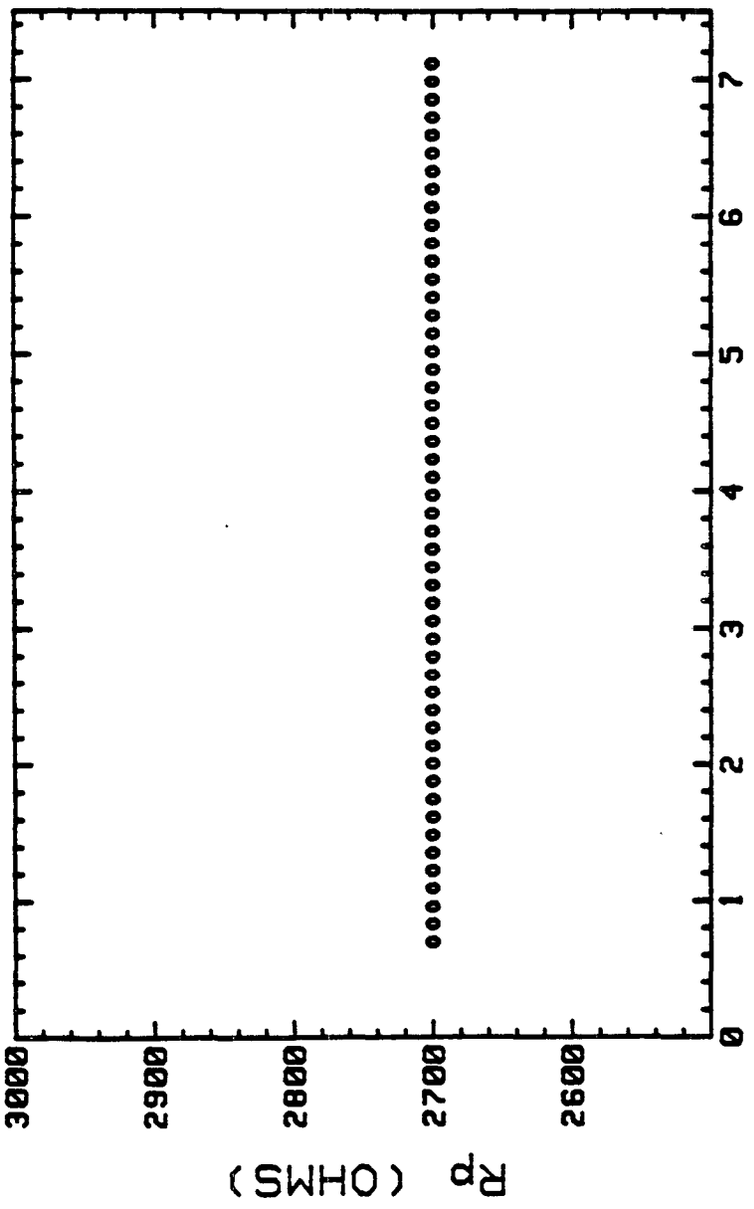

Figure 5.10 The parallel resistance versus the logarithm of frequency for the Debye circuit with R2 = 2.7 kilohms, C2 = 1 x 10^{-3} Farads, C1 = 2.5 x 10^{-11} Farads.

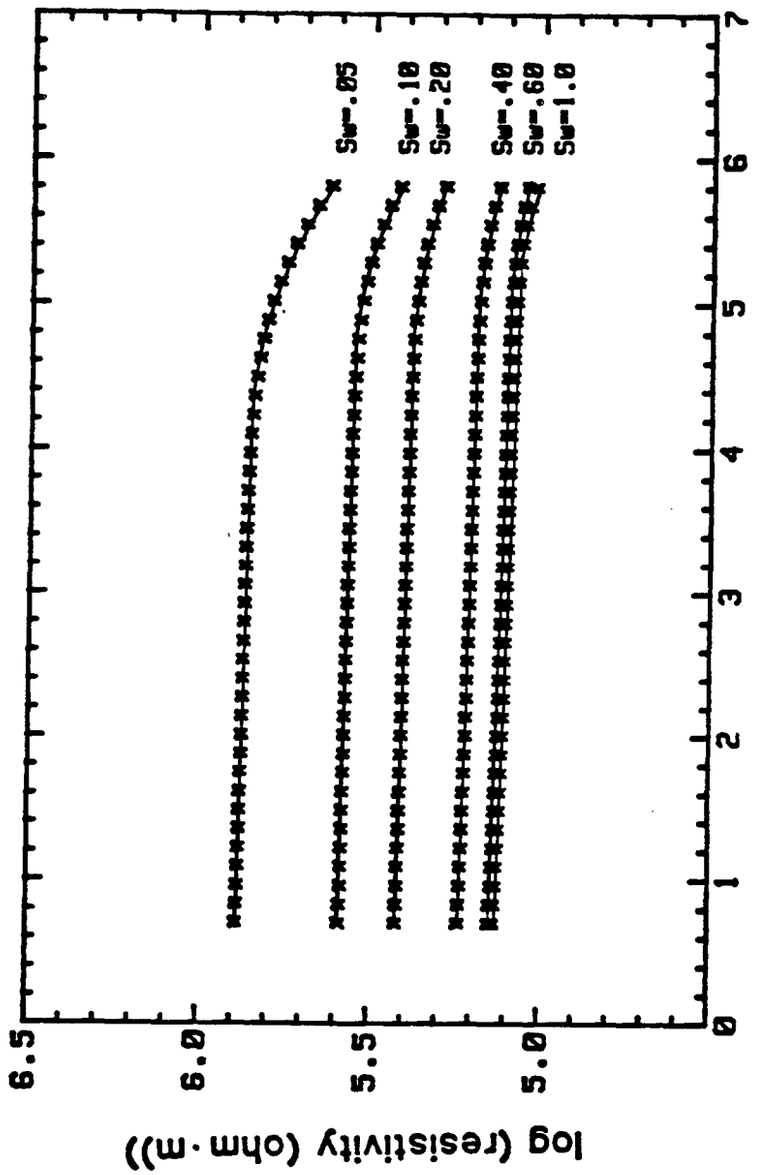

Figure 5.11 The logarithm of resistivity versus the logarithm of frequency for Berea 100 at various levels of saturation.

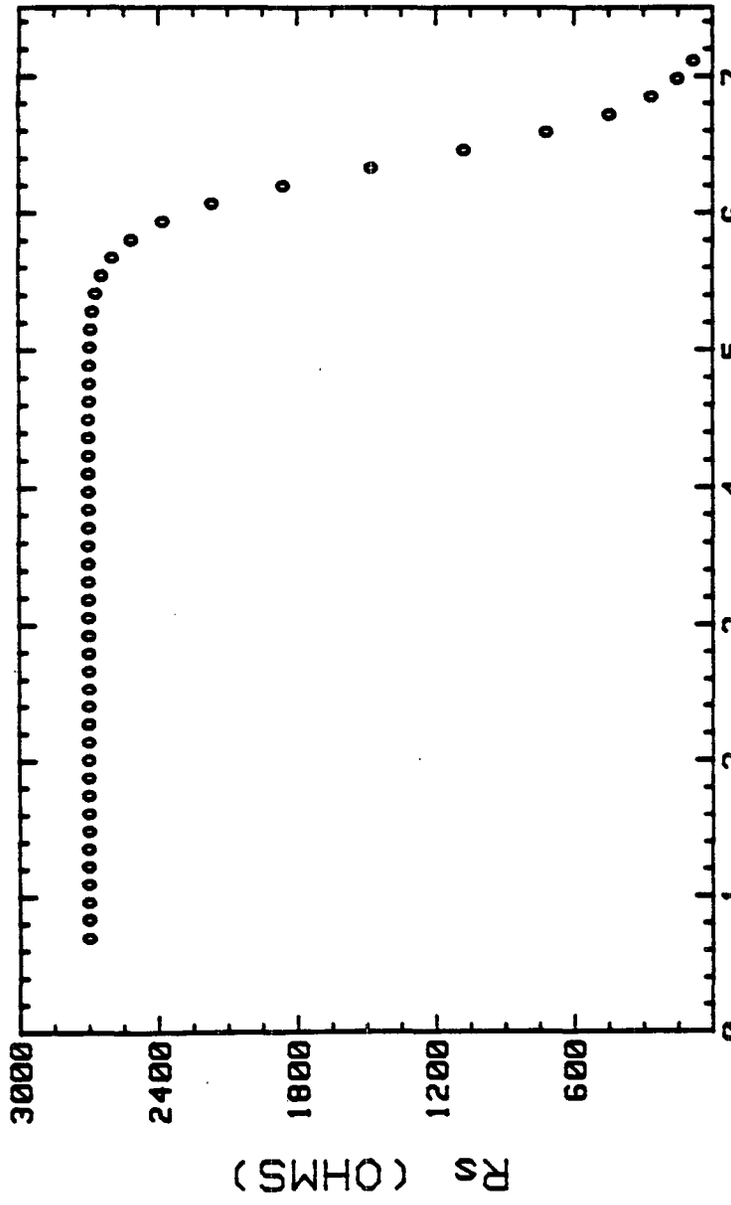

Figure 5.12 The series resistance versus the logarithm of frequency for the Debye circuit with R2 = 2.7 kilohms, C2 = 1×10^{-3}, C2 = 2.5×10^{-11} Farads.

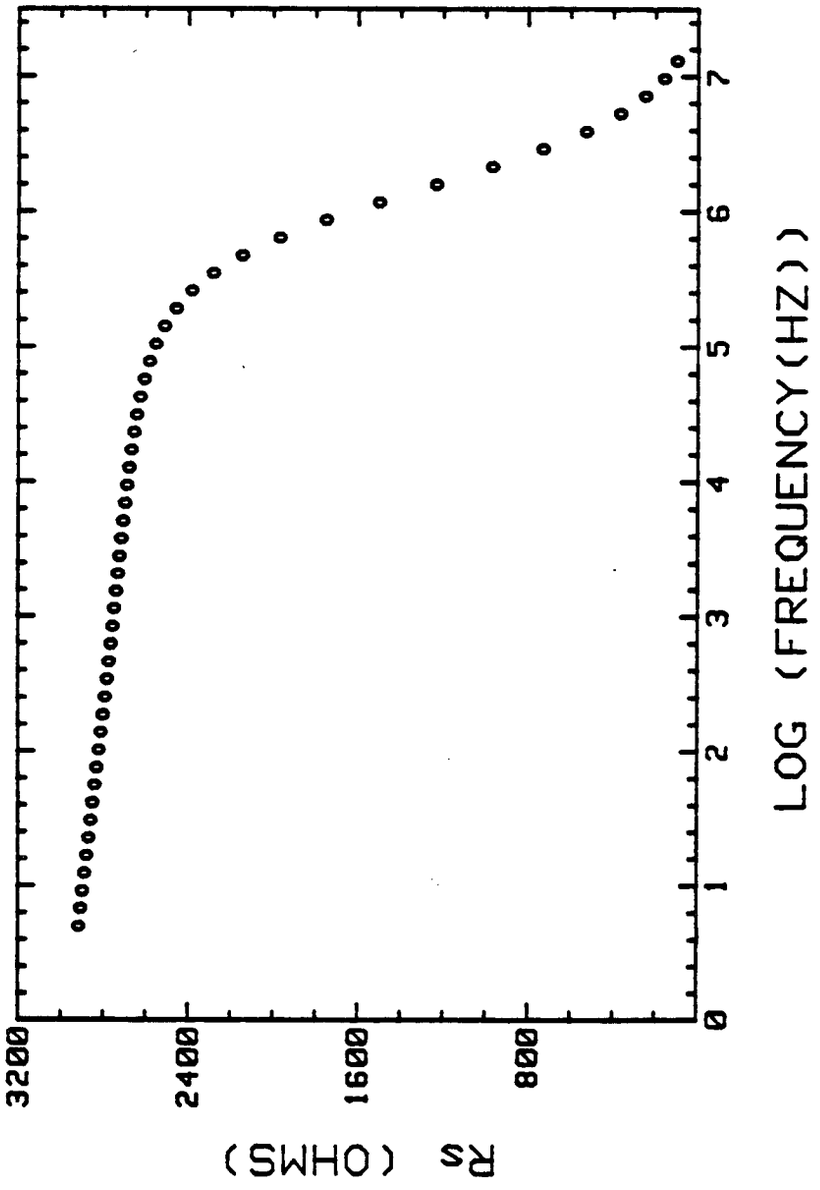

Figure 5.13 The series resistance versus the logarithm of frequency for Berea 100, Sw=.30.

Frequency Dependent Reactance

$-X_s$ for the Debye circuit is plotted in Figure 5.14 as a function of frequency. $-X_s$ for Berea 100, S_w =.90 and S_w =.11, is plotted in Figure 5.15. These data have not been corrected for polarization at the sample/electrode interface, so only the data in the high frequency region will be considered. $-X_s$ peaks at the characteristic relaxation frequency for the high frequency response. The relaxation frequency for an RC circuit is equal to $(RC)^{-1}$. The relaxation frequency for the high frequency response is thus equal to $(R_2C_1)^{-1}$ and accordingly varies with sample, saturation, and salinity of pore fluid as R_2 and C_1 vary. An example of these changes is shown in Figure 5.15. The relaxation frequency was always found to increase with increasing level of water saturation and/or increasing salinity.

The relaxation frequency for the low frequency response is equal to $(R_2C_2)^{-1}$. This relaxation frequency , because the sample response at those frequencies is most like a series RC circuit, would correspond to a peak in B_p. Given that R_2 is approximately 10^3 and C_2 is approximately 10^{-3} the relaxation frequency for the low frequency response is approximately 10 Hz. As most of the data in the low frequency region are affected by the electrode polarization, there are insufficient data to see this peak.

Dissipation Factor

The dissipation factor, the ratio between the loss and storage or between the in phase and quadrature components, can be calculated from either R_s / X_s or G_p / B_p. D as a function of frequency for the Debye circuit is given in Figure 5.16. Maximum D occurs at f_0. This is predictable through consideration of the complex impedance plot: In the linear portion as -X decreases , R is constant producing increasing D. Above f_0, R constantly decreases while -X increases then decreases, producing a decreasing D with an inflection point at the

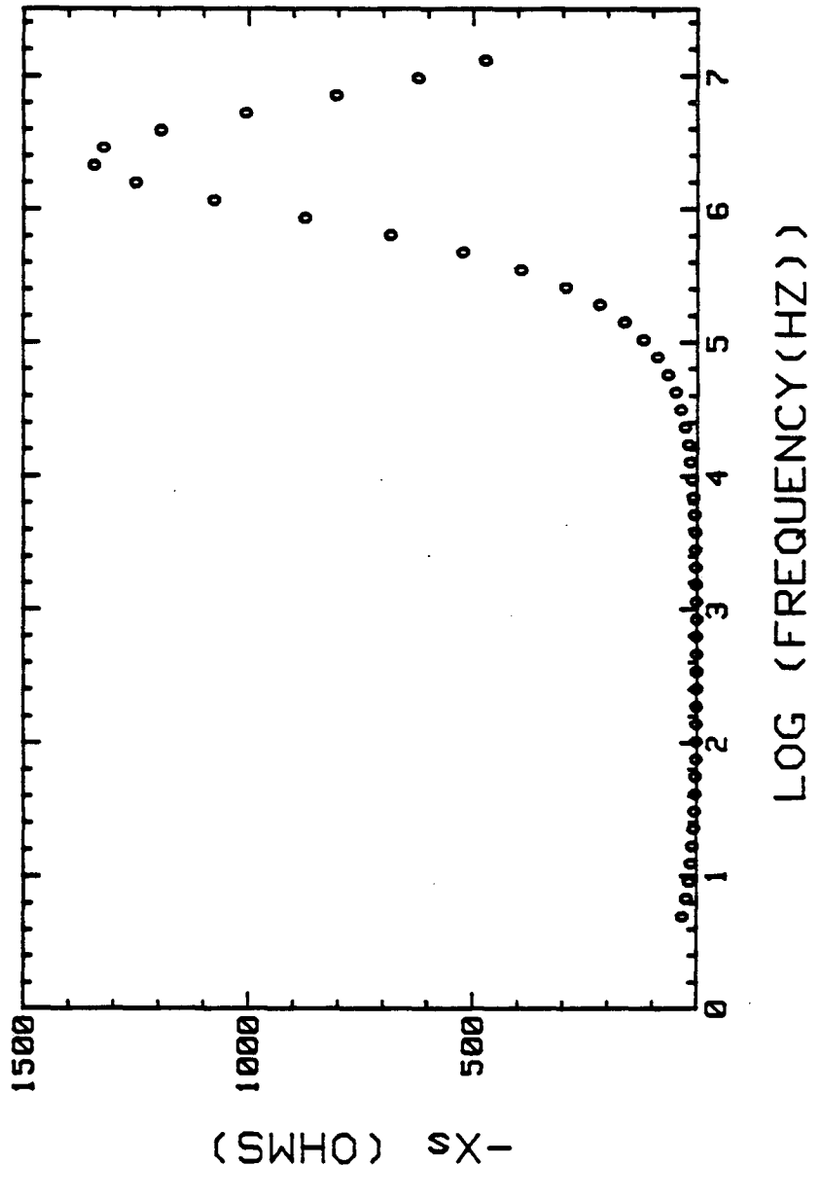

Figure 5.14 The reactance versus the logarithm of frequency for the Debye circuit with R2 = 2.7 kilohms, C2 = 1 x 10^{-3} Farads, C1 = 2.5 x 10^{-11} Farads.

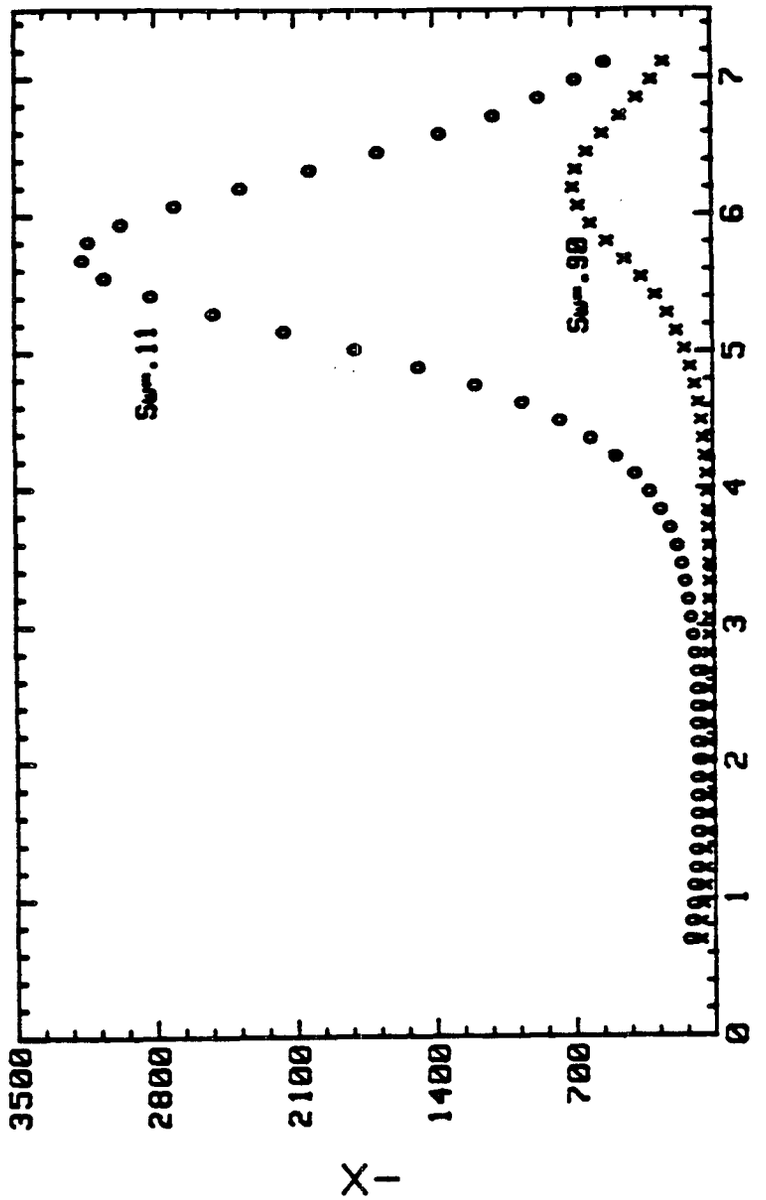

Figure 5.15 The reactance versus the logarithm of frequency for Berea 100, Sw=.11 and Sw=.90. Increasing saturation shifts the reactance peak to higher frequencies.

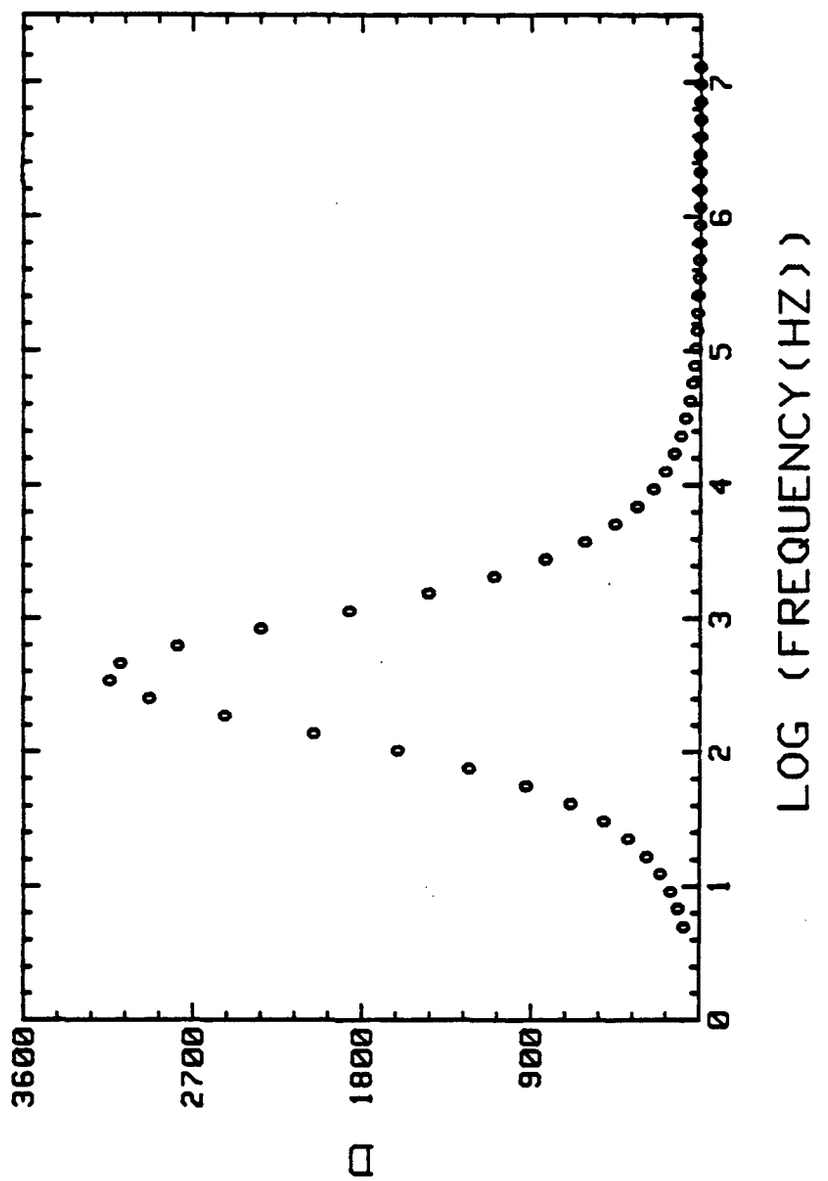

Figure 5.16 The dissipation factor versus the logarithm of frequency for the Debye circuit with R2 = 2.7 kilohms, C2 = 1 x 10^{-3} Farads, C1 = 2.5 x 10^{-11} Farads.

frequency corresponding to maximum -X. This results in a peak in D at f_0.

It has been stated that $\omega_0 = (R_1^2 C_1 C_2)^{-\frac{1}{2}}$ (Chapter 3). Substituting

$$\tau_{LF} = R_2 C_2$$
$$\tau_{HF} = R_2 C_1$$

where τ_{LF} is the relaxation time for the low frequency response and τ_{HF} is the relaxation time for the high frequency response, into the expression for ω_0 yields:

$$\omega_0 = (\tau_{LF}\tau_{HF})^{-\frac{1}{2}}$$

Whereas the peak in $-X_s$ reflects only the the relaxation time of the high frequency response, giving no information about the low frequency or total response, the peak in D is very indicative of the total electrical response, the position of the peak depending upon the values of all the circuit elements.

A plot of D as a function of frequency for Berea 100, Sw=.30, is given in Figure 5.17. In this example the low frequency polarization response has been corrected for polarization at the sample/electrode interface. The low frequency response has the characteristic constant D. At frequencies above f_0, D decreases with frequency. Decreasing D corresponds to the semicircular response in the complex plane plot. It is important to note that the frequency at maximum D does not correspond to the characteristic relaxation frequency, the frequency at maximum $-X_s$; this is due to the dispersion in the real part of the impedance (R_s). Thus while the relaxation frequency in saturated rocks is usually on the order of 10^6 Hz, the maximum dissipation frequency is usually on the order of 10^4 Hz. Maximum D may be analogous to the maximum in seismic Q in the same range; the characteristic frequency of the mechanism however is much higher and the two should not be confused.

When polarization at the sample/electrode interface is not removed a very interesting and misleading plot of D as a function of frequency is obtained

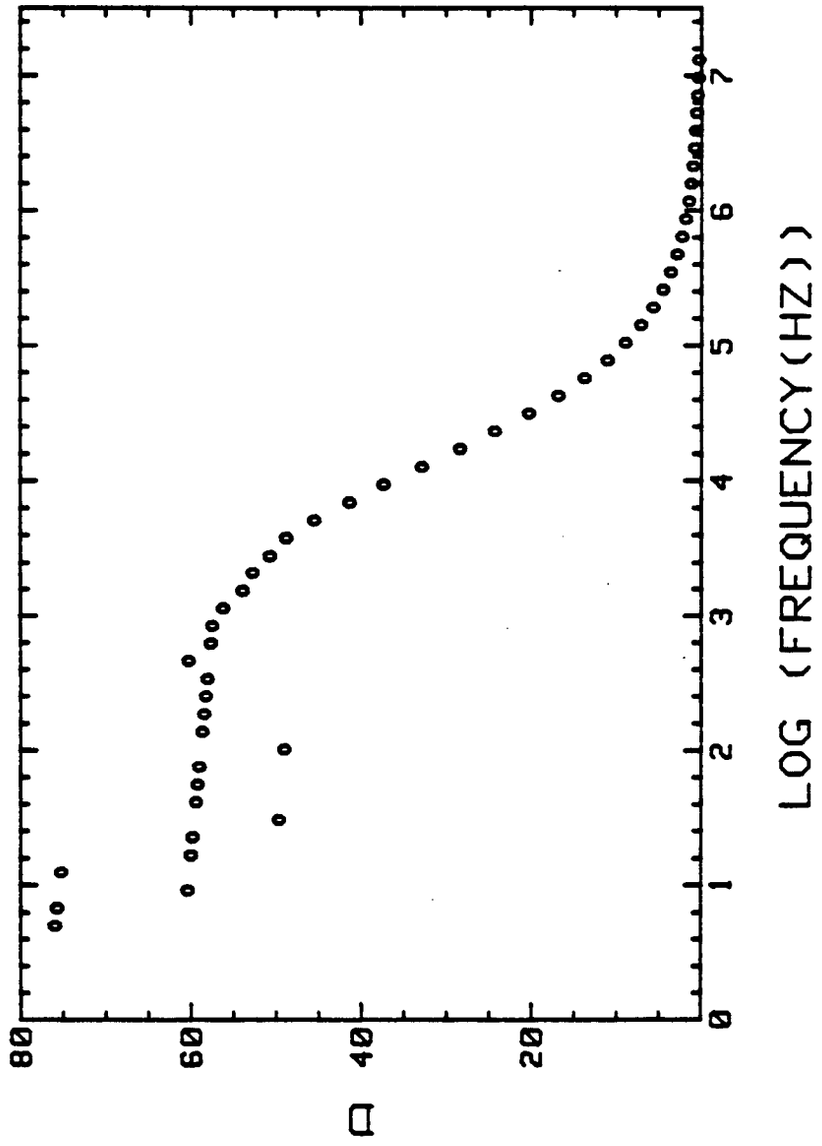

Figure 5.17 The dissipation factor versus the logarithm of frequency for Berea 100, Sw=.30.

(Figure 5.18). What appears is an apparent peak in D. This peak however is not reflective of the sample response but rather an artifact of the electrode polarization response. The only form of complex impedance plot that corresponds to increasing D is either a vertical line, which corresponds to an series RC circuit, or a line with a negative second derivative. This is the actual form of the polarization response in the complex plane - it appears linear but actually shows convex curvature which is evident when D is displayed. Not much significance should be attached to this peak in D therefore in terms of sample properties; it is an interesting feature of the polarization and deserves further study.

Dielectric Dissipation Factor

As discussed in Chapter 1 it is theoretically possible to obtain the dielectric dissipation peak by subtracting the d.c. conductance from the imaginary part of the dielectric constant. In order to do this successfully, very accurate measurements are needed at low frequencies that do not contain any effects of polarization. A dielectric dissipation peak has been separated in one data set (Figure 5.19). There is a maximum in the dissipation at 10 kHz. The imaginary part of the dielectric constant shows two slight inflection points, but not a loss peak. It is very difficult to study dielectric loss in the presence of ionic conductivity and while the d.c. ionic conduction has been subtracted, it was not possible to remove the a.c. ionic conduction. It is very possible that this masks the dielectric loss peak.

Summary

The use of equivalent electrical circuits has proven to be very useful in obtaining a general understanding of the total electrical response. There are three main circuit components, an interfacial capacitance, the d.c. resistance,

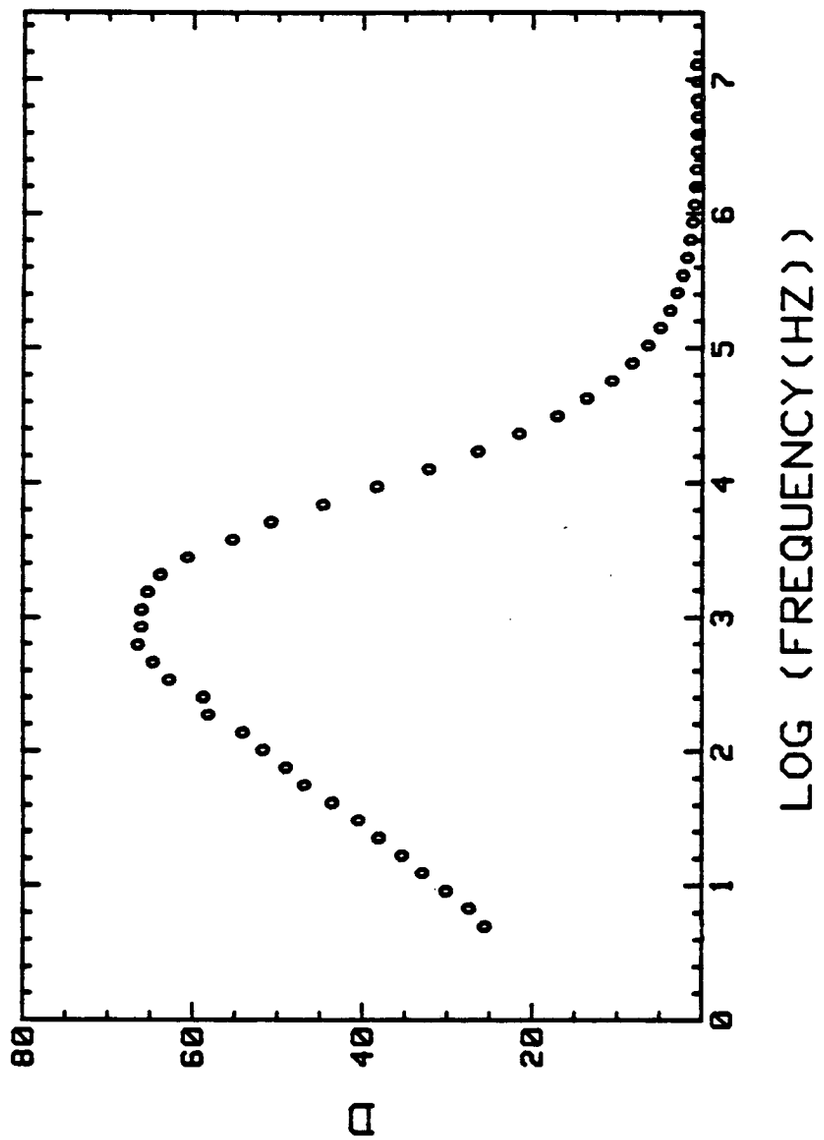

Figure 5.18 The dissipation factor versus the logarithm of frequency for Berea 100, Sw=1.0. The data are uncorrected for the polarization at the sample/electrode interface; this produces an apparent peak in D.

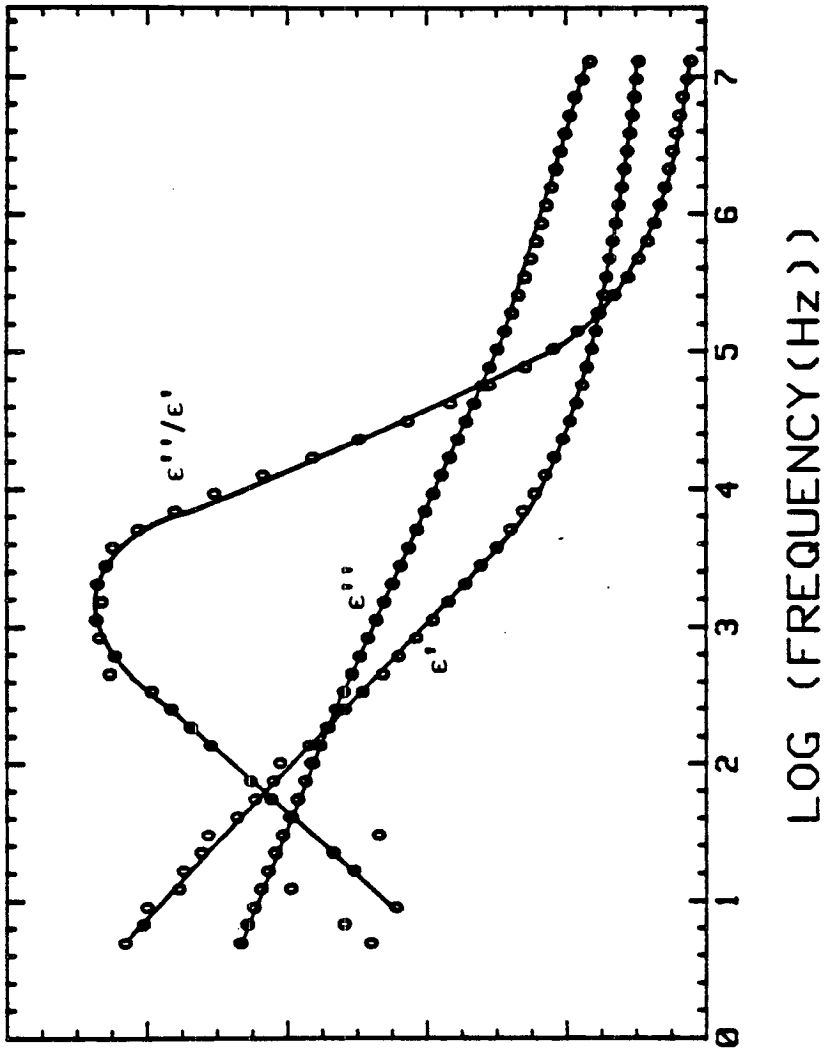

Figure 5.19 The dielectric dissipation factor ($\varepsilon''/\varepsilon'$), the imaginary part of the dielectric constant (ε''), and the real part of the dielectric constant (ε') versus the logarithm of frequency.

and a high frequency capacitance. The frequency response is very similar to that of a Debye circuit given that $C_2 >> C_1$. Maximum D occurs at the change over from a low frequency series circuit response to a high frequency parallel circuit response, the frequency at this point, f_0, being a function of sample properties; D is thus characteristic of the total sample response.

Superimposed on the Debye-like response of the rock samples is an anomalous frequency dependence. It is necessary to determine an exact equivalent circuit so that it is possible to model and interpret this frequency dependence.

CHAPTER 6

MODELLING WITH AN EQUIVALENT ELECTRICAL CIRCUIT

Introduction

There are many interacting processes occurring in rocks containing pore fluids that influence the measured electrical properties. In order to understand the basic mechanisms involved, it is necessary to unravel the total electrical response and separate the various contributions to the response. One approach to this problem is to determine the equivalent electrical circuit that can best model the electrical response and then relate the various circuit elements to specific properties or processes in the rock.

Defining an Equivalent Electrical Circuit

The total frequency response of any rock sample can be modelled as a first approximation with a Debye circuit. The Debye circuit can be re-arranged to give an equivalent circuit more readily relatable to our system (Figure 6.1). The sample response is modelled by the parallel RC circuit and the polarization at the sample/electrode interface by the capacitor in series. The values of the resistor and capacitors in this circuit are the same as those of the resistor and capacitors with corresponding subscripts in the Debye circuit shown in Figure 3.3. This equivalence holds as long as $C_2 >> C_1$; this is true for this study.

The circuit in Figure 6.1 was proposed by Scott et al. (1967) as a model for the electrical response of moist rocks with associated electrode polarization, and by Raistrick et al. (1976) to approximately model the electrical response of solid electrolytes. Arulanandan and Mitchell (1968) proposed a similar circuit to model the dielectric response of saturated kaolanite clay-water-electrolyte systems, replacing the series capacitor with an impedance to represent the

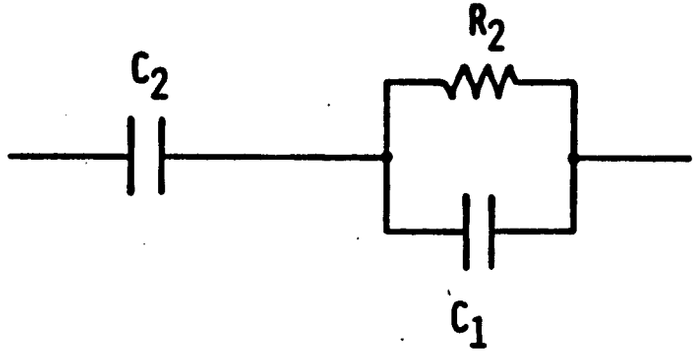

Figure 6.1 A re-arranged Debye circuit. C2 represents the polarization at the sample/electrode interface; the parallel R2-C1 circuit represents the sample.

electrode polarization. The non-ideal behavior of rock samples however, requires a more complex circuit to accommodate the anomalous frequency response. Recent attempts at modelling this non-ideal behavior of solids (Jonscher, 1975; Raistrick et al., 1976) show that a frequency dependent term of the power law type can produce the observed frequency response. Such a frequency dependent term is required in the modelling of both the interface and the sample response.

I have chosen to model the frequency response of rocks with the equivalent circuit shown in Figure 6.2, proposed by Raistrick et al. (1976). This equivalent circuit contains two frequency dependent terms in the form of diffusional admittances both of which have real and imaginary parts with power law dependence; Y_I^*, representing the interface or low frequency response, replaces the frequency independent series capacitance in Figure 6.1; Y_B^*, part of the bulk or high frequency sample response, is placed in parallel with the d.c. resistance (R_B) and high frequency capacitance (C_∞) of the system.

As most of the data have not been corrected for polarization at the sample/electrode interface I will restrict the modelling to those data at frequencies above f_0 thereby reducing the equivalent circuit to that shown in Figure 6.3, proposed by Raistrick et al. (1976) to model the high frequency response of solid electrolytes. If the contributions of R_B and C_∞ can be "subtracted" from the frequency response of the sample, an expression can be obtained for Y_B^*. It is useful to follow through the analysis of Raistrick et al. (1976) to see how the mathematical expression for Y_B can be obtained from the sample response:

Subtacting $1/R_B$ from G_p and plotting log $(G_p - 1/R_B)$ versus log frequency produces a fairly straight line with slope β (Figure 6.4). Therefore

$$G_p = \frac{1}{R_B} + A\omega^\beta$$

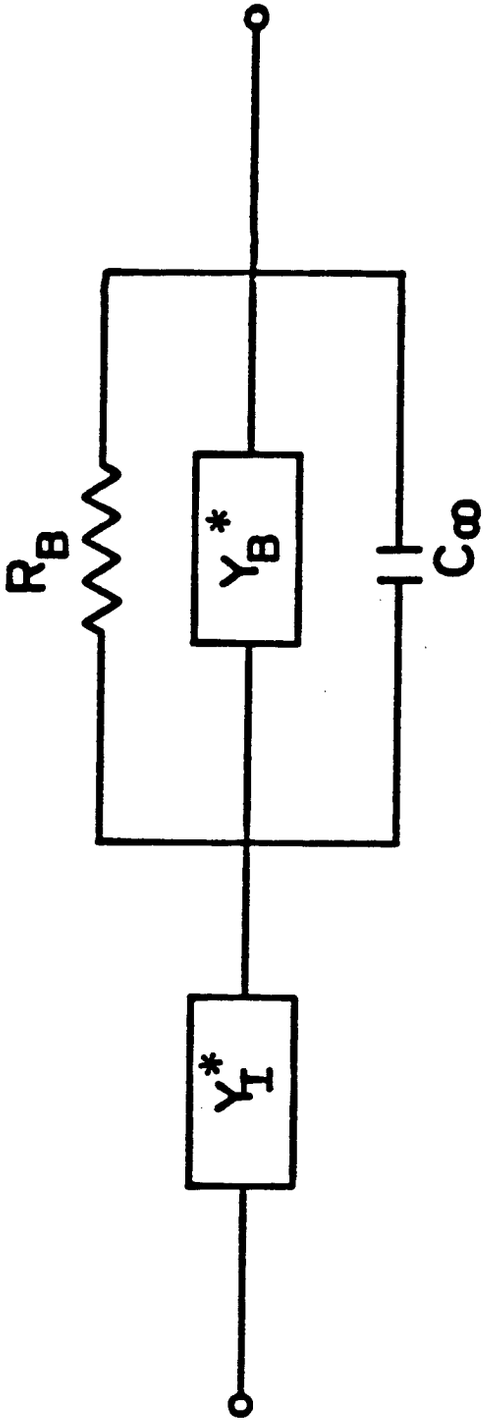

Figure 6.2 Equivalent electrical circuit (from Raistrick et al., 1976).

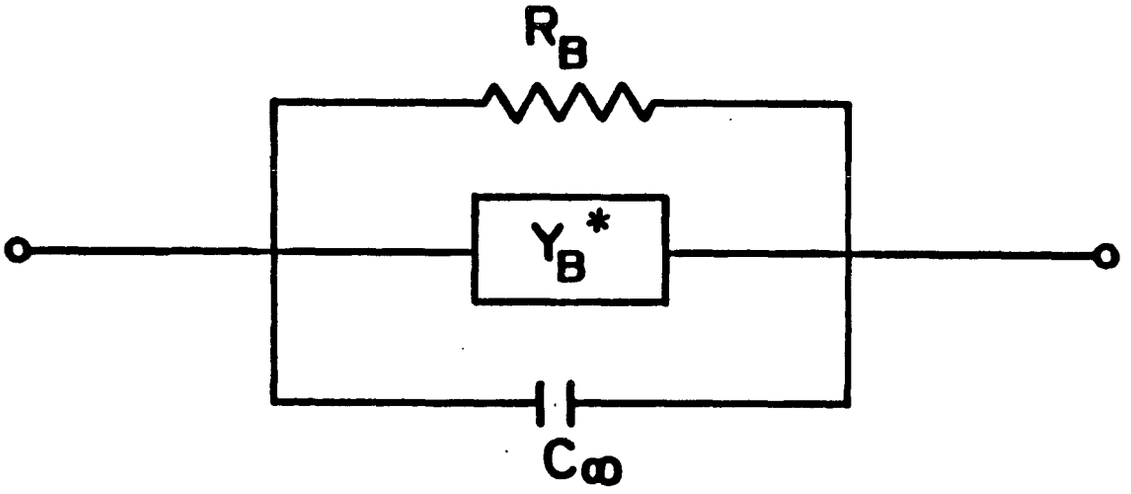

Figure 6.3 Equivalent electrical circuit for modelling the high frequency response. (from Raistrick et al., 1976)

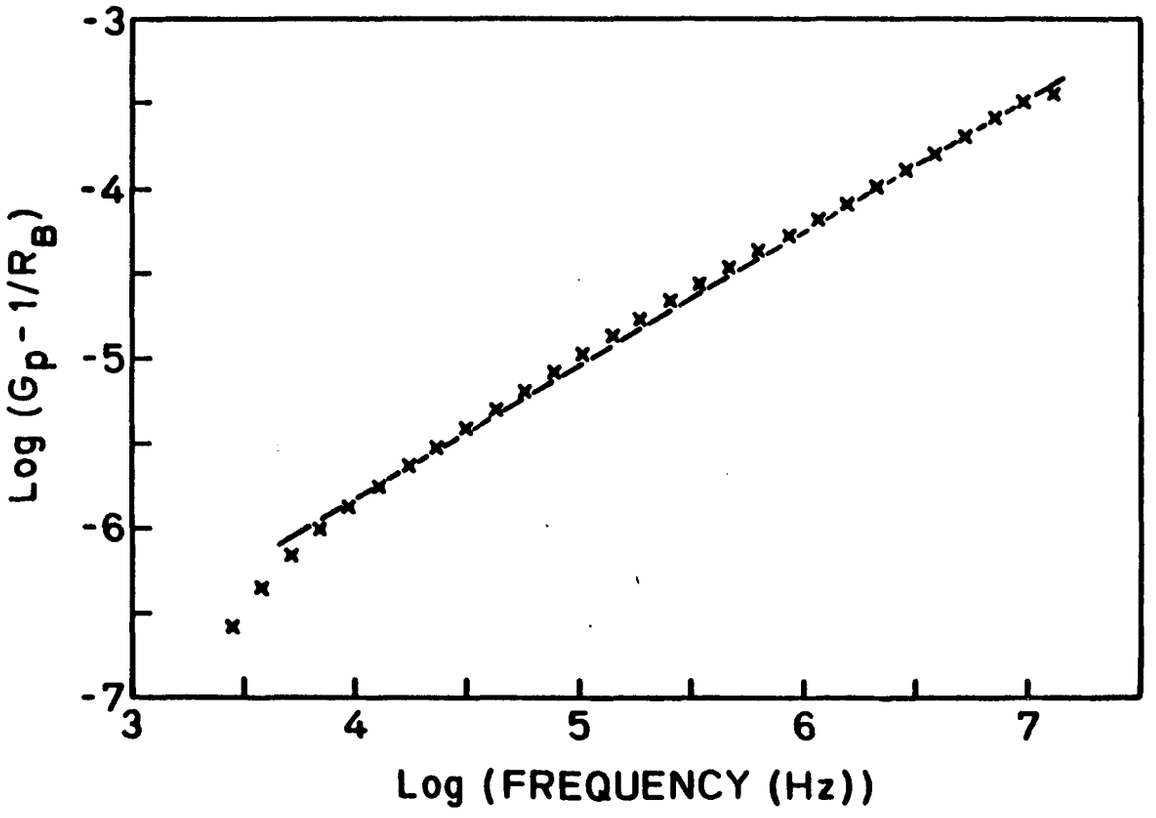

Figure 6.4 The logarithm of, the total parallel conductance minus the d.c. conductance, versus the logarithm of frequency for CH61-79.

where ω = angular frequency, A = a constant. Similarly a plot of log $(C_p - C_\infty)$ versus log frequency produces a fairly straight line with slope δ (Figure 6.5). Therefore

$$C_p = C_\infty + B\omega^\delta$$

where B = a constant. The total admittance of the circuit can be written as

$$Y^* = Gp + i\omega Cp$$
$$= 1/R_B + A\omega^\beta + i(\omega C_\infty + B\omega^{1+\delta})$$

Subtracting the contributions from R_B and C_∞ we obtain the following expression for Y_B^*:

$$Y_B^* = A\omega^\beta + iB\omega^{(1+\delta)}$$

The real and imaginary parts can be related through the Kramers-Kroenig relations resulting in a final expression for the frequency dependent admittance term:

$$Y_B^* = A\omega^\beta + iB\omega^\beta$$

where A, B, β are constants. As $B = A\tan(\frac{\alpha\pi}{2})$, (from the Kramers-Kroenig relations) this can be re-written as

$$Y_B = A\omega^\alpha(1 + \tan\frac{\pi\beta}{2})$$

The loss, or dissipation factor, D, of this term is constant with respect to frequency:

$$D = \frac{G_p}{B_p} = \frac{A\omega^\beta}{A\tan(\frac{\alpha\pi}{2})\omega^\beta} = \cot(\frac{\alpha\pi}{2})$$

The expression for the total admittance of the equivalent circuit selected for modelling the bulk sample electrical response of the rocks is therefore given by:

$$Y_T = 1/R_B + i\omega C + A\omega^\beta(1 + i\tan\frac{\pi\beta}{2})$$

the expression determined by Raistrick et al.(1976).

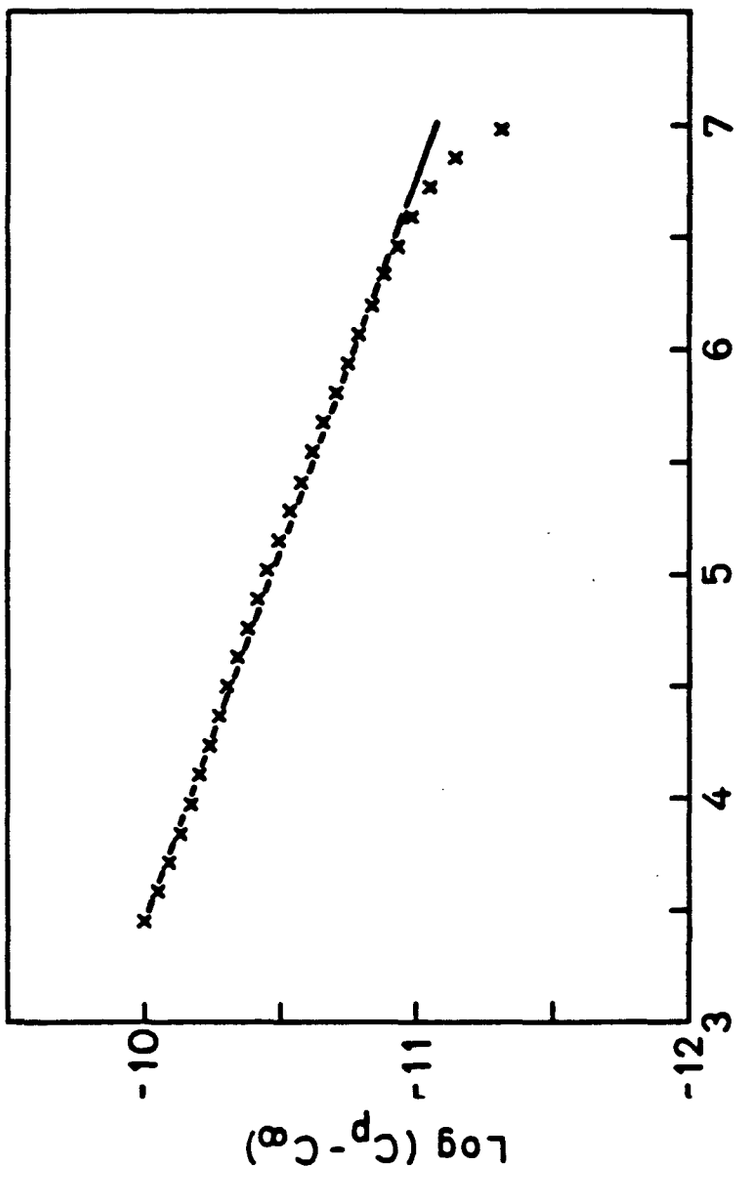

Figure 6.5 The logarithm of, the total parallel capacitance minus the high frequency capacitance, versus the logarithm of frequency for CH61-79.

Modelling the Electrical Response of the Samples

The four parameters to be determined are R_B, C_∞, A, and β. I have used a slightly modified version of a program written by Hu (1980) to fit the data from all the samples at all levels of water saturation with this equivalent circuit model. The program, based on an algorithm by Bevington (1969), combines a gradient search with a non-linear least squares fit. Two examples of the agreement between the data and the model are shown in Figure 6.6 and 6.7, where the actual data and the model data are plotted in the complex impedance plane. The selected equivalent circuit shows excellent agreement with the data, resulting in a root mean square error in most cases of less than 2%.

The discovery of an equivalent electrical circuit that shows such excellent agreement with the response of the rock samples is precisely what is needed in this study of electrical properties. It is now possible to isolate the various contributions to the electrical response. The d.c. resistance can be easily determined and separated from the total electrical response. It is also possible to determine the high frequency dielectric constant of the system; this is calculated from C_∞, which is also defined as a separate term in the circuit and represents the dipolar capacitance. The frequency dependence, which so complicates the interpretation of the measured electrical properties, is isolated and described by one relatively simple circuit component, the complex admittance term.

The determination of an equivalent electrical circuit also has widespread practical applications. With a relatively few number of data points at various frequencies it is possible to determine the four parameters $R_{d.c.}$, C_∞, A and β that completely characterize the circuit. In well-logging or core analysis, for example, measurements made in the frequency range of 100 to 500 kHz, when fit to the determined equivalent circuit, can yield the values of the d.c. resistance

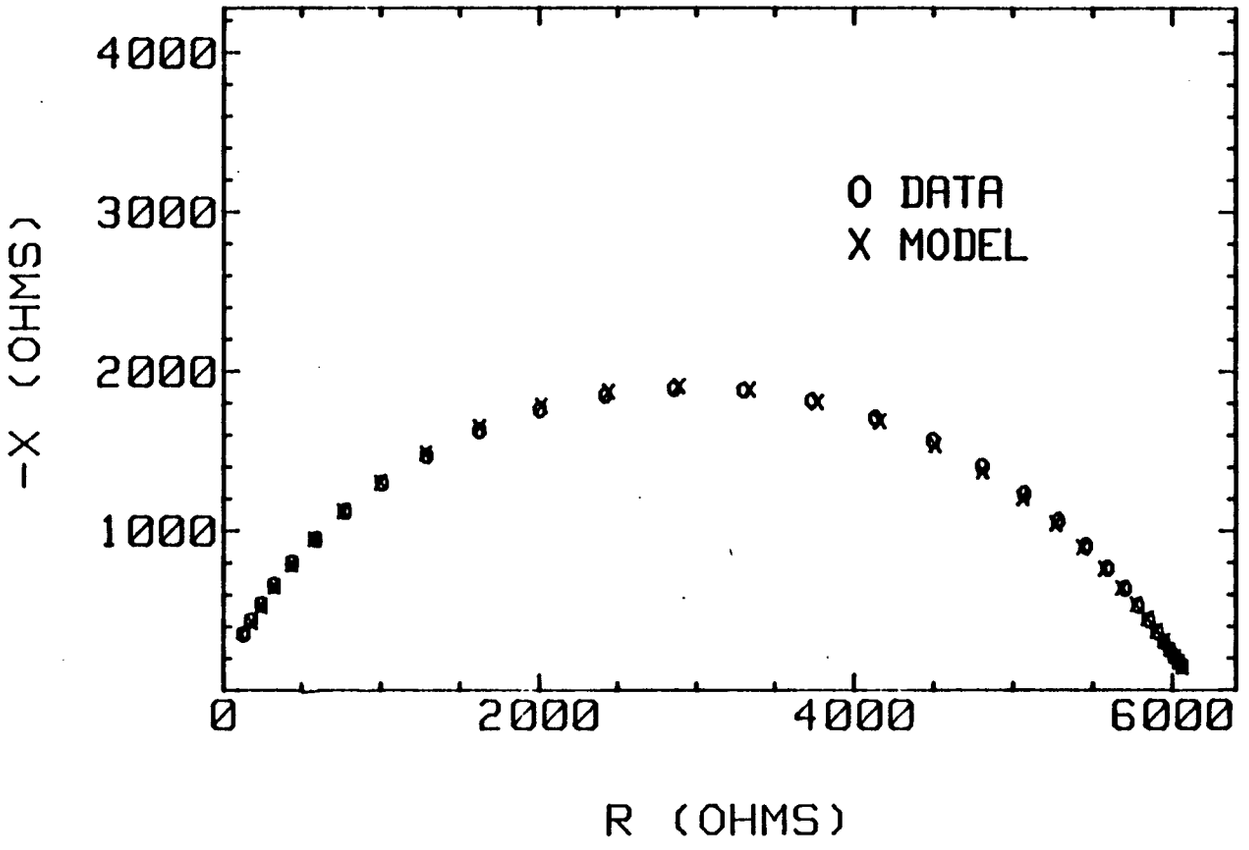

Figure 6.6 Complex impedance plot of the sample data and the model for CH66-79, Sw=.24. The root mean square error between the data and model is 1.4%.

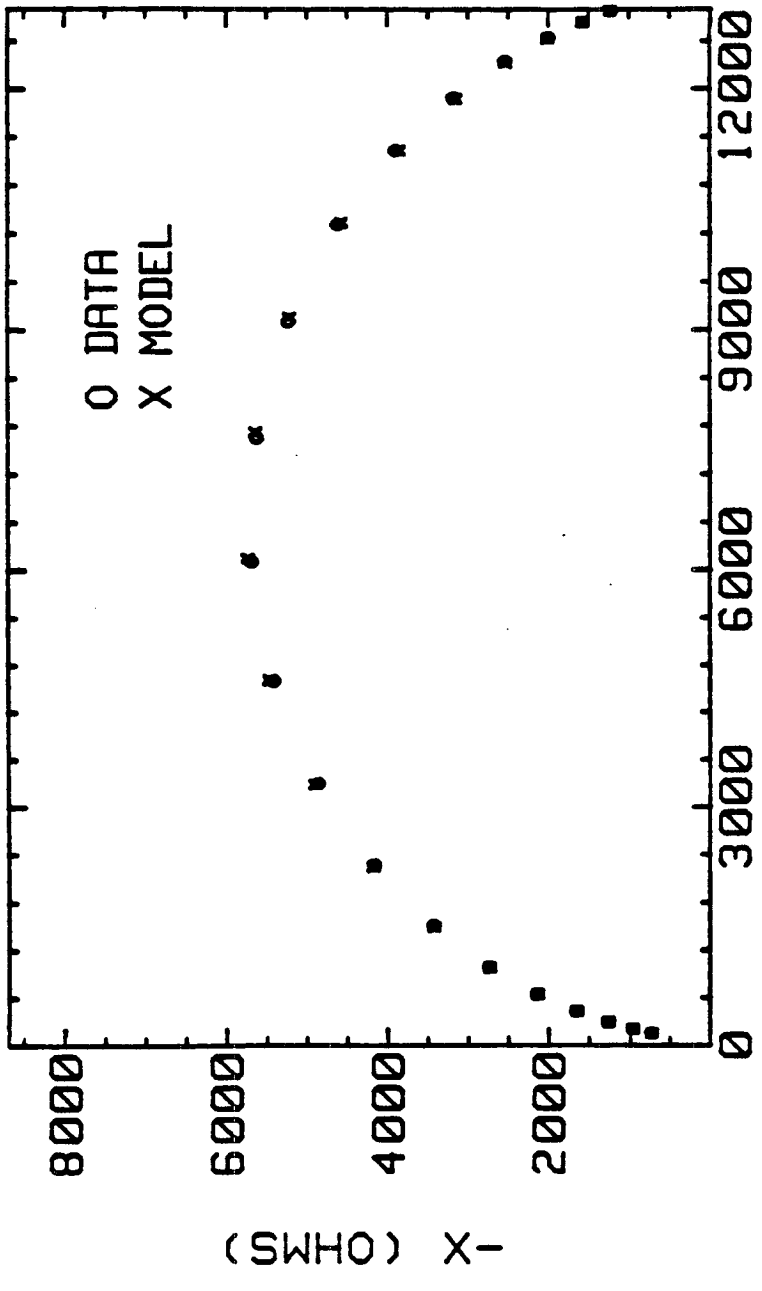

Figure 6.7 Complex impedance plot of the sample data and the model for St.Peter's, Sw=.26. The root mean square error between the data and model is 1.0%.

and the high frequency capacitance or dielectric constant. Thus the d.c.resistance can be determined without having to make measurements at the low frequencies where electrode polarization is such a major problem - measurements can be made at high frequencies and with the use of the equivalent circuit extrapolated to a lower or d.c. frequency. The high frequency dielectric constant can similarly be determined by making measurements at lower frequencies and extrapolating to higher frequencies; being able to make the measurements at lower frequencies in well-logging has the great advantage of increased depth of penetration. This technique of modelling with an equivalent circuit can thus separate the two parameters that are presently of interest in borehole applications, the d.c. resistance and the high frequency dielectric constant, without the superimposed frequency dispersion. The frequency dependence of the system, the measure of which is the complex admittance term, may itself prove to be very useful as a diagnostic tool once the source of the frequency dependence is understood.

Summary

The equivalent electrical circuit proposed by Raistrick et al. (1976) has been found to show excellent agreement with the electrical response of sedimentary rocks. Modelling with this circuit determines the d.c. resistance and the dipolar capacitance of the system. The total frequency dependence is contained in the complex admittance term, the real and imaginary parts of which show the same power law dependence upon frequency with a dissipation factor that is constant with respect to frequency.

CHAPTER 7

FREQUENCY DEPENDENCE: PROPOSED MECHANISM

Introduction

In the previous chapter it was shown that the non-Debye behavior of rock samples can be modelled by the inclusion of a complex admittance term in the equivalent electrical circuit. The specific form of the admittance term is unique in that the real and imaginary parts show the same power law dependence upon frequency and the dissipation factor is constant with respect to frequency. Frequency dependent circuit elements, and frequency dependence in general in measured electrical parameters, have been a topic of discussion for many years.

The first detailed study of a frequency dependent electrical response was Warburg's (1899) study of the interface between a metal electrode and an electrolyte. Warburg's electrode polarization response is characterized by a unique frequency dependence of the real and imaginary parts of the complex impedance such that both vary as $\omega^{-\alpha}$ where $\alpha = 0.5$. This type of frequency dependence in a system would cause the semicircles in Z^* plots to be lowered by 45° below the real axis and straight lines to be inclined at 45° to the real axis. The Warburg response, although it does provide a frequency dependent mechanism, is very restricted in both the predicted value of α and in the physical setting where such a process can occur.

Cole and Cole (1941) offered an alternate explanation for the observed frequency response which does not restrict α to 0.5. This more generalized approach is to assume a distribution of relaxation times, an approach which has been widely used in fitting impedance and dielectric data, without however identifying the physical processes involved.

The Cole-Cole relaxation model has been found to provide a good fit for laboratory complex resistivity measurements of rock samples (Madden and Cantwell, 1967; Pelton et al., 1972) and for the in situ induced polarization spectra of various mineral deposits (Pelton et al., 1978). The electrical response of the rock samples in this study is also such that it suggests a Cole-Cole distribution of relaxation times. Through consideration of the effects of sample petrography and saturation on the frequency dependence, it is possible to propose a physical source for this distribution.

Interfacial Polarization

The capacitance in rocks at low frequencies, as discussed in Chapter 4, is related to interfacial polarization. There is much information available in the literature about the capacitance associated with polarization at an electrode that is relevant to the study of interfacial polarization at low frequencies in rocks. A power law dependence, as has been earlier noted, is commonly observed in the polarization capacitance.

There are basically two types of interfacial polarization, faradaic and non-faradaic (Grahame, 1952). Faradaic polarization is that which involves an electrochemical reaction at the interface such that charges cross the interface. Non-faradaic polarization, often referred to as ideal polarization, is that in which the interface is totally blocking to charge transfer. In our system I assume that the platinum is ideally blocking. At the interfaces within the rock however, there is the possibility that some electrochemical reaction is occurring; clay membranes for example may act as semi-blocking electrodes. It has been noted that impurities can often give faradaic characteristics to systems which ideally should be blocking (Scheider, 1975).

The polarization capacitance at a blocking electrode interface can be modelled as an adsorbed layer of ions in series with a diffusive double layer

(Vorsina and Frumkin, 1939; Grahame, 1946). The charging and discharging of this double layer is one example of a non-faradaic process (Scheider, 1975). The magnitude of the capacitance of the diffuse double layer (C) can be given at low frequencies by

$$C = D\kappa / 4\pi$$

where D is the dielectric constant and κ the Debye-Huckel parameter; for a univalent electrolye,

$$\kappa = (8\pi\varepsilon^2 n / DkT)^{\frac{1}{2}}$$

where ε is the electronic charge, n is the number of each ionic species per cc, k is Boltzman's constant, and T is the absolute temperature (Gouy, 1903). The double layer capacitance is usually in the order of 10^{-6}F (Bockris and Reddy, 1970). This double layer capacitance, which is characteristic of non-faradaic polarization, is usually also associated with faradaic processes; the interface may be blocking to some species yet not to others. The double layer is therefore a significant part of the electrical response of any interface regardless of the specific polarization process.

Electrical Double Layer

The existence of a double layer in rocks at the rock/water interface and surrounding clays, has been well-documented (Fuerstenau, 1984). The low frequency capacitance found in this study for saturated rock samples, corresponding to C_2 in the Debye circuit, is of the same approximate order of magnitude as that expected for the double layer capacitance. It is well worth considering then the form of frequency dependence that has been associated with the double layer. A good review of studies of electrical frequency dependence is given by Scheider (1975); points from this are considered below.

Ferry (1948) considered equilibration rates in the diffuse double layer as

the source of the frequency dependence in faradaic polarization. This mechanism however produced lorentzian not the experimentally observed fractional power law frequency dependence unless an unusually broad distribution function was assumed. Another problem with Ferry's model was that the calculated relaxation time was $3x\ 10^{-6}$ seconds, predicting a dispersion at frequencies two orders of magnitude higher than observed. Ferry suggested that the discrepancy may have been due to a higher viscosity of the fluid in the double layer, but disregarded this as unreasonable; he concluded therefore that the double layer could not produce the dispersion because the predicted dispersion frequency was off by two orders of magnitude.

Bockris and Conway (1958) however, site evidence for the presence of high viscosity or "frozen water" in the double layer at an electrode surface. Using the higher relaxation times for this bound water, the time constants in Ferry's model could be brought to reasonable values. The form of the frequency dependence of this model however is still lorentzian.

While an electrical double layer does provide a capacitance on the same order of magnitude as that observed for the low frequency capacitance of the samples, and a frequency dispersion in the kHz range also as observed, the form of the frequency dependence has not been adequately modelled with double layer theories. There is increasing evidence to show that the microgeometry of a system may be the source of the frequency dependence. This can be considered in relation to both the high frequency and low frequency response of the rock samples.

Microgeometry and Frequency Dependence

There are a number of examples in the literature suggesting that the geometrical arrangement of the various electrical elements in a material is the source of the frequency dependence. Microscopic roughness of the electrode

surface has been suggested as the source of frequency dependence in the capacitance at an electrode (Sarmousakis and Prager, 1957; DeLevie, 1965). Scheider (1975) presents a theory relating "microscopic surface topology" to the frequency dependence observed in the electrical response of an electrolyte/electrode interface. The polarization characteristics are assumed to be determined by the manner in which ions are accumulated at the double layer that exists at the interface, the roughness of the interface introducing the observed frequency dependence.

The attempted modelling of electrical frequency dependence with equivalent electrical circuits also suggests a relationship between the microgeometry of a system and the frequency dependence. No finite combination of circuit elements can model the frequency dependence, but infinite circuits have been used to model the Warburg impedance (Nagel and Tiller), the frequency response of human skin (Tregear, 1966), and the frequency dependence due to electrode surface roughness (Scheider, 1975). Scheider (1975) used infinite ladder networks to model the surface roughness of an electrode, and found the power law exponent in the frequency dependence to be related to the type of branching in the network. It is significant that the admittance determined by Scheider (1975), both from this modelling and theoretically, has the same form as Y_B^* proposed in the circuit model of the previous chapter.

The fact that frequency dependent electrical properties can be modelled by an infinite arrangement of circuit elements suggests that the geometrical arrangement of the various electrical elements in a material is the source of the frequency dependence and the specific arrangement of these elements, like the branching type in Scheider's (1975) network, may determine the specific power law exponent of the frequency dependence. In the case of rocks this suggests

that it is the geometry of the pore space that determines the frequency response. This microgeometry can be modelled using a 3-D random network (Yale, 1984) where each pore is represented by a tube of a certain radius. To model the electrical properties using a network approach, each pore can be represented by a Debye circuit. To realistically model the elastic properties of rocks, a distribution of radii is required (Yale,1984); as the resistance of each pore is inversely proportional to the square of the radius, each pore will have a characteristic relaxation time, resulting in an observed distribution of relaxation times. Consequently even though each pore can be modelled by simple, frequency independent resistors and capacitors in the form of a Debye circuit, the modelling of the total electrical response contains a frequency dependent term reflecting the distribution of relaxation times. The R and C in the equivalent circuit for the total rock response therefore corresponds to the bulk sample properties and Y_B^*, the lumped circuit parameter representing all the non-Debye frequency dependence of the system, contains information about the microgeometry of the pore space.

Relationship Between Y_B^* and Sample Properties

Qualitatively the observations to date support the idea that Y_B^* reflects the presence and geometrical arrangement of subunits in a material. In a material exhibiting a purely Debye response, the complex admittance term, Y_B^*, is not required in the equivalent electrical circuit; the semicircular portion of the complex impedance plot is centered on the real axis. Pure liquids show this Debye response (Von Hippel, 1954). A comparative study of the electrical response of single crystal and polycrystalline PbF_2, using the equivalent circuit given in the previous chapter, showed that the complex admittance term was absent in the equivalent circuit for the single crystal, but needed in the modelling of the polycrystalline sample, suggesting that it is associated with

grain boundary effects (Raistrick et al., 1976).

In terms of the complex plane presentation of the data, the effect of Y_B^* is to depress the semicircular arc. A way of quantifying the amount of non-Debye frequency dependence in a system is therefore to quantify the depression of the semicircle in the complex impedance plane. A useful parameter for this purpose is r, defined by Hu (1980) as a measure of the amount of depression of the semicircle. r, as illustrated in Figure 7.1, is the ratio of the height to the radius of the semicircle representing the data in the complex impedance plane. r is equal to 1 for a system showing Debye behavior and decreases as the system deviates from Debye behavior.

It is difficult to interpret the specific physical meaning of the value of r in terms of rock samples. Some interesting correlations have been found however between r and sample properties. There is an observed correlation between r and the surface area to volume ratios of the samples. St. Peter's, with a very low surface area to volume ratio, has an electrical response very close to a Debye response; the semicircular arc in the complex impedance plot for this sample shows very little depression, r=.85 for S_w=.36. Berea 100 and 200, with higher surface area to volume ratios, have semicircular plots in the complex impedance plane that are more depressed than that of St. Peter's, at the same level of saturation; for Berea 100, S_w=.36, r=.76; for Berea 200, S_w=.36, r=.81. The four tight gas sandstones, with the highest surface area to volume ratios, have noticeably the most depressed semicircles with r values of .64, .64, .65, and .66 for S_w=.36. Indiana Dark, which has a high surface area to volume ratio, does not follow this trend. This sample was very difficult to model with the equivalent electrical circuit, yielding a root mean square error of 3%; this may be due to the presence of the iron oxide, goethite, in Indiana Dark and the effect of the magnetic susceptibility of this mineral on the dielectric response. In

general however, I concluded that the greater the surface area to volume ratio of a sample, the greater the deviation from a Debye response.

The frequency dependence is also very sensitive to the level of water saturation. r shows a general decrease with decreasing saturation. When a sample is fully saturated, its response is most like that of a Debye response. As the sample dries, it behaves less like a Debye circuit. When the rock approaches the very lowest levels of saturation, the deviation from a Debye response becomes so exaggerated that it is impossible to model the response with the equivalent circuit. The overall observed pattern is a decrease of r with decreasing saturation.

The correlation between the surface area to volume ratio of a sample and r can be extended to the observed changes with S_w if, instead of considering the surface area to volume ratio of the total pore space, we consider the ratio between the amount of surface bound water and the amount of bulk water in the volume of the pore space. When a rock is fully saturated, the two ratios are the same; the surface area to volume ratio of the pore space is also the ratio between the amount of water bound to the surface and the amount of water contained in the central volume of the pores. As a rock dries, it is reasonable to assume that the surface water, being physically adsorbed to the pore surface will remain while the water in the central volume of the pore space is removed. This results in an increase in the ratio of the amount of surface bound water to the amount of volume free water in the pore space as the rock dries. The observed relationship between r, the surface area to volume ratio and S_w therefore suggests that the frequency dependence in a rock sample is strongly affected by the presence of surface bound water and bulk water in the pore space.

Diffusion in Pores

The dissipation factor associated with Y_B^o is constant with respect to frequency. The low frequency response also exhibits constant D. It is possible to interpret this in terms of one mechanism that operates throughout the entire frequency range of this study, ionic diffusion in the pores.

The diffusion of ions in the pore space of a rock, in response to an applied electric field, can be described by the following equation:

$$\delta = \left(\frac{D}{f}\right)^{\frac{1}{2}}$$

where δ is the diffusion length, D is the diffusion coefficient, f is frequency. Diffusion is only important as a mechanism if the diffusion length is comparable to the pore size. Assuming D= 10^{-6} cm/sec, δ equals 10^{-3} cm at 1 Hz, 10^{-4} cm at 1 kHZ, and 10^{-6} cm at 1 MHz. The diffusion length thus ranges from 1 micron down to 100 A. This range of lengths is comparable to expected pore sizes; thus diffusion is a viable mechanism in the pore space throughout the entire frequency range of this study.

It is very reasonable to think of diffusion and the related interfacial polarization as a "constant D" mechanism. D is a measure of the ratio between energy loss and energy storage. A constant D means that the loss and storage are proportional and keep this same proportionality over a large frequency range so are closely inter-related in terms of some process. This is true of interfacial polarization. Ions are moving to interfaces where they are blocked; the movement of ions is the conduction in the rock, the energy loss; the blocking of the ions occurs at the interfaces in the rock and acts like the charging of a capacitor - the energy storage. The more ions that are conducted, the more ions that can be stored at an interface. The storage is proportional to, and in fact dependent upon, the loss.

Summary

Diffusion of ions occurs throughout the frequency range of this study (5 Hz to 13 MHz). This is a constant D mechanism that comprises the total electrical response in the low frequency region and acts effectively in parallel with the bulk sample properties in the high frequency region. In the modelling of the high frequency response, Y_B^* represents this diffusion in the pore space; the observed frequency dependence associated with this term is related to the surface area to volume ratio and the level of saturation in a sample.

CHAPTER 8

THE EFFECT OF SATURATION ON THE DIELECTRIC CONSTANT

Introduction

The dielectric constant is potentially a very useful parameter by which to measure the level of water saturation in rocks. Before it can be successfully applied as a logging tool however, a good understanding is needed of the effect of water saturation on the dielectric constant, taking into account the influence of such variables as the frequency of operation and the petrography of the rock. A strong frequency dependence has been found; there is also an observed dependence on the level of water saturation in the sample.

Effect of Saturation from 10 kHz to 10 MHz

In discussing the effect of the level of saturation on the dielectric constant, only the data at frequencies above 10 kHz will be used, as below this frequency most of the data were affected by polarization at the sample/electrode interface.

In Figure 8.1 the dielectric constant of Berea 100 is plotted versus S_w at seven different frequencies and in Figure 8.2, the dielectric constant of CH61-79 at eight different frequencies. These plots show that the dielectric constant increases much more with increasing S_w at low S_w than at high S_w. At high S_w the dielectric constant increases only gradually, and linearly, with increasing saturation. These data are representative of the data obtained for all the sandstones. I will define as S_w^0 the saturation level at which the break in slope in these plots occurs, and will discuss first the high saturation ($S_w > S_w^0$) and then the low saturation ($S_w < S_w^0$) levels.

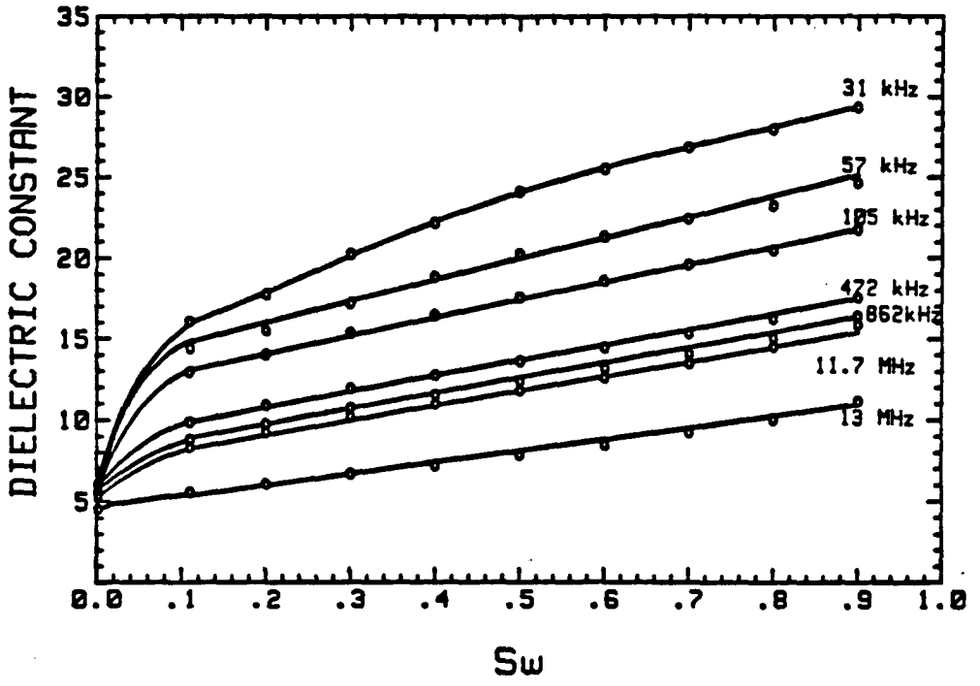

Figure 8.1 The dielectric constant of Berea 100 versus Sw at seven different frequencies.

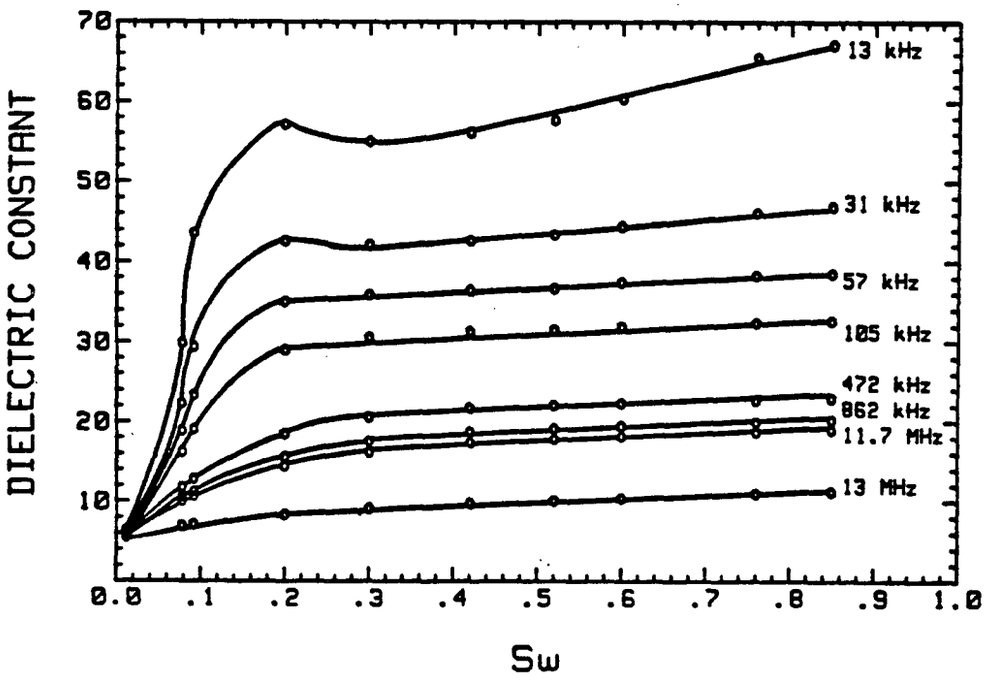

Figure 8.2 The dielectric constant of Ch61-79 versus Sw at eight different frequencies.

High Saturation Levels

At levels of saturation greater than S_w^0, the dielectric constant is found to increase linearly with increasing S_w. I can express this as

$$\Delta\varepsilon = k\Delta S_w$$

where $\Delta\varepsilon$ is the change in the dielectric constant, ΔS_w is the change in the level of saturation, and k is the proportionality constant.

As can be seen in Figures 8.1 and 8.2, k increases with decreasing frequency. For example, for Berea 100 (Figure 8.1), at 13 MHz, k = 5 and at 31 kHz, k = 17. Similarly for CH61-79 (Figure 8.2), at 13 MHz, k = 2 and at 31 kHz, k = 8. This increase in k with decreasing frequency was found for all samples and led to the conclusion that the lower the frequency, the more sensitive the dielectric constant is to the level of saturation.

I also found in the data that k was proportional to the porosity of the rock. The example given above illustrates this point, where k for Berea 100, with porosity equal to 0.197, is at any given frequency more than twice as large as k for CH61-79, with porosity equal to 0.074. This observed trend, increasing k with increasing porosity is predictable. The linear relationship between ε and S_w naturally suggests that it follows a simple volumetric mixing law of the rock and pore water. The dominant factor in the change of the dielectric constant with S_w, is the change in the volume of water which is equal to the volume of the pore space of the sample times the change in S_w. Consequently k, as observed, should be proportional to the porosity of the sample.

Low Saturation Levels

The most noticeable feature of the dependence of the dielectric constant on saturation for all the samples is its large increase at the low levels of saturation.

It appears however, that it is the frequency dependence of the dielectric constant, which varies with S_w, that largely governs the observed change of the dielectric constant with S_w. In Chapter 5 the power law dependence of C_p, and hence of the dielectric constant, was shown, with the power law exponent strongly dependent upon S_w, increasing with decreasing saturation until some critical saturation at which it dropped rapidly. The large increase in the dielectric constant at low saturations ($< S_w^0$) throughout most of the frequency range of this study is most likely due to the the rapid change in the frequency dependence of the dielectric constant with saturation at low saturations (as shown in Figure 5.8). In the previous chapter a correlation was noted between frequency dependence and the surface area to volume ratio of a sample, and also between frequency dependence and S_w. From these observations it was suggested that the frequency dependence depends upon the ratio of the volume of surface bound water to the volume of bulk free water present in the pore space of a sample, the more bound water, the greater the frequency dependence. I suggest that there is a rapid increase in the frequency dependence of the dielectric constant at low saturations due to the presence of predominantly bound water in the pore space at these saturations. This is seen as a rapid increase in the absolute value of the dielectric constant up to S_w^0. If the water in the pores of a rock is therefore considered as consisting of two phases, bulk pore water, and water bound to the rock surface, S_w^0 will be indicative of the amount of bound water in the rock.

As bound water is present on the pore surface and bulk water is present in the volume of the pore, the relative amount of bound water is proportional to the surface area to volume ratio of the pore space. Using the surface area to volume ratios determined from the nitrogen adsorption isotherms to calculate the amount of bound water will provide a lower limit on the amount of bound

water. (This will be a lower limit because nitrogen molecules will not enter pores less than approximately 20 Å in diameter (Brunauer, 1970), so cannot detect the surface area of the micropores or that associated with the clay layers.) Thus the surface area to volume ratio of a rock provides a means of predicting S_w^0 and vice versa.

In Figure 8.3 the dielectric constant of the five samples for which I have surface area measurements is plotted as a function of S_w at 31 kHz. Due to the low density of data it is impossible to accurately determine S_w^0, but some observations can be made. The tight gas sand, with relatively high surface area and low porosity, has a surface area to volume ratio of $9.45 \times 10^6\ cm^{-1}$; S_w^0 for CH61-79 appears to be around 0.15. St. Peter's by comparison, with very low surface area and high porosity, has a surface area to volume ratio of $1.57 \times 10^4\ cm^{-1}$ and accordingly S_w^0 falls between 0.005 and 0.04. The data for the two Berea samples with surface area to volume ratios of 8.40×10^4 and $1.33 \times 10^6\ cm^{-1}$ suggest S_w^0's between 0.01 and 0.04. Indiana Dark, while being the sample with the highest surface area, also has the highest porosity, resulting in a surface area to volume ratio less than that of the tight gas sand, $3.48 \times 10^5 cm^{-1}$. $S\omega^0$ for Indiana Dark falls in the range of 0.05 to 0.1.

While a greater density of data in the region of S_w^0 is needed, the available data do suggest that the samples with high surface area to volume ratios, contain a larger percentage of bound water in the pores and that this is reflected in the position of S_w^0. Assuming 10 Å of bound water on the pore walls and using the surface area to volume ratio of $1.33 \times 10^5\ cm^{-1}$ for Berea Sandstone, a calculation of the volume of bound water predicts that 1% of the water in the pore space is bound. The same calculation for a tight gas sand, with a much greater surface area to volume ratio, predicts 13% bound water. As mentioned above these are lower limits but this approach shows good agreement

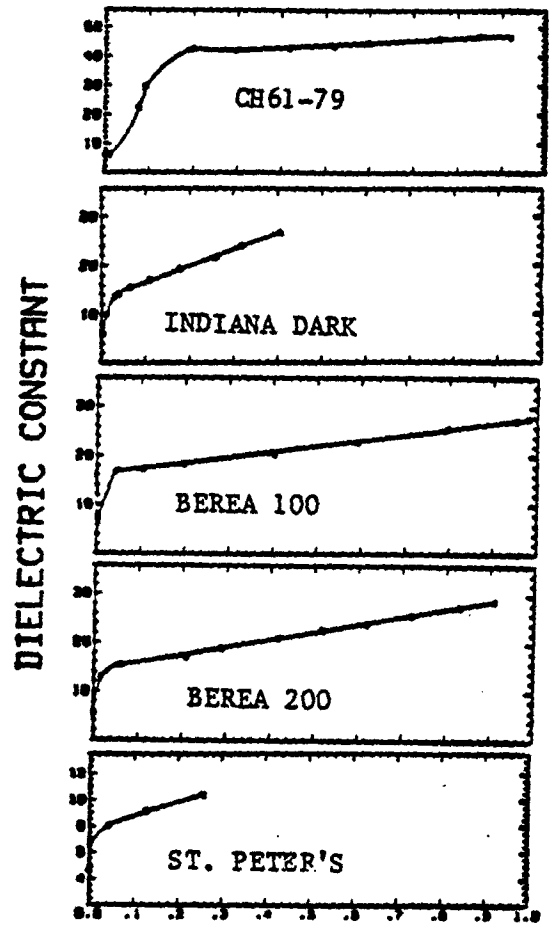

Figure 8.3 The dielectric constant versus Sw at 31kHz for five different sandstones.

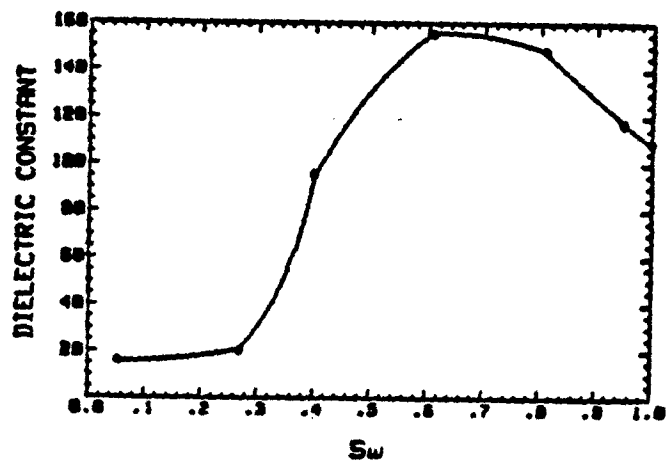

Figure 8.4 The dielectric constant versus Sw at 31kHz for a shale sample.

between the surface area to volume ratio and the value of S_w^0.

One interesting feature in Figure 8.2 is a peak in the dielectric constant at S_w = 0.2. This peak was found also in another tight gas sand at S_w = 0.2, but was apparently absent in the all other samples. saturations. Sheng and Callegari (1983) propose that a peak in the dielectric constant occurs due to the existence of small gaps between large conducting regions. Sheng and Callegari (1983) refer to this as a percolation threshhold; I interpret this to be the point in the saturation where surface coverage is complete and the water exists in isolated clusters (as described by Anderson and Parks, 1968). This peak thus occurs at S_w^0, a measure of the amount of bound water or the surface area to volume ratio of the rock.

It is informative that in a shale I also find a prominent peak at S_w = 0.6 (Figure 8.4). I have suggested that the position of a change in slope or, in some cases a peak, may be sensitive to the amount of bound water in a rock. Because in shales the surface area is high and the porosity low, a large percentage of the water in the pores is bound; consequently the peak will occur at much higher levels of saturation.

Because the change in the dielectric constant with water saturation at these frequencies, in the kilohertz to low megahertz range, is strongly affected by the frequency dependence, a very different dependence of the dielectric constant on S_w is found when only the high frequency or dipolar dielectric constant (calculated from C_∞ of the equivalent circuit in Chapter 6) is considered. The dielectric constant of water structurally bound to a solid surface is very close to that of ice (Bockris and Conway, 1958), approximately 6. The first monolayer of water adsorbed to a surface thus has the lowest dielectric constant; the dielectric constant of successively adsorbed layers increases until it reaches that of free water (Bockris and Reddy, 1970), approximately 80. In

Figure 8.5, where the high frequency dielectric constant of Berea 100 is plotted as a function of saturation, a very slow increase in the dielectric constant is seen at low saturation undoubtedly due to the low dielectric constant of the bound water. This is followed by an increasing change in the dielectric constant with saturation as the amount of water and the dielectric constant of the additional water increases.

A correlation was noted between the value of the dielectric constant at saturations above S_w^0 and the surface area to volume ratio of a sample. In Figure 8.6 is shown a plot of the dielectric constant as a function of frequency for twelve different sandstones at S_w=0.36. The dielectric constant of St. Peter's is consistently the lowest, the dielectric constant of the tight gas sandstones, consistently the highest. The trend follows the trend in surface area to volume ratios where known and the expected trend from petrography where unknown. Given that the dielectric constant of bound water is lower than that of free water, it is expected that those rocks with higher surface area to volume ratios, suggesting a higher amount of bound water, would have a lower dielectric constant. The opposite is observed; this is again not due to the high frequency dielectric constant of the system, but due to the superimposed frequency dependence. A higher surface area to volume ratio causes a greater frequency dependence resulting in a higher measured dielectric constant in the frequency range of 10 kHz to 13 MHz.

Summary

I have found that the dielectric response of partially saturated sandstones in the frequency range of 10 kHz to 13 MHz, is dependent upon the level of water saturation. There is a large increase in the dielectric constant with S_w from $S_w = 0$ to $S_w = S_w^0$. At saturations above S_w^0, the dielectric constant increases linearly with increasing S_w, the proportionality constant between the two being

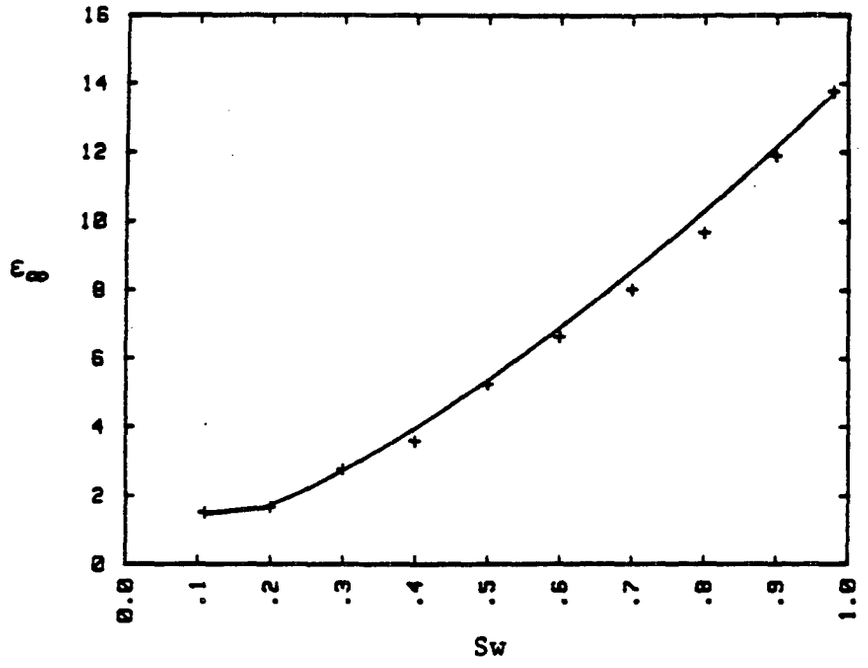

Figure 8.5 The high frequency dielectric constant of Berea 100 versus Sw.

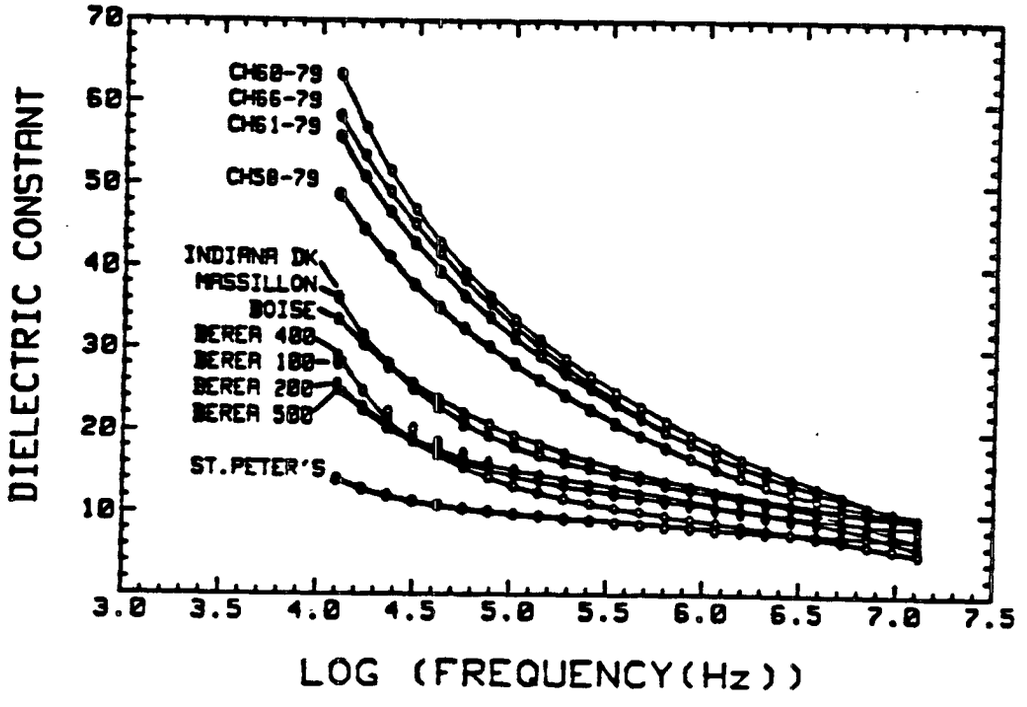

Figure 8.6 The dielectric constant versus logarithm of frequency for twelve sandstones at Sw=0.36.

dependent upon frequency and porosity. It is the surface area to volume ratio of the pore space that appears to be the dominant factor in determining S_w^0, which is interpreted as a measure of the amount of bound water in a sandstone sample. The surface area to volume ratio also determines the amount of frequency dependence and thus is the dominant factor in determining the measured absolute value of the dielectric constant in the frequency range of this study.

CHAPTER 9

THE DIELECTRIC CONSTANT: CONCLUSIONS

An essential step in developing an understanding of the dielectric constant has been to separate the effects of frequency from the effects of sample and fluid properties. Representation of the data in the complex impedance plane and the determination of an equivalent electrical circuit has proven to be a very useful technique for this purpose.

The electrical response can be divided into a low frequency and a high frequency region; the frequency dividing these two regions is dependent upon the sample properties, being mostly affected by the resistance. The low frequency region is often dominated by polarization at the sample/electrode interface; the actual sample response at these frequencies exhibits a dissipation factor that is constant with respect to frequency and is interpreted as ionic diffusion and the related interfacial polarization. The high frequency region is dominated by the bulk sample properties, the d.c. resistance of the sample and the high frequency dipolar capacitance.

The Debye circuit provides a good approximate model of the electrical response of a rock. There are two capacitors in this circuit - a relatively large capacitor, dominating the low frequency response, that is interpreted as corresponding to the electrical double layer at interfaces in the rock; and a relatively small capacitor, dominating the high frequency response, that is a bulk sample property. The gross features of the frequency dependence of the dielectric constant can be attributed to the presence of these two capacitors, one in series and one in parallel with the d.c. resistance of the system.

The frequency response of the rocks however, shows an anomalous frequency dependence that cannot be modelled with a Debye circuit. This

frequency dependence can be modelled in the high frequency region by the inclusion of a complex admittance term in the equivalent circuit of the form proposed by Raistrick et al. (1976). This admittance represents all the non-Debye frequency dependence of the system; the real and imaginary parts of this admittance show the same power law dependence upon frequency and the dissipation factor is constant with respect to frequency. Ionic diffusion is proposed as the mechanism related to this admittance term; the microgeometry of the system is proposed as the source of the frequency dependence. The high frequency electrical response of rocks shows excellent agreement with the proposed equivalent circuit resulting in a usual root mean square error in modelling of less than 2%. It is possible using this circuit to isolate the high frequency dipolar capacitance and the d.c. resistance from the associated frequency dependence.

The presence of bound and free water in the pore space of the rock has a significant effect on the change in the dielectric constant with water saturation. There is a marked increase in the dielectric constant with saturation up to some critical saturation, S_w^0, above which the dielectric constant increases more gradually and linearly with water saturation. S_w^0 is interpreted as reflecting the relative amount of bound water in the rock, and can be determined from knowledge of the surface area to volume ratio of a sample; conversely, if S_w^0 is known, the surface area to volume ratio can be determined. The absolute value of the dielectric constant throughout the frequency range of this study is largely determined by the magnitude of the frequency dependence; the frequency dependence, and thus the measured dielectric constant, are proportional to the surface area to volume ratio of a sample.

The effect of salinity has not been discussed in great detail but can be readily assessed in terms of the equivalent circuit representation of the data.

Increasing salinity decreases the resistivity of a sample, thus affecting the critical frequency separating the low and high frequency regions of the electrical response. Increasing salinity is generally found to decrease the value of the high frequency capacitance; at high frequency the dielectric constant essentially reflects the mixing of the two components - the rock and the pore water. The dielectric constant of a solution decreases with increasing salinity (unpublished data of D. Gottlob in Pottel, 1973), thereby decreasing the dielectric constant of the rock-water mixture. The measured dielectric constant throughout most of the high frequency region however increases with increasing salinity. This is due to an enhanced frequency dependence (the semicircular arc in the complex impedance plane becomes more depressed when there is a saline solution in the pores), most likely related to increased ionic diffusion in the sample with the higher salinity pore fluid.

The dielectric constant is a complex parameter sensitive to the frequency of measurement and the properties of the sample and pore fluid. Use of equivalent electrical circuits has proven to be very useful in the separation of these various effects and has contributed greatly to the understanding of this rock property. The determined equivalent circuit provides an excellent basis from which to continue the study of the many inter-related aspects of the dielectric response of sedimentary rocks.

REFERENCES

Anderson, J. H., and G. A. Parks, The electrical conductivity of silica gel in the presence of adsorbed water, *J. Phys. Chem.*, *72*, 3662-3668, 1968.

Arulanandan, K., and J. K. Mitchell, Low Frequency Dielectric Disperison of Clay-Water-Electrolyte Systems, *Clays and Clay Minerals*, *16*, 337-351, 1968.

Bauerle, J. E., Study of solid electrolyte polarization by a complex admittance method, *The Journal of Physics and Chemistry of Solids*, *30*, 2657-2670, 1969.

Bevington, P. R., *Data Reduction and Error Analysis for the Physical Sciences*, McGraw-Hill , 1969.

Bockris, J. O'M., and B. E. Conway, Determination of the faradaic impedance at solid electrodes and the electrodeposition of copper, *J. Chem. Phys.*, *28*, 707-716, 1958.

Bockris, J. O'M., and A. K. N. Reddy, *Modern Electrochemistry*, *V. 2*, Plenum Press, New York, 1970.

Brunauer, S., Surface areas of porous solids, in *Proceedings of the International Symposium on Surface Area Determinations*, edited by Everett and Otterwill, pp. 63-73, IUPAC, 1970.

Brunauer, S., P. H. Emmett, and E. Teller, The B.E.T. method, *J. Am. Chem. Soc.*, *60*, 309, 1938.

Calvert, T. J., R. N. Rau, and L. E. Wells, Electromagnetic propagation...a new dimension in logging, *S.P.E. 6542*, 1977.

Clark, V., *Effect of volatiles on seismic attenuation and velocity in sedimentary rocks*, Ph.D. dissertation, M.I.T., Cambridge, 1980.

Cole, K. S., Electric phase angle of cell membranes, *J. of General Physiology*, *15*, 641-649, 1932.

Cole, L. S., and R. H. Cole, Dispersion and absorption in dielectrics I. Alternating

current characteristics, *J. Chem. Phys.*, *9*, 341-351, 1941.

Collett, L. S., Laboratory investigation of over-voltage, in *Overvoltage Research and Geophysical Applications*, edited by J. R. Wait, Pergamon Press, New York, 1959.

Collett, L. S., and T. J. Katsube, Electrical parameter of rocks in developing geophysical techniques, *Geophysics*, *38*, 76-91, 1973.

DeLevie, R., *Electrochim. Acta.*, *10*, 113, 1965.

Ferry, J. D., Frequency dependence of the capacity of a diffuse double layer, *J. Chem. Phys.*, *16*, 737-739, 1948.

Fricke, H., The theory of electrolytic polarization, *The Philosophical Magazine*, *14*, 310-318, 1932.

Fuerstenau, D. W., Interfacial phenomena in mineral-water systems, in *Physics and Chemistry of Porous Media*, *A.I.P. Conference Proceedings*, *107*, edited by D.C. Johnson and P.N. Sen, New York, 1984.

Fuller, B. D., and S. H. Ward, Linear system description of the electrical parameters of rocks, *IEEE Trans. Geosci. Electronics* , *GE-8*, 7-18, 1970.

Grahame, D. C., Properties of the electrical double layer at a mercury surface. I. Methods of measurement and interpretation of results, *J. Am. Chem. Soc.*, *63*, 1207-1215, 1941.

Grahame, D. C., Properties of the electrical double layer at a mercury surface. II. The effect of frequency on the capacity and resistance of ideal polarized electrodes, *J. Am. Chem. Soc.*, *68*, 301-310, 1946.

Grahame, D. C., Mathematical theory of the faradaic admittance, *J. Electrochem. Soc.*, *99*, 370C, 1952.

Guoy, G., *Ann. Chim. Phys.*, *29*, 145, 1903.

Ho, C., *Application of ac techniques to kinetic studies of electrochemical Systems*, Ph.D. dissertation, Stanford University, Stanford, 1980.

Hu, Y. W., *Ionic conductors based on lithium orthosilicate and related structures*, Ph.D. dissertation, Stanford University, Stanford, 1980.

Johnscher, A. K., The interpretation of non-ideal dielectric admittance and impedance diagrams, *Phys. Stat. Sol. (a), 32*, 665-676, 1975.

Keller, G. V., and P. H. Licastro, Dielectric constant and electrical resistivity of natural-state cores, *U.S. Geol. Surv. Bull, 1052-H*, 257-285, 1959.

Madden, T. R., and D. J. Marshall, A laboratory investigation of induced polarization, *U.S. Atomic Energy Comm. R.M.E*, 3156, 1958.

Meander, R. A., and P. T. Cox, Dielectric constant logging, a salinity independent estimation of formation water volume, *S.P.E. 5504*, 1975.

Nagel, L. E., and W. A. Tiller, Dielectric response in human skin, in preparation,

Olhoeft, G. R., Electrical properties in Initial report of the petrophysics laboratory by G. R. Hunt, G. R. Johnson, G. R. Olhoeft, D. E. Watson, and K. Watson, *U.S.G.S. Circular 789*, 1979.

Olhoeft, G. R., Electrical properties of rocks, in *Physical Properties of Rocks and Minerals, 11-2*, edited by W.R. Judd Y.S. Touloukian, R.F. Roy, pp. 548 , McGraw-Hill, New York, 1981.

Poley, J. Ph., J. J. Nooteboom, and P. J. de Waal, Use of v.h.f. dielectric measurements for borehole formation analysis, *Soc. Pet. Well Log. Ana., Log Analyst, May-June*, 8-30, 1978.

Raistrick, I. D., and R. A. Huggins, Considerations in the use of electrical measurement techniques to evaluate potential new electrolytes and mixed conductors, *Proc. Symposium and Workshop on Advanced Battery Research and Design, Argonne National Laboratory*, B-277, 1976.

Raistrick, I. D., C. Ho, and R. A. Huggins, Ionic conductivity in some lithium silicates and aluminosilicates, *J. Electrochem. Soc., 123*, 1469-1476, 1976.

Sarmousakis, J. N., and M. J. Prager, Impedance at polarized platinum

electrodes in various electrolytes, *J. Electrochem. Soc.*, *104*, 454-459, 1957.

Scheider, W., Theory of the frequency dispersion of electrode polarization: Topology of networks with fractional power law dependence, *J. Phys. Chem.*, *79*, 127-136, 1975.

Schwan, H.P., Electrode impedance and measurements in biological materials, *Annals of the New York Academy of Science*, *148*, 191-209, 1968.

Scott, A. H., and H. L. Curtis, Edge correction in the determination of the dielectric constant, *Journal of Research of the National Bureau of Standards*, *22*, 747-775, 1939.

Scott, J. H., R. D. Carroll, and D. R. Cunningham, Dielectric constant and electrical conductivity measurements of moist rock: A new laboratory method, *Journal of Geophysical Research*, *72*, 5105-5115, 1967.

Sharbough, A. H., and S. Roberts, Dielectric measurement procedures, in *Methods of Experimental Physics*, *6*, edited by K. Lark-Horovitz and V.A. Johnsons, Academic Press, New York, 1959.

Sheng, P., and A. J. Callegari, Differential effective medium theory of sedimentary rocks, *App. Phys. Lett.*, *44*, 738-740, 1984.

Shi, C., *Electrical conductivity of silica in the presence of water and methanol vapor*, Ph. D. dissertation, Stanford University, Stanford, 1972.

Tarkhov, A. G., Resistivity and dielectric constant of rocks in alternating current fields, *Vses. Nauchn.-Issled. Geol. Inst. Materialy, Geofiz*, *12*, 3-42, 1948.

Tregear, R. T., Physical functions of the skin, *Theoretical and Experimental Biology*, *V. 5*, Academic Press, London, 1966.

Vinegar, H. J., and M. H. Waxman, Induced polarization of shaly sands - the effect of clay counterion type, *SPWLA Logging Symposium Transactions*, 1984.

Von Hippel, A. R., *Dielectric Materials and Applications*, 438 pp., M.I.T. Press, Cambridge, 1954.

Vorsina, M. A., and A. N. Frumkin, , *Compt. rend. Acad. Sci. U.R.S.S.*, *24*, 918, 1939.

Warburg, E., Ueber das Verhalten sogennanter unpolisirbarer Electroden gegen Wechselstrom, *Ann. Phys. Chem.*, *67*, 493-499, 1899.

Wolff, I., *Physics (New York)*, *7*, 203, 1936.

Yale, D. P., ***Network modelling of flow, storage and deformation in porous rocks***, Ph.D. dissertation, Stanford University, Stanford, 1984.